2013

MONITORING DAIRY COW FEED INTAKE USING MACHINE VISION

Anthony N. Shelley
University of Kentucky, anshel2@uky.edu

STUDENT AGREEMENT:

I represent that my thesis or dissertation and abstract are my original work. Proper attribution has been given to all outside sources. I understand that I am solely responsible for obtaining any needed copyright permissions. I have obtained and attached hereto needed written permission statements(s) from the owner(s) of each third-party copyrighted matter to be included in my work, allowing electronic distribution (if such use is not permitted by the fair use doctrine).

I hereby grant to The University of Kentucky and its agents the non-exclusive license to archive and make accessible my work in whole or in part in all forms of media, now or hereafter known. I agree that the document mentioned above may be made available immediately for worldwide access unless a preapproved embargo applies.

I retain all other ownership rights to the copyright of my work. I also retain the right to use in future works (such as articles or books) all or part of my work. I understand that I am free to register the copyright to my work.

REVIEW, APPROVAL AND ACCEPTANCE

The document mentioned above has been reviewed and accepted by the student's advisor, on behalf of the advisory committee, and by the Director of Graduate Studies (DGS), on behalf of the program; we verify that this is the final, approved version of the student's dissertation including all changes required by the advisory committee. The undersigned agree to abide by the statements above.

Anthony N. Shelley, Student

Dr. Daniel Lau, Major Professor

Dr. Zhi David Chen, Director of Graduate Studies

MONITORING DAIRY COW FEED INTAKE USING MACHINE VISION

THESIS

A thesis submitted in partial fulfillment of the
requirements for the degree of Master of Science in
Electrical Engineering in the College of Engineering
at the University of Kentucky

By

Anthony Neal Shelley

Lexington, Kentucky

Director: Dr. Daniel Lau, Professor of Electrical Engineering

Lexington, Kentucky

2013

ABSTRACT OF THESIS

MONITORING DAIRY COW FEED INTAKE USING MACHINE VISION

The health and productive output of dairy cows can be closely correlated to individual cow feed intake. Being able to monitor feed intake on a daily basis is beneficial dairy farm management. Each cow can be addressed individually with minimal time required from those working with the animals. This is essential as time management is closely tied to resource management in a dairy operation. Anything that can save time and resources and increase profitability and herd health is a paramount advantage in dairy farming. This study examined the use of machine vision structured light illumination three-dimensional scanning of cow feed to determine the volume and weight of feed in a bin before and after feeding dairy cow. Calibration and control tests were conducted to determine the effectiveness and capability of implementing such a machine vision feed scanning system. Such a system is ideal as it does not obstruct workflow or cow feeding behavior. This is an improvement over existing systems as the system in this research study can be implemented into existing farm operations with minimal effort and costs.

KEYWORDS: Dairy Cow, Feed Intake, Structured Light Illumination, Three-Dimensional Scanning, Machine Vision

Anthony Neal Shelley

April 26, 2013

MONITORING DAIRY COW FEED INTAKE USING MACHINE VISION

By

Anthony Neal Shelley

Daniel L. Lau
Director of Thesis

Zhi David Chen
Director of Graduate Studies

April 26, 2013

ACKNOWLEDGEMENTS

The following thesis could have never come to fruition without the generous help from Dr. Daniel Lau and Dr. Jeffrey Bewley, who guided and kept me on track throughout the entire process. The insights gained with this research will undoubtedly aid me in my future attainment of a Doctorate of Philosophy in Electrical Engineering.

I must also thank my family for without their financial as well as moral support, I could have never made it through this process: Claude Herman Shelley, Virgie Alice Shelley, Andrew Nicholas Shelley, and Zona Mae Shelley. Although no longer with me in the flesh, but eternally with me in the spirit, I am eternally grateful for my grandfather, Willie Havens Shelley, who along with the rest of my family and the guidance of A Watchful Eye have fashioned me into the man I am today. Providing a lamp unto my feet and a light unto my path.

$\varphi\alpha$

TABLE OF CONTENTS

LIST OF FIGURES

CHAPTER I: INTRODUCTION

Precision dairy farming refers to the use of technologies for managing individual animals to improve management strategies and farm performance. The ability to monitor the health of only the herd is antiquated and leads to great disparity between expected farm results and the actual results. Modern dairy farming is constantly focusing more attention to individual cow health and productivity. There are several benefits to the individual monitoring of a cow. A sick cow can be identified and removed from the herd much sooner to protect herd health. Determining optimal reproductive times can be monitored as well as individual calf delivery to avoid the loss of calves to death or disease. The diet of each individual cow can be rationed to fit their specific dietary needs to ensure maximum milk yields.

One precision dairy farming technology, feed intake monitoring, is very beneficial in tracking more than just dietary health of the individual cow. Individual feed monitoring helps to monitor the productivity of each cow versus the quantity of feed being consumed. This aids in farm budgeting, milk yield forecasting, and feed nutrition rationing. When feed is wasted by a cow, that is a direct loss of profit from the farm, as the money spent on that feed cannot be recovered. Being able to forecast milk production is essential for budgeting and resources management in a dairy farming operation as decreasing milk yields can lead to huge losses for the dairy farming operation. Ration balancing is important for maintaining and improving the herd diet. In general, the healthier the cow eats and the more feed it consumes, the greater the milk yield. By keeping track of how much feed the individual cow consumes, the producer can determine what combination of feedstuffs they prefer and in what rations. Feedstuffs are the feed ingredients used in mixing a feed ration that is balanced, meets dietary needs,

and helps promote individual cow health and productivity. In this manner, feed does not go to waste as often and in smaller amounts than traditional feed rationing without feed intake monitoring.

Currently, there are only a handful of methods that work to identify how much feed is distributed to or consumed by dairy cow. Each of these feed intake monitoring methods has its own benefits as well as a degree of faults. One method is visual inspection, which relies upon guessing how much feed is distributed and consumed. However, the difficulty in manually collecting data at the time of feeding has limited the extent of this type of monitoring [1]. The problem here is that you only get a best estimate of the distribution and consumption. This method does not tell you accurately how much the cow actually ate. The waste feed is rarely if ever quantified in a dairy production with this method. The feed that goes to waste is typically all collected together and sent to compost with no record of individual consumption. A second method of feed intake monitoring is employing an electronic system that will automatically record feed intake data. The most common practice here is to utilize radio frequency identification (RFID) to monitor the consumption by individual cows. Common systems that utilize this technology include GrowSafe [2] and Calan Gates [3], just to name a few systems. An RFID transponder located on the cow, typically in an ear tag or collar, interacts with an RFID reader located at the feeding area for traceability of an individual animal. In order to read the low-frequency multiple RFID tags at once, the Growsafe system developed a mat that is to be placed in front of feeders that collects individual cow data simultaneously. Most of the research completed in this area focuses on feeding behavior with feed intake only a secondary focus or as supporting informative

data, such as the research studies conducted by E. D. M. Mendes et al. [4], P. D. Krawczel et al. [5], T. J. DeVries et al. [6], and N. Chapinal et al. [7].

The purpose of this study is to develop a feed intake monitoring system that quantifies how much feed is distributed to the individual cow as well as how much is actually consumed. A machine vision system was chosen and implemented, in particular a 3D imaging system, to record and monitor the change in feed bins before and after feeding. In this manner, the producer will have a more accurate record of how much feed the cow is actually consuming as opposed to what the producer believes the cow is consuming. This can greatly aid in early detection of sickness or other health issues, monitoring milk output, feed efficiency, and several other factors of day-to-day dairy production that affect herd health and profitability of the farm. The incorporation of a machine vision system is optimal as the system can be placed in an area that does not obstruct the workflow of the farm, does not add additional work, and does not interfere with the feeding habits of dairy cow.

The novelty of this study is that a system is proposed and tested that has the capability to accurately record as near a true value of feed consumption and feed efficiency as possible. Our solution is to use computer-automated inspection from video surveillance in order to monitor feed intake. The system represents a marked improvement over existing systems or evaluation methods that only consider the amount of feed distributed and not the total amount actually consumed. The system setup is novel in its own right, as other existing technologies do not incorporate the SLI technology that this setup employs.

BACKGROUND

Precision dairy farming technologies are new to the dairy farming industry, and it will undoubtedly take time for them to become adopted and integrated into everyday operations. Much progress has been made in the past few years towards realizing this goal, with technologies such as computerized milk yield recordings, biometric identification, and health monitoring systems being readily adopted. In order for the dairy industry to continue to increase its production output capabilities and maintain herd health, further adoption of precision dairy farming practices must be promoted and accepted by large scale commercial operations as well as small scale independent family dairy producers. One such technology area is feed intake monitoring systems, which monitor how much feed is given to each cow, and how much of it is consumed by the individual cow. Several techniques have been attempted and various methods used to advance the realization of practical feed intake monitoring systems that are cost effective and beneficial to all dairy operations.

In order to understand the importance of feed intake monitoring in dairy cow, it is first important to understand the feed intake of dairy cow. Research in this area requires knowledge of both nutrition and behavior [8]. Dairy cows need to consume a lot of feed to achieve today's expected milk production. According to Dr. Lee Chiba, feed represents about 50 percent of the total production costs and, therefore, the feeding program more than any other single factor can determine the productivity of lactating dairy cows and the profitability of the dairy farm.[9] About 75 percent of the differences in milk production between cows is determined by environmental factors with feed making up the largest portion of these differences, reports Dr. Chiba. There is a close

relationship among milk production, dry matter intake, and body weight changes that must be considered throughout the lactation cycle of dairy cow.

There are four phases to the lactation cycle of dairy cow. The first phase is the Early Lactation Phase and it typically last between 0 to 70 days, or about 10 weeks. This phase is important as milk production increases rapidly following calving, peaking at 4 to 10 weeks after calving.[10] Because feed intake lags behind milk production, body fat will be mobilized to meet energy requirements for milk production.[9] Professor Michael Looper of the University of Arkansas states after calving, most cows can eat 20 pounds of grain per day if healthy.[10]

The second phase is the Peak Dry Matter Intake Phase and typically last 70-140 days, or again about 10 weeks in duration, into the lactation cycle. This period is marked by slowly declining milk production after reaching peak production. Feed intake should be near maximum and can supply nutrients for the cows, according to Michael Looper, and cows should be maintaining weight or slightly gaining. Grain should be fed according to the level of production as well as the cow's individual body condition score.[10]

The third phase is the Mid to Late Lactation Phase and occurs in the 140-305 days of the lactation cycle. The dry matter intake exceeds the needs during this phase because this is the main period to restore body reserves for the next upcoming lactation cycle. This phase is characterized as a period of declining milk production and should be the easiest to manage, says Michael Looper. The cows should be pregnant and animals should be slightly gaining weight so that they will be in a body condition score of 3.5 to 4 on a 5 point scale at dry off. Michael Looper also claims that a drop in milk production

of 8 to 10 percent per month is normal throughout the declining phase of milk production.[10]

The fourth phase is the Dry Period Phase and is characterized as the 50-60 days before the next lactation cycle begins or the last 50-60 days of the current lactation cycle. The dry period is a critical phase of the lactation cycle, according to Michael Looper, since a sound dry cow program can increase milk production or severely affect milk production during the following lactation and it can serve to minimize metabolic problems around the time of calving [10].

Maximizing dry matter intake in early lactation is very important.[11] Overestimation or underestimation of dry matter intake can be very costly if milk production is compromised. Professors John K. Bernard and Monty J. Montgomery of the University of Tennessee state that lactating dairy cows must consume large quantities of dry matter to provide the nutrients needed to maintain high levels of milk production and that the consequences of low dry matter intake are lower peak milk yields, lower total milk production, excessive loss of body weight, and poor reproductive performance.[12] According to professors Bernard and Montgomery, research has shown a two pound increase in milk production for each pound increase in dry matter intake and as milk production continues to increase, management of dry matter intake becomes more critical.[12] A number of factors affect dry matter intake, including forage quality, nutrient balance of rations, feeding method, ration palatability, moisture content, environmental stress, physical facilities, and general management practices.[12]

Feed should be available whenever the cows want to eat.[13] Rick Grant states that the times when bunks are often empty and cows typically eat are right after milking

and during freestall and alleyway scraping.[13] As well, Rick Grant believes that producers should work to minimize the time spent in holding areas and the milking parlor.[13] In general, the maximum amount of time that cows should be without access to feed is 6 to 8 hours daily, according to Rick Grant, because, beyond this point, significant declines in dry matter intake will occur.[13] The cow in this research study are fed at 1pm every day and their feed bins are checked again around 7pm every day. This allows the individual cow to eat as much as possible from the first bin during this 6 hour period before the feed from the second bin is offered to the cow. Rick Grant reports that, generally, 65 to 70 percent of daily dry matter intake occurs during daylight.[13] J.L. Albright of Purdue University states that cow have a distinct diurnal grazing pattern, which includes a major meal beginning approximately at sunrise.[14] Further, J.L. Albright indicates that cow are crepuscular, that is, most active at sunrise and again at sunset.[14] T. J. DeVries et al. also note this diurnal feeding pattern in their research as it suggests feeding is most active just before and after milking times [15]. As the feeding frequency is allowed to increase, the amount of feed consumed increases.

Feed efficiency is another important component in monitoring herd health and feed intake. According to Michael F. Hutjens of the University of Illinois, feed efficiency reflects the level of fat-corrected milk yield produced per unit of dry matter consumed with an optimal range of 1.4 to 1.8 pounds of milk per pound of dry matter while values in the field can vary from 1.1 to 2.0 pounds of milk per pound of dry matter intake.[16] According to Michael Hutjens, the “new focus” on maximizing efficiency reflects as cows consume more feed, digestive efficiency decreases as the relationship between net energy-lactation intake and milk production is subject to diminishing

returns.[16] The “traditional focus” was that as cows consume more feed to support higher milk production, the proportion of digested nutrients captured as milk is proportionally higher.[16] With lower milk prices, one way to maintain profitability without sacrificing milk production or herd health is by enhancing feed efficiency, states Michael Hutjens.[16] Days in milk, age, growth, changes in body condition score, body weight, forage quality, feed additives, and environmental factors will impact feed efficiency values.[16] Michael Hutjens reports that actual feed intake is critical for an accurate feed efficiency value and feed refusals should be removed (subtracted) as this feed has not been consumed.[16]

The amount of dry matter intake is one of the most discerning factors in milk production. In order to manage dry matter intake, producers must take it upon themselves to monitor the dry matter intake of their dairy cows. Promoting feed intake by lactating dairy cow is critical in terms of improving milk production, health, and body condition of the animal [17]. Understanding what causes declines and increases in feed intake will help producers to make more informed decisions as well as helping to maintain and support higher milk yields and the overall profitability of the dairy herd.

PREVIOUS RESEARCH

As already stated, one method of monitoring dairy cow feed intake is by simply utilizing human visual inspection to monitor the amount of feed output and consumption, but the difficulty in manually collecting data at the time of feeding has limited the extent of this type of monitoring [1]. This method is very inaccurate as no real quantifying measure is used to keep track of the feed. The producer has no idea of how much feed was eaten, wasted, or otherwise used. As a means to enhance dry matter intake estimation, several mathematical models have been proposed to predict and monitor dry

matter intake. A recent research study J.S. Rim et al. [18] compared various visually based dry matter intake prediction equations. The research study concluded that all of the models under-predicted actual observed dry matter intake [18]. The study also concluded that an accurate estimation of dry matter intake will always be a challenging task and that in order to achieve this goal, more mechanistic approaches, rather than simple empirical associations, are recommended for investigating diet and animal interactions under nonstandard environmental conditions, animals, or feeds [18].

The second method of monitoring dairy cow feed intake discussed involves utilizing weighing scales and RFID in a system, such as GrowSafe and Calan gates, to quantify how much feed is distributed and consumed. Previous research studies have focused mainly on feeding behavior instead of monitoring feed intake. Recent advances in the development of computerized recording systems, such as those used in the studies previously noted using the second method of feed intake monitoring, have resulted in a renewed interest in obtaining information on feeding behavior.

K.S. Schwartzkopf-Genswein et al. [19] conducted a research study to validate a RFID system for monitoring the feeding patterns of feedlot cow. The study determined that the RFID nature of the system did have some inherent factors that would produce errors, such as non-grounded (looped) metal panels used to construct feedlot pens and the transponder tags in the ear themselves [19]. Another factor of error potential in accurately monitoring feed intake is simply the limited RFID read range of the system, meaning that actual feeding data has the potential to go unrecorded when the RFID tag is out of range [19]. A similar study by T. J. DeVries noted similar errors in the RFID technology from physical structures acting as unintended antennae [6].

In the study by T. J. DeVries et al. [6], 12.6% of the observations that animals were confirmed present at the feed alley using video, the GrowSafe system failed to record animal presence. These observations were likely due to several sources of error: (i) external sources of radio frequency can cause lost signals; (ii) instances where the cow lifted her head out of the 50-cm read range but still remained over the tombstone; and (iii) reductions in the read range could have occurred due to changes in the orientation of the neck collar that place the transponder further from the mat. Another 3.5% of observations when the GrowSafe systems indicated that a cow was present at the feed alley, the video showed that the cow was not present. These extraneous observations were likely due to interference caused by the physical structures of the facility. For example, there were several physical structures (e.g., gates, fencing, lying stall partitions, and components of the feed alley neck rail) that may have acted as unintended antennae for signals.[6]

Research conducted by A. Bach et al. [20] monitored both feeding behavior and feed intake using weighing scales. This research required that the system automatically detect cow presence at the feed bunk and then monitored the amount of feed consumed at each presence detection. The system did have occasions where the system computer failed to recognize the presence of cow, and therefore any feed consumed during that time was not recorded. This study also reaffirmed the inability of human observers to keep track of feed intake as there were at least 96 occasions where the human observers did not detect cow presence at the feed bunk but the computer did [20].

The research study of T. Schultz [21] implemented the use of computerized corral feed stations for dairy cow. The mechanical feed stations monitored the feed intake of

individual cows fed in large groups, making it easier to spot changes in each animal's condition.[21] The study consisted of the following setup:[21]

> The feeding system consisted of a bulk concentrate feed storage tank with a flex auger that automatically moved feed to a small hopper in a specially designed feed dispensing stall. Here the cow, with a coded transponder hanging from her neck, emitted an electronic identification specific for that cow. This signal was received by a transmitter-receiver connected to the feed delivery motor, which was connected by cable to a computer. The computerized feeding system used in these observations was "Surge Infarmation."
>
> The computer had been programmed to feed each cow according to her previous milk yield. Feed delivery was set for six equal feedings during a 24-hour period, and any one visit was limited to 25% of the total. Each corral, with an average of 86 cows, had one feed tank and four feed stations. Previous research has shown that one station is adequate for 22 cows, as a general recommendation. The cows were production-grouped by daily milk yield as high (70 to 90 pounds), medium (50 to 70 pounds), or low (30 to 50 pounds) to observe milk production effects on feed station use.

The cows received nearly all of their daily feed allowance via the computerized corral feeder. This research concluded that the use of computerized, mechanical feed stations has proved beneficial in meeting individual cow nutritional needs by reducing feeding errors and monitoring feed intake as an indicator of cow health [21].

It has been suggested that lower feed intake by cows, utilizing such systems as a Calan gate system, may be due to the fact that the visual stimulation associated with food is removed, and the lack of competition that exists with individual feeding compared to group feeding.[22] The fact that the number of cows that can feed at any time is reduced by such individual feed intake monitoring systems also plays a role in feed intake. The reduction in available feeding space and increased competition for limited feeding space increases the agonistic behavior among cows.[22] None of these systems analyze the feed intake on a dry matter basis, which is where most of the nutritional value comes

from the feed. These systems instead work on an as-fed basis where the average moisture content of the feed is approximately half of the volume of the feed.

Another concern with using such systems is that they were built to fit local conditions, namely being suitable for closed, free, or tied stall barns. The system utilized needs to be able to be exposed to harsh, uncontrolled, and changing environmental conditions and must perform reliably under conditions of a commercial dairy. The frequent need for reprogramming according to specific experiments and the multitude of parameters involved require a different system design compared to existing designs. The ideal system would be designed and implemented for measuring, controlling, and monitoring individual feed intake of free-housed dairy cows while not interfering with feeding habits and not introducing additional work or inhibiting workflow on the farm.[23] Given the absence in reliable monitoring of the actual feed consumption of the individual cow, there is a continual waste of feed, which affects the profitability of the farm. Without monitoring the subtle changes in intake of the cow, the early detection of sickness or other health factors can go unnoticed until it is too late to rectify or can make what would have been a simple solution, if detected earlier, much more complicated to resolve.

UNIVERSITY OF KENTUCKY DAIRY

The University of Kentucky Coldstream Dairy Research Farm is one such dairy production facility that does take into consideration all of these effects on dry matter intake and which works hard to maintain and improve dairy cow herd performance. The University of Kentucky Coldstream Dairy Research Farm is located about 8 miles north of the main university campus. It was originally constructed in the 1960's and has been continually updated and used as a research facility. Among the various components of

the complex are a free stall barn with 108 stalls for the milking herd; a tie-stall barn with 36 stalls, used primarily for cows on research trials that require individual feeding; a small free stall barn with 18 stalls and Calan individual feeders, used primarily for nutrition research; a milking parlor that holds eight cows (essentially 2 "double 2" parlors); heifer, dry cow, and maternity facilities; and a management building that includes an office, teaching facilities and laboratory space.[24]

The animals located at the farm that were used in this study were part of a dairy cow herd that consists of about 95 Holsteins and 35 Jerseys and the average annual milk yield production of the herd is about 23,000 pounds for the Holsteins and 16,000 pounds for the Jerseys.[24] The tie-stall barn was used in this research study with a continuously changing small number of test cows, typically 2-4 cows. This allowed testing to be conducted for a number of cows at once instead of just a single cow and with differing dietary and eating habits which provided a stronger and more diverse research base on which to collect data from.

IMAGING SYSTEM

Our ultimate goal is to bring machine vision technologies to precision dairy farming so that problems such as feed intake can be addressed in a completed automated fashion using video surveillance. Video surveillance has the advantages of being easy to install without interfering with the existing dairy workflow since cameras can be installed on the ceiling and other non-obtrusive locations. The term, “machine vision,” is used to encompass technologies that allow a computer to “see” via means of using cameras to capture visual data which is then processed using an analog to digital conversion and other possible digital signal processing tools in order to view the scene of the cameras as desired, typically as a means of recognition, analysis, or inspection of the scene.

Within the broad range of imaging technologies associated with machine vision, we have a particular interest in the area of 3D machine vision where cameras record not only a visible light scene/texture, but also the distance of all visible objects from the camera. In some literature, this is referred to as 2.5-dimensional imaging since you only measure the Z-coordinate of the visible surfaces, not a true 3D cross section such as that produced by X-ray computed tomography. Methods of 2.5D imaging include stereovision, time of flight, and structured light and utilize either an active or a passive lighting architecture. With passive lighting, the lighting of the scene is from ambient light. With active lighting, the lighting of the scene is controlled by the system itself. Ambient light may remain in the scene, but is not the dominant source.

Passive stereovision was a predominant choice, as such systems are relatively cheap, can be stationary, and can collect image data in a short period. In the case of stereo imaging, two cameras are used to capture the same scene with differing perspectives in order to create a disparity between them. A computer then overlays these two scenes to find corresponding pixels and the separation of these matching pixels is known as the disparity, which gives rise to the 3D nature of the imaging technique. Several correspondence matching issues arise when using a passive stereovision system, and can therefore lead to correspondence mismatching and inaccurate results.

Yet other 3D imaging setups, such as time of flight systems, were ruled out due to the amount of time required to collect data or the need for repositioning of the subject as the system utilized needed to be stationary and time efficient. Time of flight technology is an active lighting system architecture that finds the distance to the target's surface by measuring the round trip time of a pulse of light. Time-of-flight systems utilize a laser

range finder or a flash-like light source in order to detect the distance to a point. Time of flight systems are limited by the number of data points that they capture at a given time and their relatively limited field of view. Therefore, time of flight systems can lead to accuracy errors.

The resolution and accuracy of stereovision systems, which employ the use of two or more cameras, can be improved upon by reducing the stereometric system to just one camera and a projector in a system architecture known as structured light illumination (SLI). By using an active stereovision SLI system instead of a passive two camera stereovision setup, the costs are further decreased, image data collection timing is faster, and resolution and accuracy of the scan are improved. Therefore, an SLI system was the optimal system choice for this research. SLI systems work on the basis of projecting a light pattern across the scene being observed in order to create depth and surface information from the deformation of the known projected pattern. The SLI system in this research utilizes known fringe phase modulated patterns to gather depth information. The accuracy of SLI systems is because they resolve the pixel correspondence matching problem that other systems encounter and they allow for error detection and correction. SLI systems are also more precise because they can capture the entire field of view at once instead of one point at a time. The SLI system used in this research study is shown in Figure 1.1 and further geometrically detailed in Figure 1.2. Based upon the basic geometric principles behind SLI scanning, the system is able to utilize triangulation software to determine the volume, and therefore the weight, of feed in the bin.

Figure 1.1 – Complete imaging system.

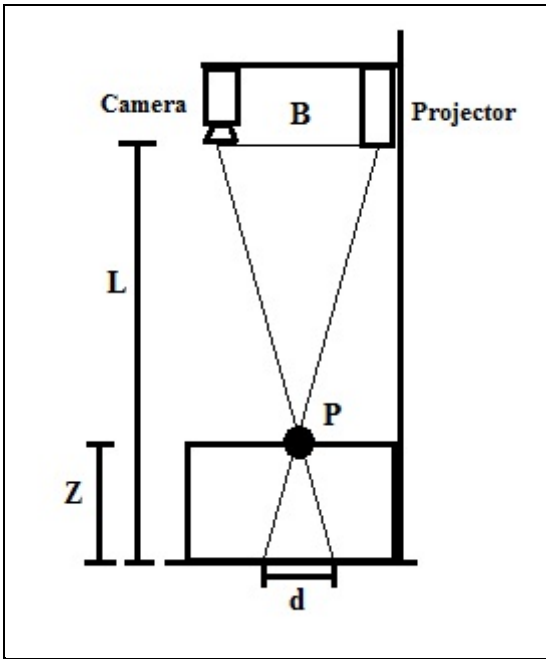

Figure 1.2 – System geometry.

The feed intake monitoring system measures feed intake by the change in volume between the 3D feed surfaces recording by our 3D imaging system before and after a cow has consumed their allotted individual daily feed. With the research proposed in this study, the hope was to learn whether such a system can accurately determine the volume and thus the weight of feed in a bin just based on the theory of SLI. The research was also conducted to determine if such a system can be adopted in a real-world dairy farm setting to monitor the amount of feed offered, consumed, and refused. This would include identifying what factors limit the capabilities of this technology as well as determining if such a system has the potential to be automated.

The future goal of the research conducted in this study is to have a feed intake monitoring system that is capable of accurately determining how much feed was delivered, how much was actually consumed, and to automatically record these values in a real-world dairy operation setting. As for now, the research focuses on just developing a system that is accurate with the benefits of automation to be added in a later version. As seen by previous research, the measurement estimation capability and accuracy is the most difficult obstacle and therefore is the main aim of this research.

RESULTS

There were several objectives of this research study. The first objective was to be able to collect and store control test images of feed bins at differing known weights. The second objective was to be able to collect and store images of dairy cow feed in feed bins before and after feeding. The next step was to be able to process images to output a correlated value, such as volume or weight. The final objective of this research study was to analyze the results to determine the effectiveness of 3D scanning for monitoring feed intake of dairy cow.

Lighting for this research study was assumed to remain consistent, which was accomplished by creating and placing the system inside of an enclosed box. Another assumption of this research study was that the end user will be proficient enough with computers to use the software and system involved. A final consideration was that the feed is laid out in a bin or a feeding structure similar in shape as to have consistent dimensions and unmoving so as to continuously remain in view of the camera, such as the feeding bins utilized in this research study.

One limitation of this experimental setup was that the lighting will change in an actual natural feeding environment. The ability of the end user to accommodate an Ethernet cable infrastructure for connection between the system and the computer is also a limitation in a real-world setting. The control test data collection will be from a small sample population of the herd, but this should be adequate to scale to larger populations without any loss of accuracy of the system as this works on an individual cow basis. In addition, the system used in this study was utilized in a controlled environment. Such a system would need more robust and resilient hardware to withstand the harsh conditions of a farming environment.

The results of this study initially showed a linear correlation between the volume of feed in the bin and the computed weight value of the feed in the bin. The image weight values are tested against known scale measured weight values of the same bin of feed in order to determine if this correlation does indeed exist and to determine if this system can accurately produce weight values for the bin of feed. Externalities were also discovered and discussed in order to determine their impact on the accuracy of the system. Ultimately, these externalities were deemed to impart large enough variances in

the image calculated weight when compared to the scale measured weight to invoke a second review of the relationship of the calculated image value to image weight value. Upon further review, it was determined that a single strictly linear relationship is not the optimal choice, but instead correlation with the position of the feed in the bin must as well be considered. Assuming a singular linear correlation of the image value resulted in overestimation or underestimation of the image weight value compared to the scale measured weight value. Statistical analysis using t-testing of the calibration data led to a discovery that some feed biasing was being underestimated or overestimated consistently. This results in proposing a solution of developing lookup tables (LUT) with their own distinct correlation based upon feed bias in the bin. In this manner, the error of the image weight value calculated is greatly reduced. This research study, therefore, concludes based upon the results that a machine vision SLI 3D imaging system can accurately estimate the weight value of feed.

The future of our system is to eliminate the bins and to operate in ambient light without the shroud in a natural feeding environment. The expense of using a near-IR light system that would work in such an environment is too high and is why we did not use it in this research study. Again, a future system would also be fully automated as opposed to the manual data collection conducted in this study. A future system would also incorporate other precision dairy farming technologies in order to enhance the benefits of monitoring dairy cow feed intake.

CHAPTER II: STRUCTURED LIGHT ILLUMINATION (SLI)

A structured light illumination (SLI) system is composed of a digital camera and projector arranged such that, for example, the camera is positioned above the projector such that the captured and projected images are column-wise aligned. In Figure 2-1, such a SLI system is depicted from the perspective of the YZ-plane such that the camera and projector lines of sight are in the direction of the negative Z-axis. In this chapter, we will refer to the projected image as $P[r, s]$ where r is the row coordinate of the projector's spatial light modulator and s is the column coordinate. The captured image will, likewise, be referred to as $C[m, n]$ where m is the image row coordinate and n is the column coordinate. For a VGA projector/camera pair, m and r are in the range $[1{,}480]$ and n and s are in the range $[1, 640]$.

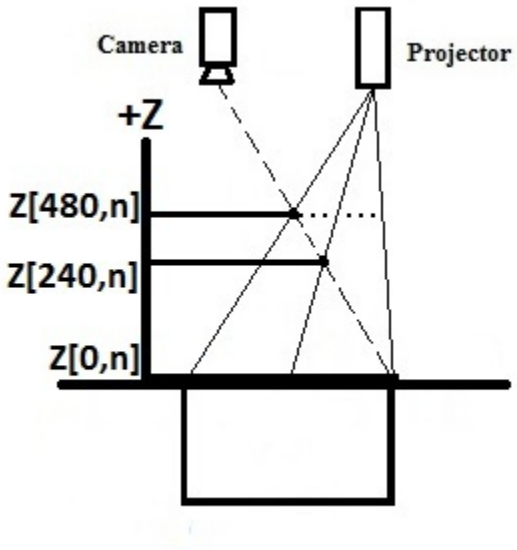

Figure 2.1 – SLI system side view representing row, phase, and gray-level values normal to the surface of the object being scanned.

In the illustration of Figure 2-1, a line of sight for a single pixel of the camera, noted $[m_0, n_0]$, is shown as the dotted line emanating from the camera lens and terminating on the $Z = 0$ plane. Also shown in Figure 2-1 are the lines of sight for three

pixels of the projector, $P[r = 1, s = n_0]$, $P[r = 240, s = n_0]$, and $P[r = 480, s = n_0]$, illustrated by solid lines emanating from the projector's lens and terminating on the $Z = 0$ axis. From the principles of epipolar rectification, i.e. the fact that the camera and projector images are aligned column-wise, we know that the three illustrated lines of sight from the projector intersect the illustrated line of sight of the camera pixel but at unique Z coordinates. For this reason, we can refer to the unique Z value as a function of the projector row coordinate such that $Z(r = 1)$, $Z(r = 240)$, and $Z(r = 480)$ represent the three possible points of intersection between the three projector lines of sight with the one camera line of sight.

The exact conversion of r to a Z value is then a function of the intrinsic and extrinsic parameters of the projector-camera pair derived through calibration [25], where intrinsic parameters characterize the physical properties of the sensor/spatial light modulator and the component lenses, while the extrinsic parameters characterize the position of the devices in world coordinate space. Specifically, Kai et al. [25] employ the equation:

$$z[m, n] = \frac{e[m,n] \cdot r + f[m,n]}{g[m,n] \cdot r + 1} \tag{2.1}$$

to map the projected image row r to a Z-value of the camera pixel $C[m, n]$ using the scalar values $e[m, n]$, $f[m, n]$, and $g[m, n]$. Since each pixel of the camera will have its own unique set of scalar values, e, f, and g, we indicate these parameters as functions of the camera pixel coordinates $[m, n]$.

In order to derive a specific X and Y coordinate for each pixel of the camera, we can use the principles of the pin-hole camera model, which is depicted in Figure 2-2.

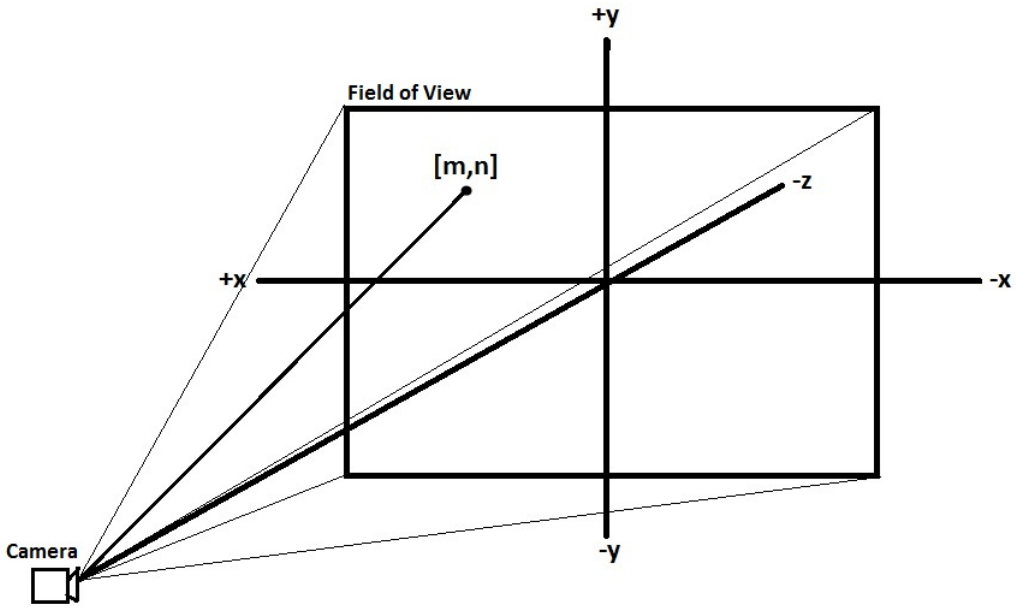

Figure 2.2 – Camera field of view shown with axial representation of camera pixel coordinates. A pixel [m,n] is shown in the field of view.

Here and with the camera looking down the negative Z axis, the lines of sight for each camera pixel can be written parametrically with X and Y being a linear function on Z such that:

$$x[m,n] = a[m,n] \cdot z[m,n] + b[m,n] \tag{2.2}$$

and:

$$y[m,n] = c[m,n] \cdot z[m,n] + d[m,n]. \tag{2.3}$$

Like e, f, and g, the parameters a, b, c, and d are scalar constants derived from calibration with each camera pixel having its own unique values such that a, b, c, and d are functions of the camera pixel row and column coordinates $[m,n]$.

So in order to derive a unique X, Y, and Z coordinate for each pixel of the camera, representing the 3D position of the target surface visible to the camera, the goal of a structured light illumination system is to determine the projector row coordinate, r, for the projected pattern, $P[r, s = n]$, as seen by the camera pixel, $C[m,n]$. For a very simple

means of deriving the particular projector row coordinate that a particular camera pixel sees, suppose that we set all the pixels of P to black, then $P[r,s] = 0$ for all r and s. We then capture a first image from the camera, which we label $C_1[m,n]$, such that:

$$C_1[m,n] = a \cdot f(x,y,z) + n_1[m,n], \tag{2.4}$$

where $f(x,y,z)$ is the amount of light reflected off the target surface whose position in 3D space is given by (x,y,z); a is the amount of ambient light incident upon the surface at (x,y,z); and $n_1[m,n]$ represents the noise component in the camera sensor.

Suppose now that we set all pixels of our projector to white, i.e. $P[r,s] = 1$ for all r and s, then the image captured by our camera, which we label $C_2[m,n]$, is given by:

$$C_2[m,n] = a \cdot f(x,y,z) + P[r,s] \cdot f(x,y,z) + n_2[m,n], \tag{2.5}$$

which reduces to:

$$C_2[m,n] = a \cdot f(x,y,z) + 1 \cdot f(x,y,z) + n_2[m,n], \tag{2.6}$$

where $n_2[m,n]$ is the noise component in the sensor for this second image and $P[r,s]$ is the light projected onto the target surface, at (x,y,z), coming from the projector pixel $[r,s]$. Since we are projecting solid white for all r and s, we can substitute in 1 for this term. Assuming $n_1[m,n]$ and $n_2[m,n]$ are small compared to a and $f(x,y,z)$, then we can now determine the value of $f(x,y,z)$ separate from the ambient light, a, according to:

$$f(x,y,z) = C_2[m,n] - C_1[m,n] \tag{2.7}$$

and we can derive a according to:

$$a = \frac{C_1[m,n]}{f(x,y,z)}. \tag{2.8}$$

If we were to now set $P[r,s]$ equal to $\frac{r}{480}$ such that the first row of the projected image is solid black, the 240th row is equal to gray-level 0.5, and the 480th row is equal to solid white, then the captured image, $C_3[m,n]$, is then described according to:

$$C_3[m,n] = a \cdot f(x,y,z) + \frac{r}{480} \cdot f(x,y,z) + n_3[m,n], \tag{2.9}$$

where we have replaced $P[r,s]$ in the equation with $\frac{r}{480}$. We can determine the value of $r \cdot f(x,y,z)$ separate from the ambient light, a, according to:

$$r = (C_3[m,n] - C_1[m,n]) \cdot f^{-1}(x,y,z) \cdot 480 \tag{2.10}$$

or, as a single step, we can define r according to:

$$r = \frac{C_3[m,n]-C_1[m,n]}{C_2[m,n]-C_1[m,n]} \cdot 480. \tag{2.11}$$

It is because of these results that the minimum number of projected/captured image pairs that can be used to accurately reconstruct a 3D scene is three.

If we now take into account the effects of sensor noise, then equation 2.11 can be re-written to produce a noisy estimate of r_n according to:

$$r_n = \left(\frac{C_3[m,n]-C_1[m,n]}{C_2[m,n]-C_1[m,n]} \cdot 480\right) + \sigma = r + \sigma, \tag{2.12}$$

where σ represents the accumulative effects of noise in C_1, C_2, and C_3. This uncertainty translates into an error in Z according to:

$$Z_n[m,n] = \frac{e[m,n]\cdot(r+\sigma)+f[m,n]}{g[m,n]\cdot(r+\sigma)+1} = \frac{e[m,n]\cdot r+e[m,n]\cdot\sigma+f[m,n]}{g[m,n]\cdot r+g[m,n]\cdot\sigma+1}. \tag{2.13}$$

Given our method of setting $P[r,s] = \frac{r}{480}$, it is clear that noise, having fixed variance, will be especially troublesome in areas where r approaches 0, depending on the values of e and g. In particular, large values of g mean that the noise term becomes the dominant term in the denominator. Exactly how much effect σ has on Z is therefore affected by the

patterns projected but also by the intrinsic and extrinsic parameters of the projector-camera pair such that, spreading the projector-camera pair further apart reduces the effects of noise.

Assuming that the projector-camera pair are fixed, another means of minimizing σ relative to the projected signal power is needed. For instance, replacing each captured image C_1, C_2, and C_3 with average images produced by taking multiple shots of each should, theoretically, reduce the variance of the noise in each image by a factor of N, the number of component images averaged together. Indeed, the more patterns used by a SLI system, the better accuracy that can be achieved. Based on the information from only one pattern, it is hard to achieve both high accuracy and reliability. Multi-pattern strategies are well known for their robustness to object color and measurement accuracy. Mostly, the multi-pattern strategies are based on temporal coding, where a set of patterns are successively projected onto the measuring surface. The depth information for a given pixel is usually formed by the sequence of illumination values for that pixel across the projected patterns. The bits of the depth information are multiplexed in time. This kind of pattern strategy can achieve high accuracy in measurement due to the fact that as multiple patterns are projected, the coded depth information basis tends to be small (usually binary) and, therefore, a small set of primitives is used, which are easily distinguishable among each other. Moreover, a coarse-to-fine paradigm is followed, where the position of a pixel is encoded more precisely as the patterns are successively projected.

Many of the multi-pattern techniques can be classified as: (i) techniques based on binary codes which projected sequences of binary patterns in order to generate binary

codewords (depth information), (ii) techniques based on n-ary codes which are a basis of n primitives used to generate the codewords (depth information), and (iii) phase shifting method (PSM) which involves projecting the same pattern, but shifting it in a certain direction in order to increase resolution. Among these multi-pattern approaches, PSMs achieve higher spatial resolution and accuracy as they project a periodic intensity pattern several times by shifting it in every projection.[26]

Typically, PSMs project a set of time-multiplexed patterns, $\{I_n: n = 0,1, \dots N - 1\}$, onto a target object such that an off-axis imaging sensor observes the scene and captures the wave patterns distorted by the surface topology under inspection. Generally, the patterns $\{I_n^c\}$ are designed as:

$$I_n^p(x^p, y^p) = A + B \cdot s(x^p, y^p), \tag{2.14}$$

where A is a temporal DC value and B is the amplitude (or projector modulation) value of a periodic signal function $s(x^p, y^p)$. The coordinates (x^p, y^p) are the corresponding coordinates in the projector. The captured images, $\{I_n^c: n = 0,1, \dots N - 1\}$, are then denoted as:

$$I_n^c(x^c, y^c) = \alpha(x^c, y^c) I_n^p(x^p, y^p) + \alpha(x^c, y^c)\beta(x^c, y^c), \tag{2.15}$$

where the superscript c indicates that I_n^c is now in the camera space and (x^c, y^c) are the two-dimensional camera coordinates. In Eq. (2.16), $\alpha(x^c, y^c)$ represents the albedo with $\alpha(x^c, y^c) \in [0,1]$ where 0 is pure black and 1 is pure white. The term $\alpha(x^c, y^c)\beta(x^c, y^c)$ represents the albedo image from ambient illumination with intensity $\beta(x^c, y^c)$.[25]

Through a decoding function and a phase unwrapping algorithm, the phase Φ that represents the coordinate of x^p or y^p, can be obtained from the "wrapped" (or coded) phase Φ, which is expressed as:

$$\Phi(x^c, y^c) = g\left[\frac{U(x^c,y^c)}{V(x^c,y^c)}\right], \tag{2.16}$$

where:

$$U(x^c, y^c) = \sum_{n=0}^{N-1} a_n I_n^c\,(x^c, y^c) \tag{2.17}$$

and:

$$V(x^c, y^c) = \sum_{n=0}^{N-1} b_n I_n^c\,(x^c, y^c). \tag{2.18}$$

The terms a_n and b_n are two coefficients in summations such that, in $U(x^c, y^c)$ and $V(x^c, y^c)$, the terms of $\beta(x^c, y^c)$ and the DC value, A, in images are canceled, while the division between the two summations cancels the terms of $\alpha(x^c, y^c)$. The term $g(\cdot)$ is a function that estimates the phase values, $\Phi(x^c, y^c) \in [0,2\pi)$, out of image intensity values. As we can see, the PSMs are trying to calculate the coding information. To do so, at least three patterns should be projected, since there are three unknown parameters, namely α, β, and Q.[26]

In summary, there are a variety of different light pattern strategies. Among these strategies, PSM, which projects a pattern several times by shifting it spatially in every projection, is typically used. In contrast to patterns based on binary code and n-array, PSM overcomes the discrete nature of patterns. In addition, because the pattern resolutions are exponentially increasing among the coarse-to-fine light projections and the fringe gap tends to 0, the resolution of PSM is greatly improved.[26]

Among the many proposed SLI methods, the technique of Phase Measuring Profilometry (PMP), which is a PSM method, is one of the most widely used and precise

strategies. The canonical PMP technique employs a set, $\{I_n: n = 0,1, \dots N-1\}$, of sinusoidal wave patterns such that at the point (x^p, y^p) in projector space, the intensity value is assigned as:

$$I_n^p(x^p, y^p) = A^p(x^p, y^p) + B^p(x^p, y^p)\cos(\Phi(y^p) - \tfrac{2\pi n}{N}), \tag{2.19}$$

where n represents the phase-shift index, N is the total number of phase shifts, A^p is the temporal DC value, which is normally 0.5, and B^p is the amplitude of the temporal AC signal, which is also normally 0.5. Thus, the sinusoidal signal covers the entire dynamic range of the projector [0,1]. The term $\Phi(y^p)$ is the phase information and is designed according to:

$$\Phi(y^p) = \cos(2\pi f y^p) = \tfrac{2\pi F y^p}{H}, \tag{2.20}$$

where H is the pattern height (number of points in pattern), H is the number of periods, and f is the frequency of the sine wave. Note the dependence of the phase term, $\Phi(y^p)$, on y^p as this is the parameter that will be used when triangulating with the camera, which is assumed to be positioned vertically above/below the projector. Thus, we denote $I_n(x^p, y^p)$ as $I_n(y^p)$.[25,26]

After projecting the patterns, the reflection process can be expressed as:

$$I_n^c(x^c, y^c) = A^c(x^c, y^c) + B^c(x^c, y^c)\cos\left(\Phi(x^c, y^c) - \tfrac{2\pi n}{N}\right) \tag{2.21}$$

$$I_n^c(x^c, y^c) = \alpha(x^c, y^c)\left[A + B\cos\left(\Phi(y^p) - \tfrac{2\pi n}{N}\right) + \beta(x^c, y^c)\right], \tag{2.22}$$

where (x^c, y^c) is the two-dimensional camera coordinate, $\alpha(x^p, y^p)$ represents the albedo within [0,1] where 0 is pure black and 1 is pure white and $\alpha(x^c, y^c)\beta(x^c, y^c)$ is the albedo image from ambient illumination with intensity $\beta(x^c, y^c)$. $I_n^c(x^c, y^c)$ is the

intensity of that pixel. The A^c term is the average pixel intensity across the pattern set, derived by Liu as:

$$A^c = \frac{1}{N}\sum_{n=0}^{N-1} I_n^c, \tag{2.23}$$

where the image A^c is equal to an intensity or texture photograph of the scene.[25,26] The B^c term is the intensity modulation of a given pixel and is derived from I_n^c by Liu as:

$$B^c = \frac{2}{N}\left\{\left[\sum_{n=0}^{N-1} I_n^c \sin\left(\frac{2\pi n}{N}\right)\right]^2 + \left[\sum_{n=0}^{N-1} I_n^c \cos\left(\frac{2\pi n}{N}\right)\right]^2\right\}^{0.5}, \tag{2.24}$$

such that B^c can be thought of as the amplitude of the sinusoid reflecting off of a point on the target surface.[25,26] According to Liu, if I_n^c is constant or less affected by the projected sinusoid patterns, B^c will be close to zero and, therefore, B^c is employed as a shadow noise detector filter such that the shadow-noised regions, with small B^c values, are discarded from further processing.[25,26] A^c looks similar to a standard video frame image absent any indication of the projected pattern sequence I_n^p.[25,26] In contrast, B^c looks very similar to A^c except that it only shows the texture in those areas of the scene that significantly reflect the projected sequence I_n^p. B^c has great significance as an indicator of projected signal strength, as the binarized image shows only those pixels greater in magnitude to a user defined threshold. It is these pixels that will ultimately be used to reconstruct a three-dimensional surface with ignored pixels being considered too noisy as to relay any reliable depth information.[25,26]

The albedo and ambient illumination effects are added into the patterns and therefore the phase information $\Phi(y^p)$ can then be obtained from a decoding function. Phase unwrapping is the process that converts the wrapped phase to the absolute phase. The phase information can be retrieved from the intensities of the fringe patterns. Of the

reliable pixels with sufficiently large B^c, Φ represents the phase value of the captured sinusoid pattern derived as:

$$\Phi(x^c, y^c) = \tan^{-1}\left[\frac{\sum_{n=0}^{N-1} I_n^c(x^c, y^c)\sin\left(\frac{2\pi n}{N}\right)}{\sum_{n=0}^{N-1} I_n^c(x^c, y^c)\cos\left(\frac{2\pi n}{N}\right)}\right] \tag{2.25}$$

$$\Phi(x^c, y^c) = \tan^{-1}\left[\frac{\alpha(x^c, y^c)B\sin(\Phi(y^p))}{\alpha(x^c, y^c)B\cos(\Phi(y^p))}\right]. \tag{2.26}$$

The decoding function removes the effects of albedo and ambient illumination such that the designed phase information is recovered. Generally, if a high frequency signal is employed, the obtained phase Φ needs to be further "unwrapped" into unit frequency Φ in order to find the unique correspondence over the full resolution. Once $\Phi(x^c, y^c)$ is obtained, the 3D world coordinates of a point can be calculated from $(x^c, y^c, \Phi(x^c, y^c))$ in a pre-calibrated system. To resolve the image into world coordinates and to determine depth information, at least 3 patterns should be projected and captured since $\Phi(y^p)$, $\alpha(x^c, y^c)$, and $\beta(x^c, y^c)$ are unknowns. As the most widely used pattern strategy, PMP is easy to implement and well developed for $N > 3$ patterns.[25,26]

Shown in Figure 2.3 are the eight sequential scans for the low frequency pattern projected. Similarly, the mid frequency and high frequency patterns also have eight sequential patterns, resulting in a total of twenty-four pattern projections. Shown in Figure 2.4 are the resultant output images for the individual scan. The first three images show a single pattern of the twenty-four, respectively, low, mid, and high frequency patterns projected. Also shown are the resulting A^c and B^c components of the scan and the final phase image of the scan. It is this final phase unwrapped image of the bin of feed from the SLI system that we utilize to determine the image value and, therefore, the bin feed weight.

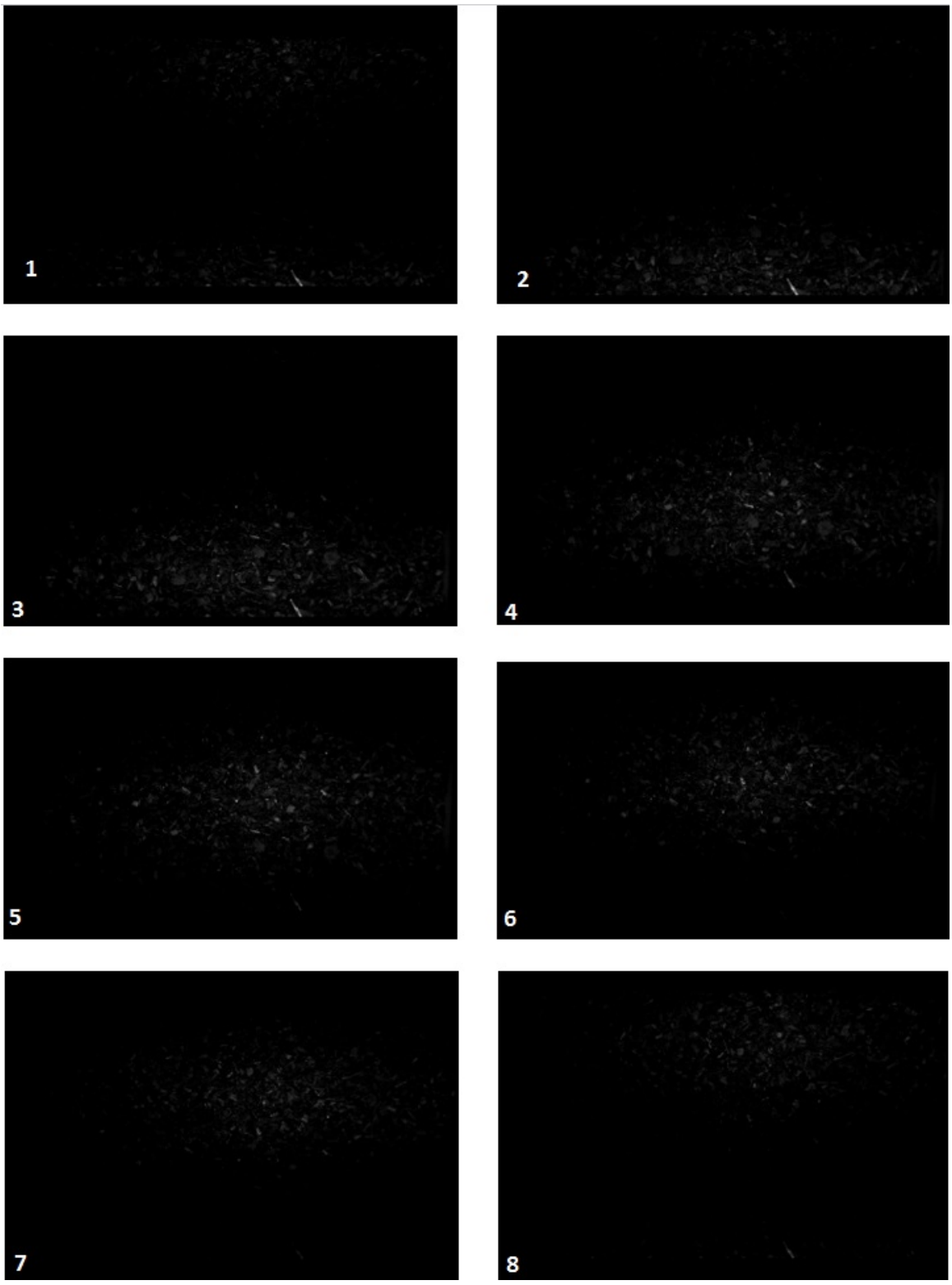

Figure 2.3 – The 8 sequential scans shown in order for the low frequency pattern.

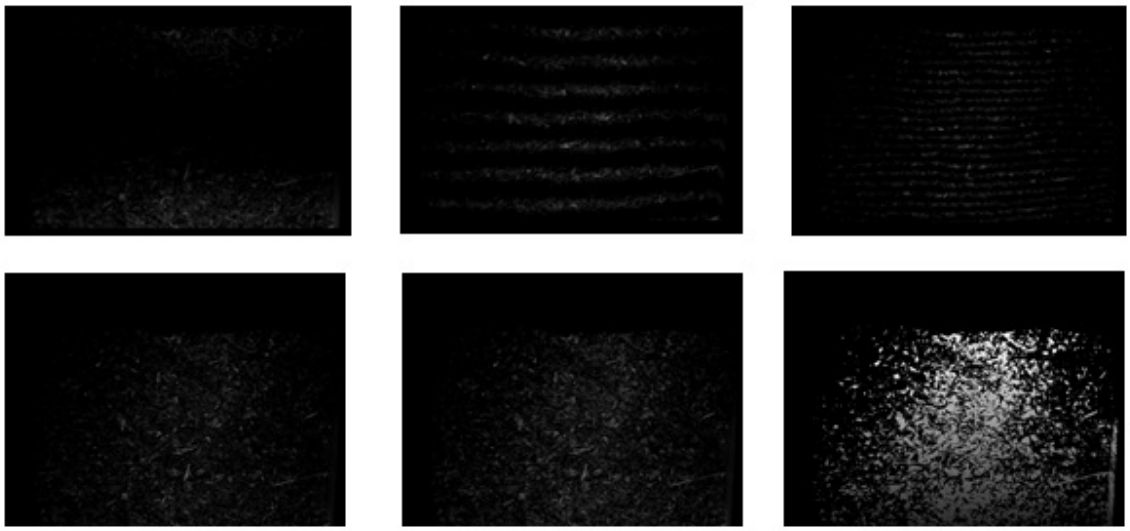

Figure 2.4 – Low frequency (top left), mid frequency (top center), and high frequency (top right) patterns used for scans. Resulting DC or real component, A^c (bottom left), modulation or imaginary component, B^c (bottom center), and resultant absolute phase image (bottom right) for a 50lb. bin of feed.

CHAPTER III: METHODOLOGY

The majority of current feed intake monitoring systems are based upon monitoring only the amount of feed output for the cow to eat. They do not also take into consideration the amount of feed wasted or otherwise uneaten by the individual cow. The disparity between the amount of feed given and the amount consumed can lead to over-estimating or under-estimating the amount of feed consumed. This can lead to health problems going unnoticed far longer than needed which can turn a small health risk into a much larger problem by the time it is detected. In addition, with the ever increasing costs associated with feeding cows, producers cannot afford to waste feed. This continuous over-feeding of cows only leads to a loss of profitability of the dairy farm operation as the feed goes to waste rather than being utilized by the cow for milk production. As well, under-feeding leads to diminished returns from the cow when it comes to milk production. Cows can also be malnourished or become thin as the individual cow will use her energy stores for some time before milk production is limited. The more accurately the feed intake of the individual cow can be monitored, the more productive and economically viable the farming operation will be.

There were several objectives of this research study. The first objective was to be able to collect and store control test images of feed bins at differing known weights. The second objective was to be able to collect and store images of dairy cow feed in feed bins before and after feeding. The next step was to be able to process images to output a correlated value, such as volume or weight. The final objective of this research study was to analyze the results to determine the effectiveness of 3D scanning for monitoring feed intake of dairy cow.

The cows utilized in this research were only fresh cows. This means that they had recently given birth to a calf. These cows were placed in the research barn in the feeding stalls, shown in Figure 3.1. Each cow was isolated in their own individual feeding stall, as shown in Figures 3.2 and 3.3. This restricted cows to only eating from their feed allotment and not from other cow's feed allotment. The cows were fed at 1pm every day and milked at 4:30am and 3:30pm every day. Each cow received two bins of feed to eat that would suffice between feedings. In most cases, each bin was filled with 50 pounds of feed, which gave each cow access to 100 pounds of feed. Some bins were filled with 45, 55, or 60 pounds of feed resulting in a total feed amount of 90, 110, or 120 pounds of feed. The amount of feed allotted was determined by farm management on a per cow basis. The feed was weighed using the scales shown in Figure 3.4 and then scanned. The scales had to be set to zero with the empty bin weight of approximately 7.5 pounds as the 0 pound weight since every empty bin was of the same type and, therefore, of the same empty weight. In this manner, only the weight of the feed was weighed and not including the weight of the bin itself.

The first bin was placed in the bottom of the feeding stall, as shown in Figures 3.5 and 3.6, for the cow to eat. At the end of the working day, typically 6 or 7pm, the feed in the bin would be checked to see how much had been consumed. If the bin was completely or moderately empty, then the first bin of feed was switched out with the second bin and any leftover feed from the first bin was poured in on top of this second bin in the bottom of the feeding stall, as can be seen in Figure 3.7. The bins were collected at 1pm the following day and weighed again to determine how much feed was

leftover and then scanned. The old feed was disposed of and new feed was placed in the bins, restarting the process.

Figure 3.1 – Feeding stalls in the research barn.

Figure 3.2 – Individual stall interior (cow side) view.

Figure 3.3 – Individual research stall with a research cow.

Figure 3.4 – Scales used to measure feed weight with a 50lb. bin of feed.

Figure 3.5 – Exterior (feeding) side view of an individual feeding stall.

Figure 3.6 – Feeding bin from exterior (feeding) side view.

Figure 3.7 – Feeding bins placement.

Once the controlled feeding process was determined, the research study was then able to determine the process for scanning the feed to produce an image weight value that corresponds to a scale weight value of the exact same bin of feed. The first step was to build and calibrate the SLI system scanner. This involved determining what hardware to select for the system and how best implement such a system. The hardware selected for this SLI scanning system included a Prosilica GC640 camera, a DLP projector, and a Toshiba Satellite C655 laptop computer. The camera and projector were installed onto an 80-20 aluminum frame as shown in Figure 3.8 and calibrated beforehand at the distance of the camera and projector to the floor, in this case a distance of approximately 54.5 inches from the camera to the floor and approximately 53 inches from the projector to the floor.

Figure 3.8 – Feed intake system. (Top left) Scanning system camera (top) and projector (bottom) shown and (top right) system mounted on scanning frame. (Bottom left) side view and (bottom right) top view of SLI scanning system.

In order to control the lighting and the environmental conditions, a sturdy container was constructed for which to place the system since ambient lighting can drastically affect the performance of the SLI scanner. If the ambient light is too high, the camera image becomes oversaturated with light. Likewise, if the lighting, in this case active lighting from the DLP projector, is too low, then the camera image cannot collect

an adequate amount of pixel data to accurately reconstruct the scene. So, a PVC frame was constructed as shown in Figure 3.9 with strengthening supports on the sides and the top. The front was left open for entrance in and out of the box. The entire structure was then covered with thick, black plastic as shown in Figure 3.10 to block exterior lighting, thus giving complete control of the lighting to the projector and a consistent lighting source that would not require adjustment of the camera iris for differing lighting conditions. Power and computer connection chords were fed through corners of the box as can be seen in Figure 3.10. Once placed in its final destination, a wooden frame was bolted to the floor as can be seen in Figures 3.11 and 3.12 that would ensure that the feed bin was in exactly the same location for every scan as well as centered in the field of view of the camera. The completed imaging system is shown in Figure 3.13 with the imaging system inside of the control container and a feed bin in place for a scan.

Figure 3.9 – (Top left) rear side view, (top right) front view, and (bottom) front inside view of the PVC frame.

Figure 3.10 – (Top left) side view, (top right) front view, and (bottom) front inside view of the system shroud enclosure.

Figure 3.11 – Wooden frame that the bin sits inside of during the scanning process.

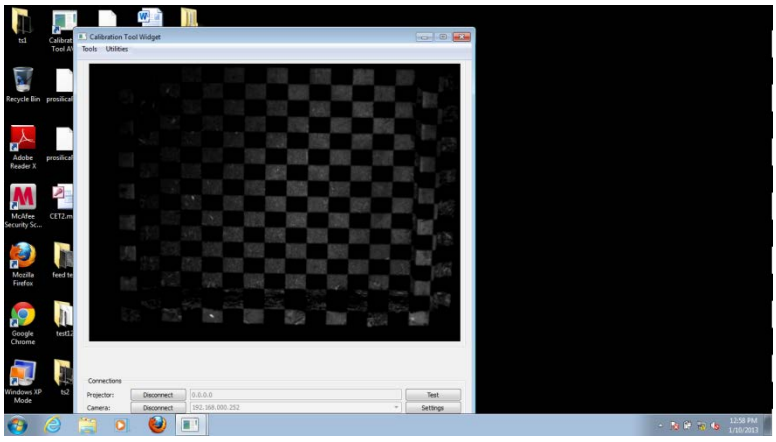

Figure 3.12 – Field of view for the camera with the positioning frame shown in place.

Figure 3.13 – Complete imaging system (front inside view).

Having placed a feed bin inside the scanning frame, our scan software proceeded by projecting a series of sinusoidal gratings, each projected frame recording to memory using the GC640 camera. These captured images were then processed as described in Chapter 2, to produce a 2D matrix of size 640x480 where each pixel in the matrix is represented by the 4D vector (x, y, z, t) where x, y, and z represent the 3D surface point of the feed while t is a measure of texture. Given that the frame holding the scanner also included a guide for the feed bin, we know that the outer-most boundary pixels of the matrix correspond to the plastic bin, and hence, we cropped out a center section of the matrix for analysis. Of these center pixels, many of the values were undefined since the amount of light reflected from the projector to the camera is below the noise floor of the sensor; therefore, given a sparse matrix of feed surface values, we needed a process that estimated the volume of feed based upon an average 3D scan. This process involved the steps of: (i) generating a Voronoi mesh [27,28,29,30] from the defined values, (ii) calculating the volume of each triangle in the mesh relative to a scan of an empty bin, and (iii) generating a weighted average volume based upon the total area covered by all triangles in the mesh. This final average volume of step (iii) became the estimate of feed volume that we compare to the scale measured weight of feed.

Shown in Figure 3.14 is the process of converting a recorded scan into a Voronoi mesh used by our software for estimating feed volume by means of Delaunay triangulation.[27,28,29,30] Figures 3.15 to 3.22 illustrate (top left) raw scan data produced by means of the SLI and (top right) the 3D interpolated surface produced by means of Voronoi tessellation. Again, the Z-axis is the view down onto the bin which was the same position as the initial phase image (top right), the negative Y-axis is the

view from the back (long) side of the bin (bottom left), and the positive *X*-axis is the view from the right (short) side of the bin (bottom right).

```
fid=fopen('11_7_list.txt','r');
fod=fopen('results.csv','w');

M=[];
maskList=find(mask==0);
while (1)
    fileString=fgetl(fid)
    if ~ischar(fileString), break, end

    P=imread(fileString);
    P=double(P)/(2^16-1);
    P=P*2*pi;
    P(find(P==0))=nan;
    P(maskList)=nan;

    zp=(E.*P+F)./(G.*P+1);
    xp=A.*zp+B;
    yp=C.*zp+D;

    l=find(~isnan(xp));

    if (~isempty(l))
        tri=delaunay(xp(l),yp(l));
        if (size(tri,1)>0)
            [a,v]=triArea(tri,xp(l),yp(l),zp(l));
            averVol=sum(v)./sum(a);
            subplot(2,2,1);imshow(fileString);xlabel('x');ylabel('y');
            subplot(2,2,2);plot(xp,yp);xlabel('xp');ylabel('yp');
            subplot(2,2,3);plot(xp,zp);xlabel('xp');ylabel('zp');
            subplot(2,2,4);plot(yp,zp);xlabel('yp');ylabel('zp');
            ha = axes('Position',[0 0 1 1],'Xlim',[0 1],'Ylim',[0
1],'Box','off','Visible','off','Units','normalized', 'clipping' ,
'off');
            text(0.5,
1,sprintf('%s',fileString),'HorizontalAlignment','center','VerticalAlig
nment', 'top');
            file_name = fileString;
            s = regexprep(file_name, '\', '_');
            path = 'C:\Users\dllau\Desktop\SCANS\images\11_7\';
            saveas(gcf, [path, s], 'tif');

            M=[M; averVol];
            fprintf(fod, '%s, %f\n', fileString, averVol);
        end;
    end;
end;
fclose(fid);
fclose(fod);
```

Figure 3.14 – Software used to create visualization images.

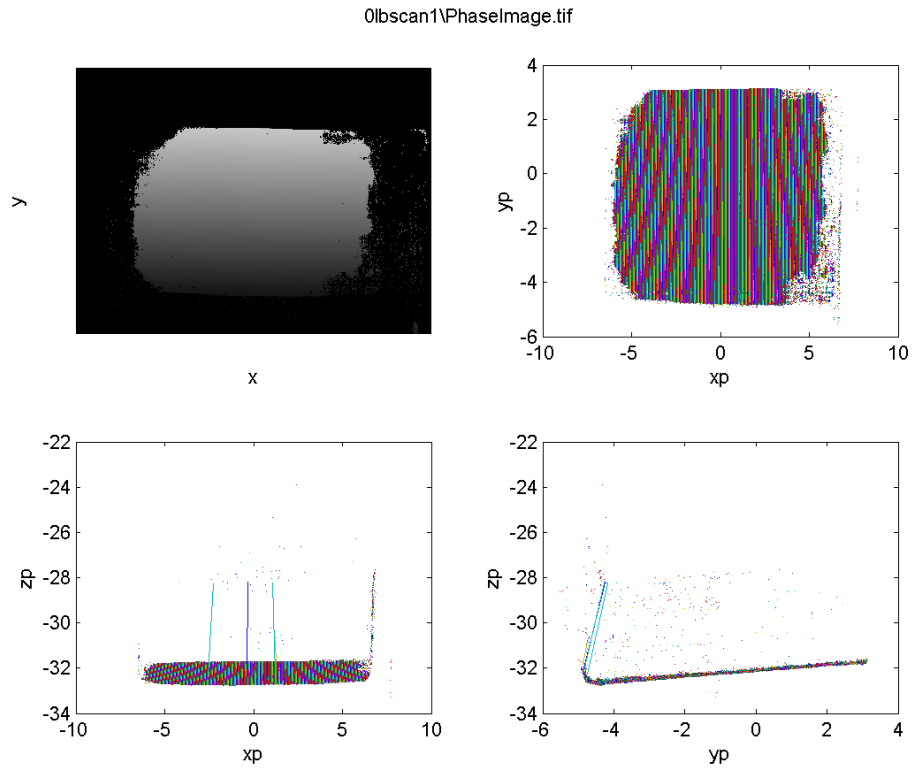

Figure 3.15 – 0lb. scan of an empty feed bin.

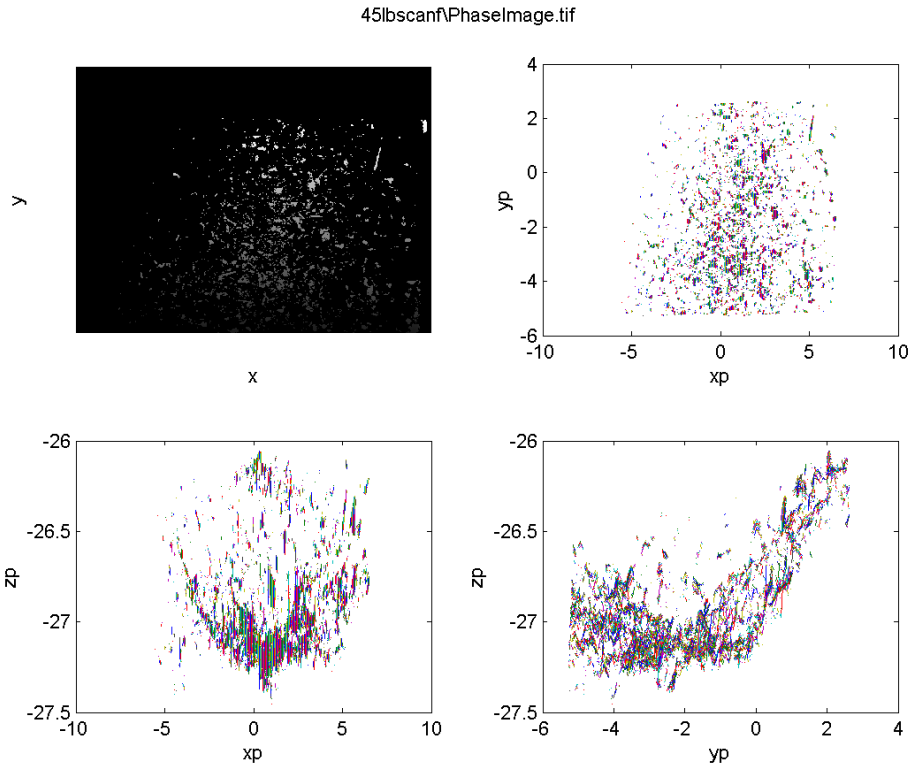

Figure 3.16 – 45lb. scan that is "flat (F)."

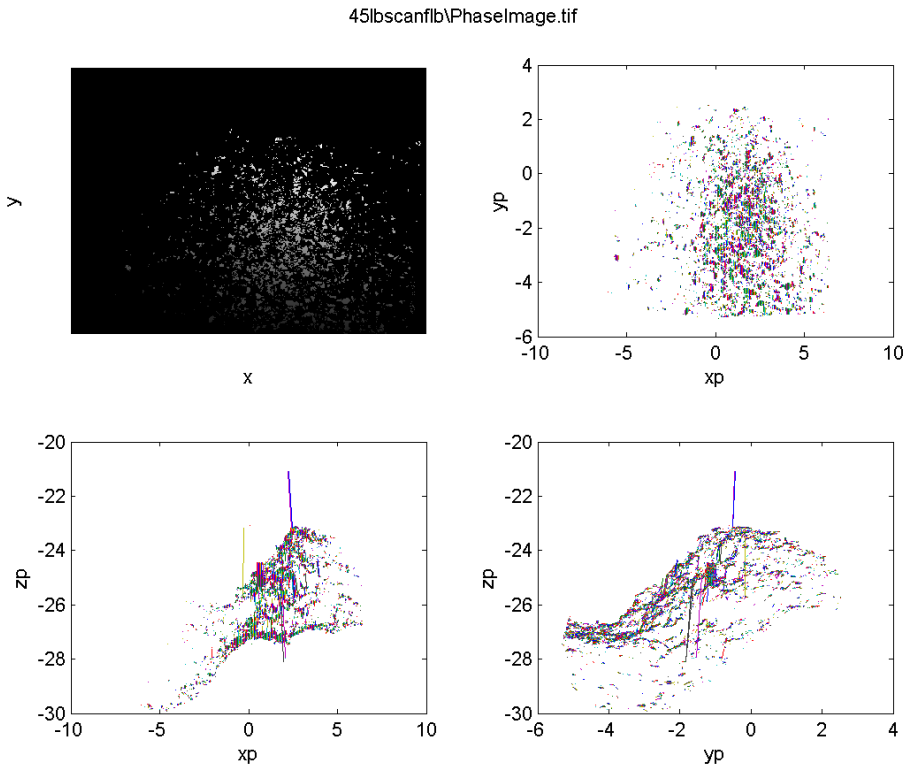

Figure 3.17 – 45lb. scan that is "front left biased (FLB)."

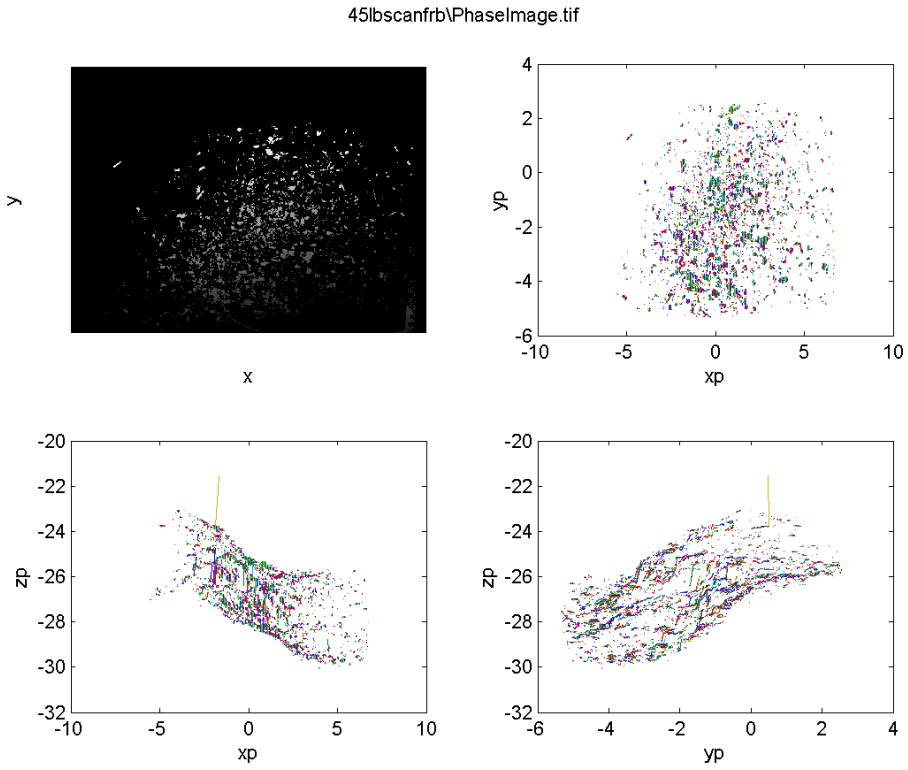

Figure 3.18 – 45lb. scan that is "front right biased (FRB)."

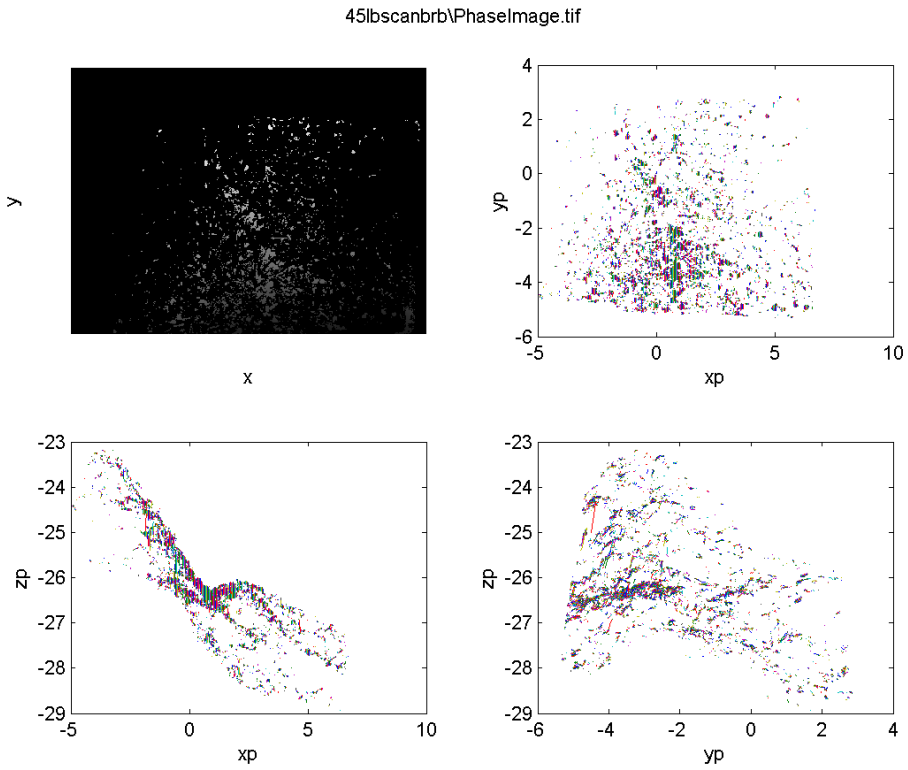

Figure 3.19 – 45lb. scan that is "back right biased (BRB)."

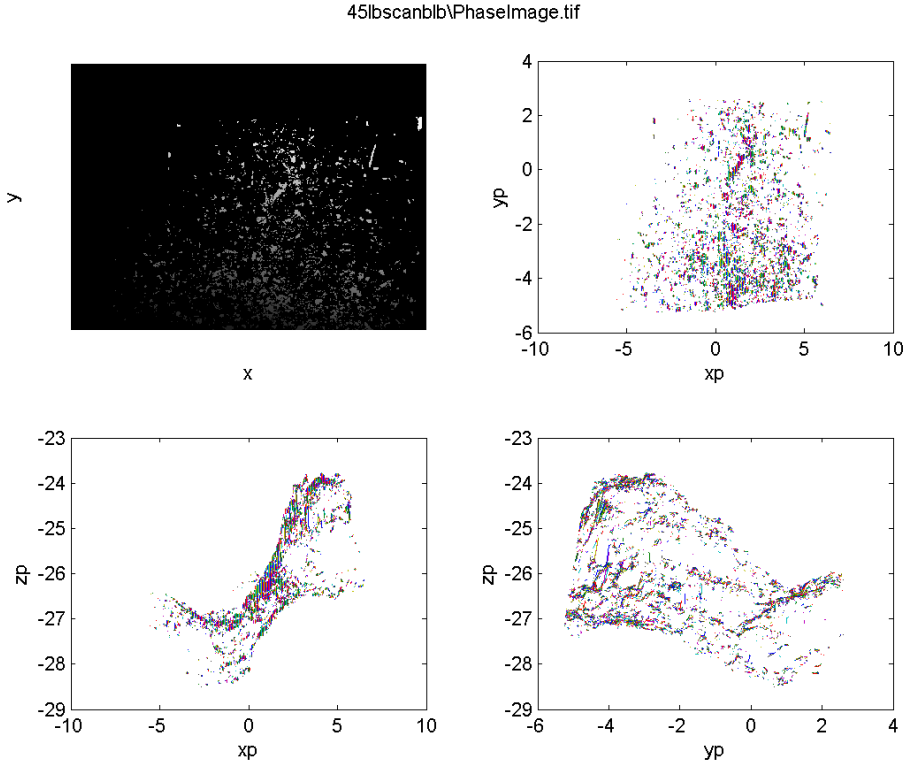

Figure 3.20 – 45lb. scan that is "back left biased (BLB)."

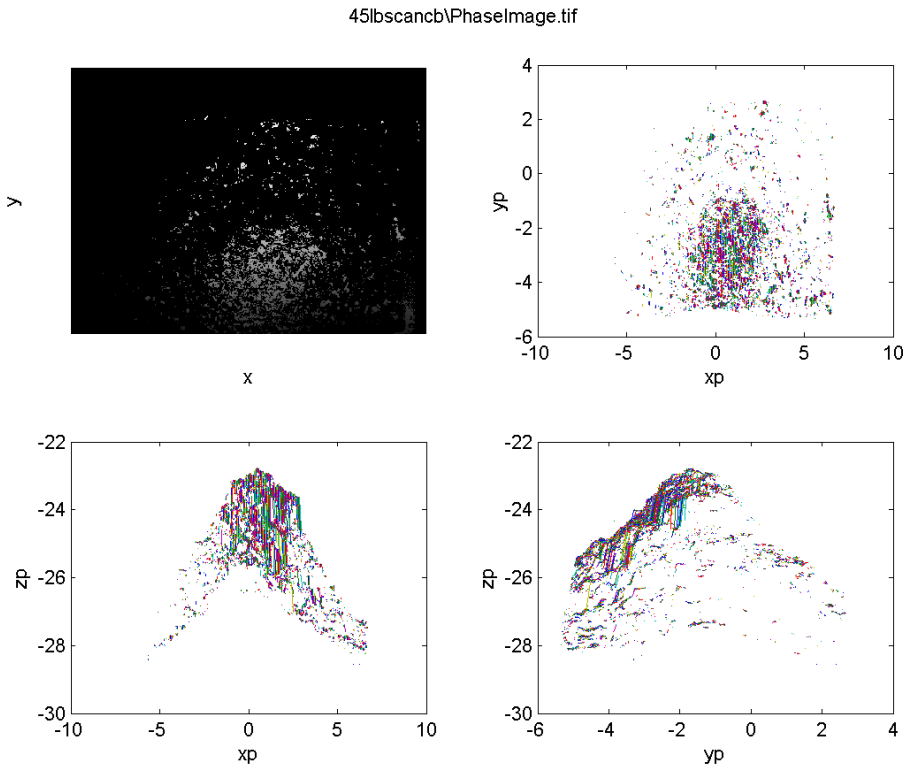

Figure 3.21 – 45lb. scan that is "center biased (CB)."

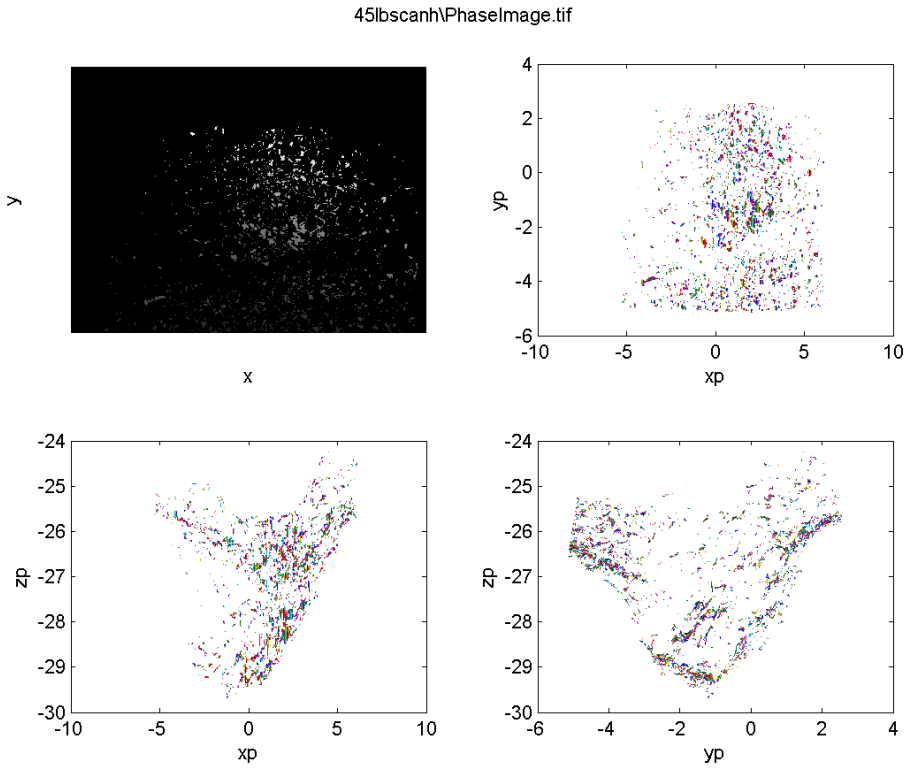

Figure 3.22 – 45lb. scan with a "hole (H)."

From the scan data produced by our software, the research study was then able to proceed in correlating this volumetric calibration scan data to weight information. The scale weight value was already known and was the standard against which to test the SLI scan data. The SLI system only scans the contour of the feed, which represents the outer dimension of the feed shape in the bin. Since the shape and contour data for all 5 pound intervals of feed in the bin are known, the volumetric relationship of these 5 pound intervals could be determined. Once the correlation between feed volume and image data was identified and determined, the process could move forward to determining an output value for the bin of feed that would represent the weight of the bin.

To derive a single value of feed weight based upon the volume estimated produced by our scanner, a linear mapping of volume to weight was determined be means of linear regression. This correlation was further tested using statistical analysis to determine if a linear correlation was the best representation for the data and to determine the error of this correlation choice. The results of this step of the process are the proceedings of Chapter 4. The end result is to have a calibrated system that can produce an image weight value that closely corresponds to a scale weight value of the exact same bin of feed. Once the system was calibrated with known weight values, it was then tested in a controlled setting with test cows. The results and proceedings of this step of the research study are Chapter 5, along with the conclusions of the abilities and accuracy of the SLI scanning system of this research study and future recommendations.

The third step of the research study was the collection of calibration scans of known weight values of feed in a bin. The calibration test scans consisted of two different types of test scans. The first type of scan was output feed scans and the second

type was weighback feed scans. The purpose for the output feed scans was to determine the accuracy and precision of the system at known scale measured weight values. The known scale measured weight of each bin of feed was compared to the weight measurement produced by the imaging system for the scan data of the same bin of feed. The purpose for the weighback feed scans was, likewise, to determine the accuracy and precision of the system at known scale measured weight values. In addition, the weighback scans were important for determining whether or not feeding or eating produced any major changes in the scans. Factors such as moisture added from the cow's mouth, tossing of the feed in the bin, feeding habits, and drying of the feed over time were considered.

A bin of feed was then scanned at intervals of 5 pounds from 0 pounds up to 50 or 60 pounds. The upper limit of 60 pounds for test scanning was used since farm management only fed the cows 100 to 120 pounds of feed per day (50 to 60 pounds per bin of feed), also because this is the limit of feed that that bin will hold without spilling over the sides and this is the limit of feed that the bin can hold and still fit under the feeding stall without pushing feed over the edges as it is slid into place. The resulting initial scans at an iris setting were deemed too dark, and therefore the camera iris was opened further to allow more light. The data and camera settings would have sufficed for accuracy, but better precision was desired. The camera iris change was the only change made to the system and took place during the initial calibration test scans. The second camera iris setting proved to be the optimal choice. It was not too much light to saturate the image while having enough light to produce accurate contour scans of the feed in the bin.

For the output feed calibration scans of each 5 pound increment level, there were multiple scans conducted. The feed was scanned in several positions: flat scan (F), center bias (CB), "hole" scan (H), back left corner bias (BLB), back right corner bias (BRB), front left corner bias (FLB), and front right corner bias (FRB). The scans were saved with titles that corresponded to the biasing of the feed in the bin. Figure 3.23 shows a guideline phase image with all of the biasing title acronyms and the biasing locations outlined on the figure. The flat scans are not shown in Figure 3.23 since there is no bias in the feed bin. The "hole" scan was a result of pushing the feed to the corners of the bin and leaving a void in the middle. Feed biasing was the act of placing the feed in one particular spot in the bin to favor that area with more feed than any other location in the bin. The biasing of the feed in the bin in different corners and positions was conducted in order to determine if this had any dramatic effect on the accuracy of the scans and ultimately the scan calculated image weight value for the feed in the bin. Examples of the biasing of the feed in the bin can be seen in Figure 3.24.

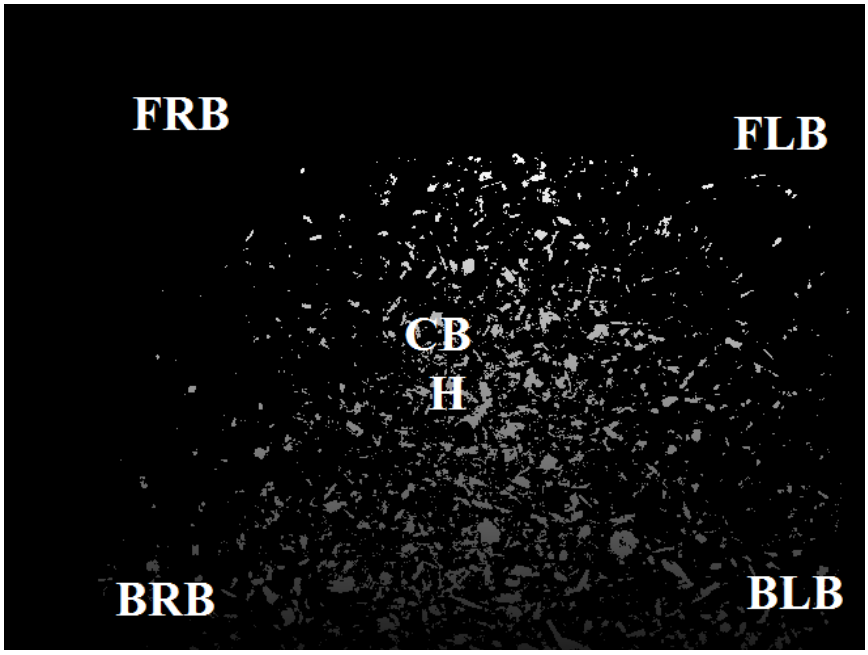

Figure 3.23 – Phase image with biasing acronyms and the biasing locations shown.

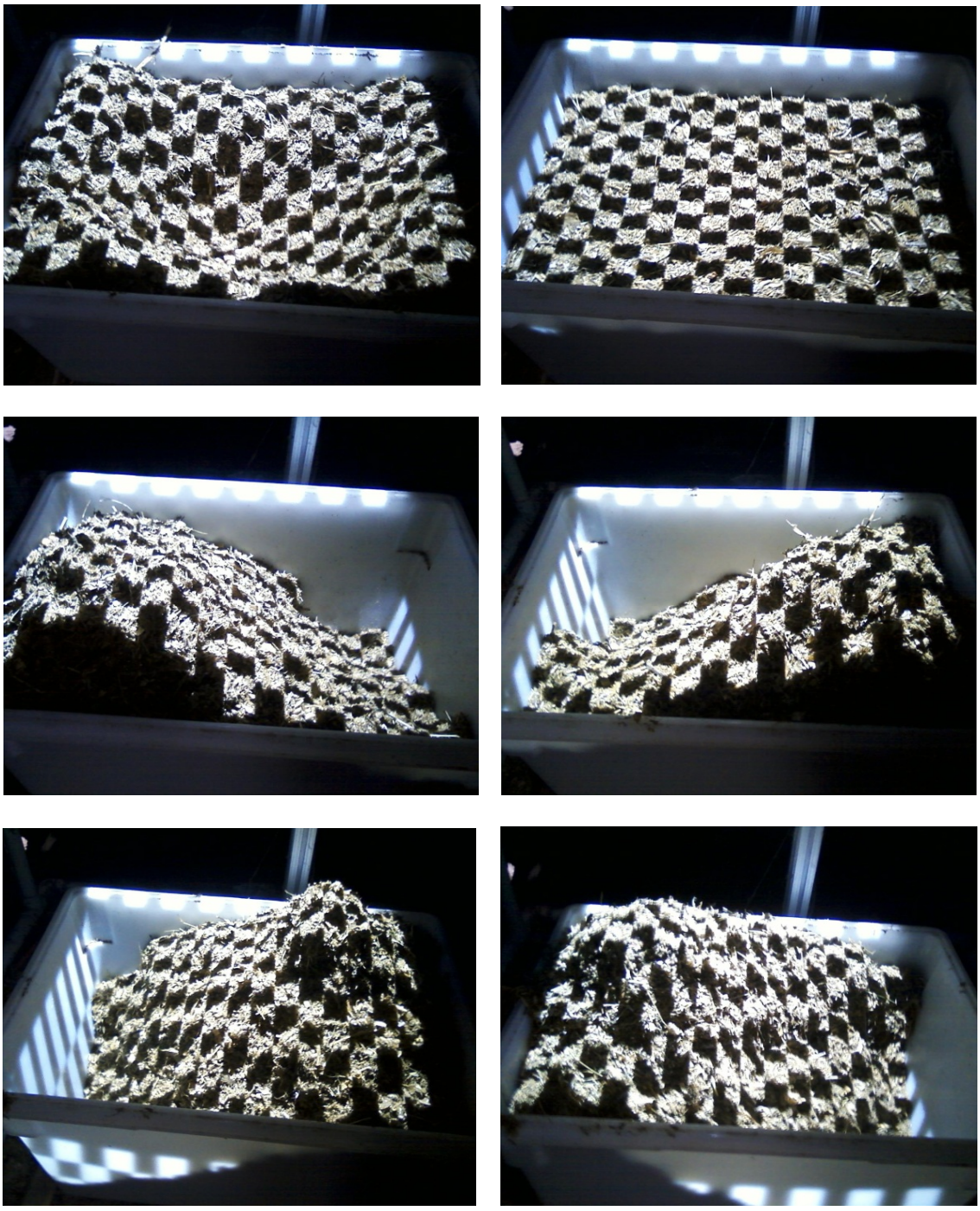

Figure 3.24 – Biasing positions - (top left) hole (H), (top right) flat (F), (center left) front left biased (FLB), (center right) front right biased (FRB), (bottom left) back right biased (BRB), and (bottom right) back left biased (BLB).

A single set of weighback calibration test scans were the final calibration test scans conducted. The purpose of these scans was to determine if any external factors influenced a difference in the feed weights or scans. Some of these factors were environmental, such as change in moisture content due to time the feed was left uncovered and allowed to accumulate or evaporate moisture with the air and surrounding environment. Yet other factors were directly related to the cow, such as feed moisture content added by the cow (i.e. from the cow's mouth via drinking water and saliva) or feed tossing and other feeding habits of the individual cow. The calibration test weighback scans were conducted in exactly the same manner as the calibration test output feed scans. The same scanning procedure used for output feed scans was used for the calibration test weighback scans which concluded with similar scan data.

The next and final step in collecting scan data was to scan control samples of output feed and weighback. These scans were the evaluation of the culmination of effort in this research study to test the accuracy and precision of the resulting feed image weight value software and of the entire imaging system in a controlled testing scenario. This required scanning the feed as it was put out for feeding and then scanning again the next day before refilling the bin with new feed. Only one scan per feed bin was needed as the calibration test scans were used to develop the baseline correlation needed for quantitative analysis. The feed was scanned "as-is," without any biasing or otherwise modification of the feed in the bin.

CHAPTER IV: FINDINGS AND ANALYSIS

The next step in the research process was to analyze the calibration test data to develop a process that would produce a weight value for each phase image or scan. The calibration test datasets resulted in the plots shown in Figures 4.1 to 4.4. The larger dataset is that of the individual scans and the smaller dataset is the average value for each 5 pound increment level tested.

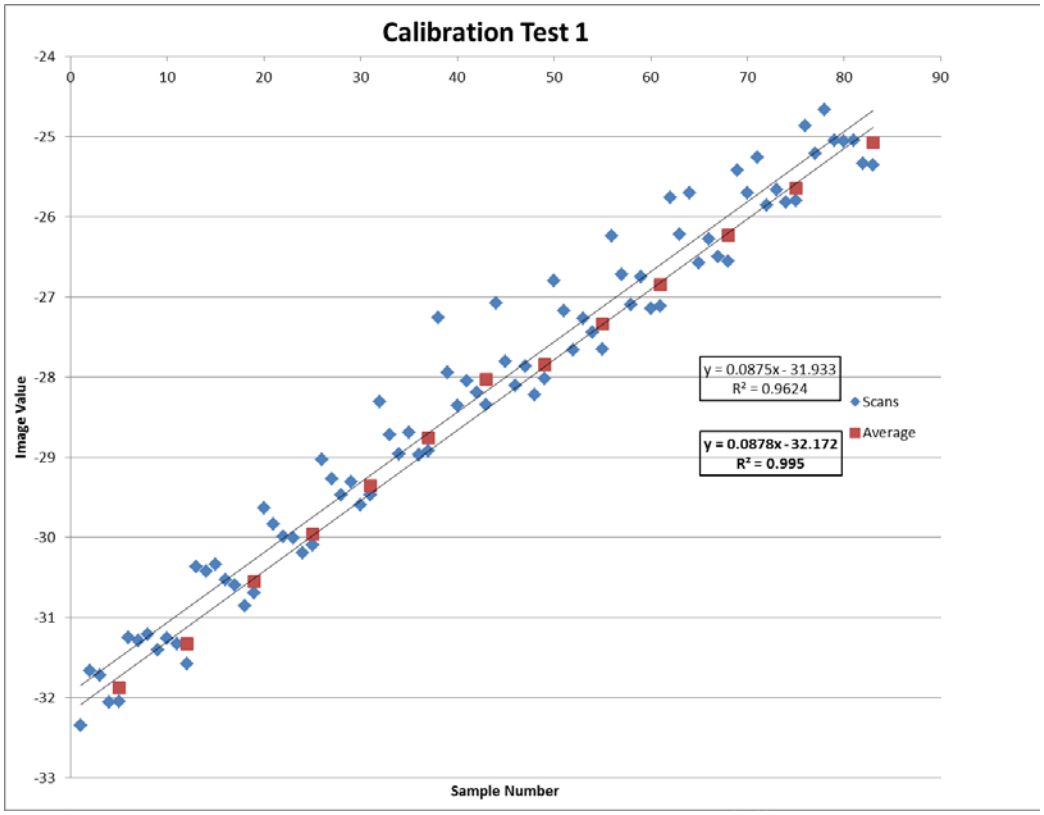

Figure 4.1 – Calibration test results conducted on 10/26/12.

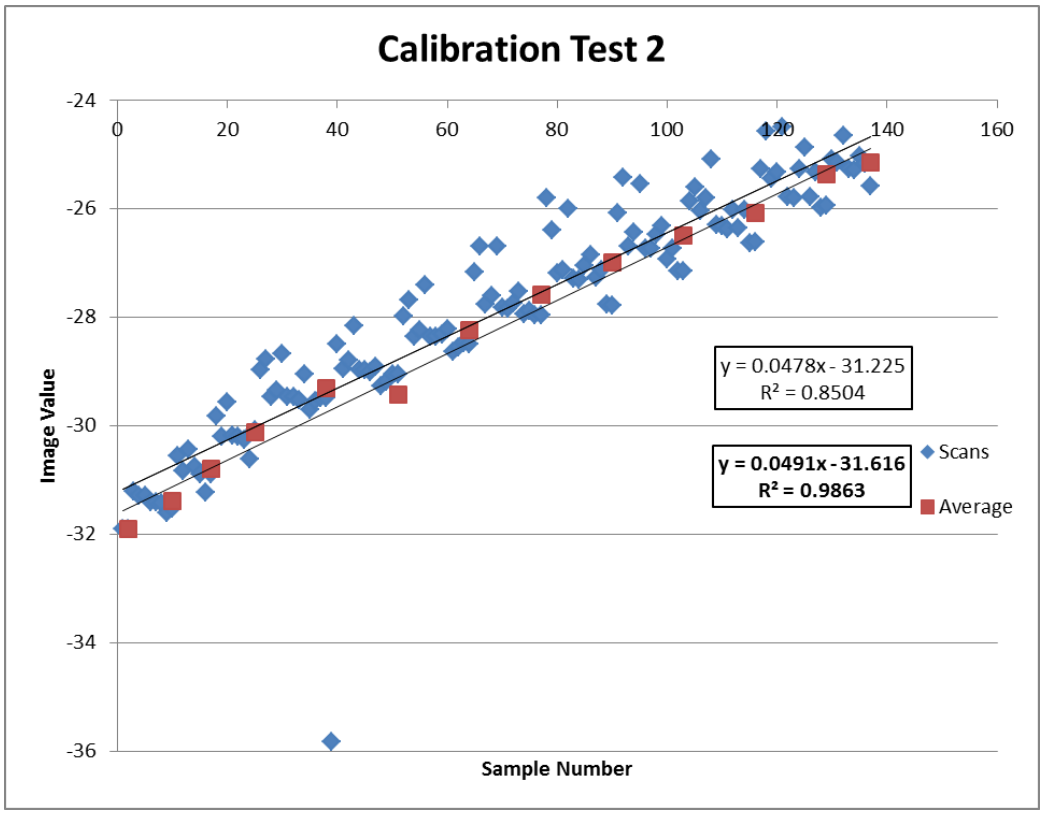

Figure 4.2 – First set of calibration test results conducted on 10/27/12.

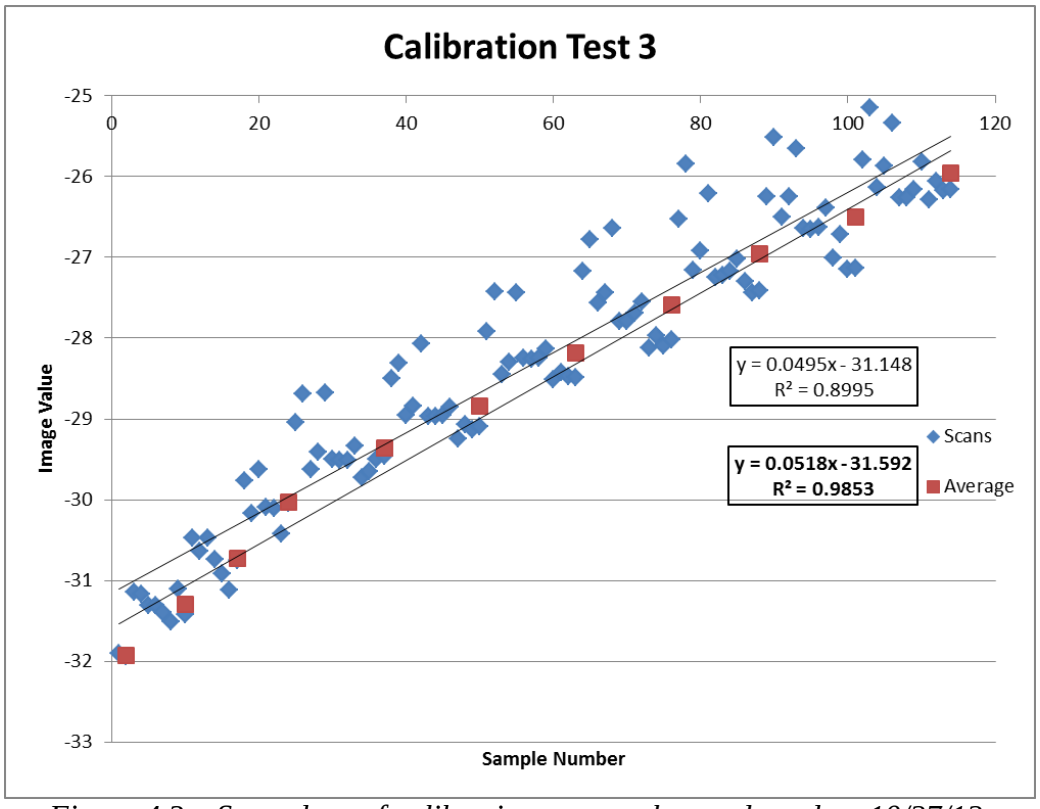

Figure 4.3 – Second set of calibration test results conducted on 10/27/12.

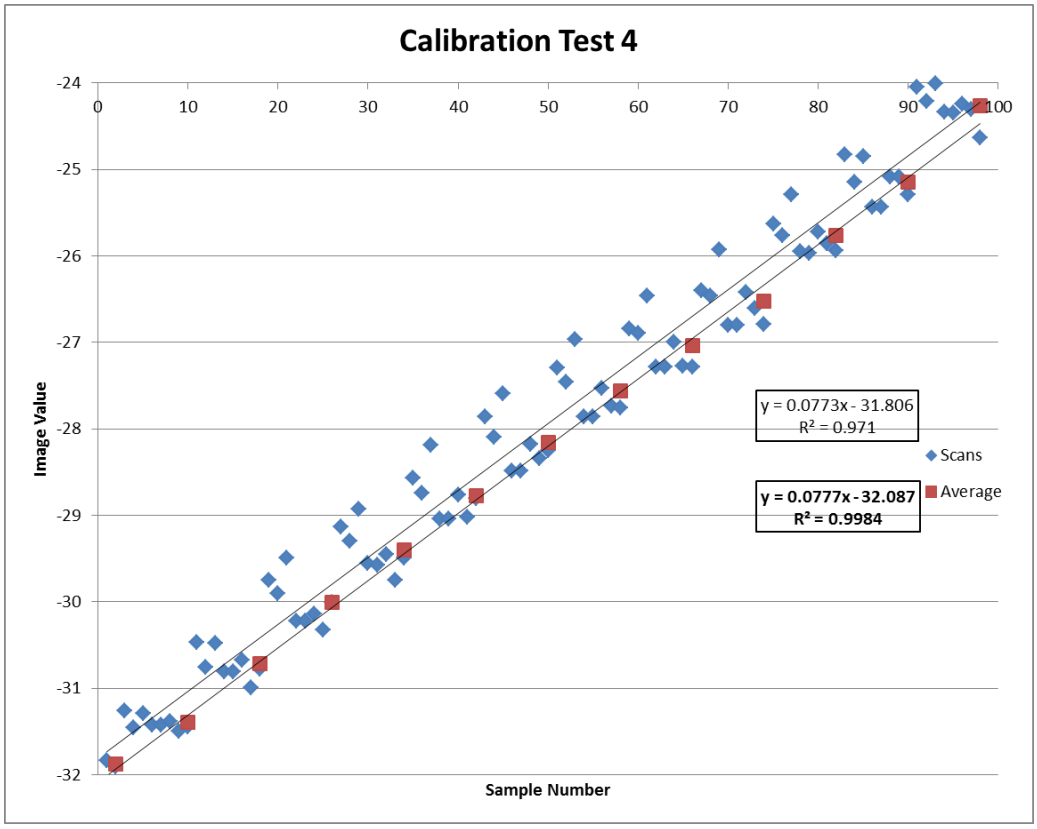

Figure 4.4 – Calibration test results conducted on weighback feed on 11/7/12.

In order to accomplish the task of determining an image weight value, a baseline value for each 5 pound increment level needed to be determined. Each calibration test 5 pound increment scan set was then averaged to determine an average value for that weight, such as the sample dataset shown in Figure 4.5.

Image Title	Image Value	Average Value
30lbscanblb\PhaseImage.tif	-27.86382246	
30lbscanbrb\PhaseImage.tif	-28.09839196	
30lbscancb\PhaseImage.tif	-27.5883515	
30lbscanf\PhaseImage.tif	-28.48376053	
30lbscanf2\PhaseImage.tif	-28.48740013	
30lbscanflb\PhaseImage.tif	-28.18144889	
30lbscanfrb\PhaseImage.tif	-28.34066949	
30lbscanh\PhaseImage.tif	-28.25337713	-28.16215276
35lbscanblb\PhaseImage.tif	-27.29985071	
35lbscanbrb\PhaseImage.tif	-27.46116538	
35lbscancb\PhaseImage.tif	-26.9709789	
35lbscanf\PhaseImage.tif	-27.86144033	
35lbscanf2\PhaseImage.tif	-27.86391075	
35lbscanflb\PhaseImage.tif	-27.53280576	
35lbscanfrb\PhaseImage.tif	-27.74223737	
35lbscanh\PhaseImage.tif	-27.75714872	-27.56119224
40lbscanblb\PhaseImage.tif	-26.84784216	
40lbscanbrb\PhaseImage.tif	-26.8902608	
40lbscancb\PhaseImage.tif	-26.466576	
40lbscanf\PhaseImage.tif	-27.28320027	
40lbscanf2\PhaseImage.tif	-27.28651453	
40lbscanflb\PhaseImage.tif	-26.99331792	
40lbscanfrb\PhaseImage.tif	-27.2713019	
40lbscanh\PhaseImage.tif	-27.28074459	-27.03996977
45lbscanblb\PhaseImage.tif	-26.40577464	
45lbscanbrb\PhaseImage.tif	-26.46189139	
45lbscancb\PhaseImage.tif	-25.93341983	
45lbscanf\PhaseImage.tif	-26.79866239	
45lbscanf2\PhaseImage.tif	-26.8060244	
45lbscanflb\PhaseImage.tif	-26.41955168	
45lbscanfrb\PhaseImage.tif	-26.60508284	
45lbscanh\PhaseImage.tif	-26.79315518	-26.52794529
50lbscanblb\PhaseImage.tif	-25.62987803	
50lbscanbrb\PhaseImage.tif	-25.76230366	
50lbscancb\PhaseImage.tif	-25.29307289	
50lbscanf\PhaseImage.tif	-25.95448737	
50lbscanf2\PhaseImage.tif	-25.96559585	
50lbscanflb\PhaseImage.tif	-25.71993362	
50lbscanfrb\PhaseImage.tif	-25.85599459	
50lbscanh\PhaseImage.tif	-25.93728367	-25.76481871

Figure 4.5 – Partial list example of calibration test scan data and calculated averages.

This was completed for each 5 pound weight increment scan set in each calibration test dataset. The weighback calibration test was conducted to determine if there was any significant difference between fresh feed and feed that had been left out for a twenty-four hour period, with the results showing that there was no noticeably significant difference. A table summarizing the averaging values for the calibration test data can be seen in Figure 4.6. The table shows the 5 pound averages for each calibration test dataset and the total average value across all calibration test datasets for each 5 pound increment. The one outlying dataset of calibration test data is the original test at the "2.8" setting on the iris. The other four are at the "4" setting on the iris, the optimal setting. Figure 4.7 plots the first 5 calibration test datasets. The calibration dataset with the "2.8" iris setting was eliminated from further analysis as this set of data was conducted at a differing iris setting than the others and the current setting of the system. The other four dataset plots lay almost directly on top of one another, which was the expected result as no further changes were made to the system. The average of all the average data points from the calibration test datasets for a particular 5 pound weight increment was calculated and thus produced the resulting plot seen in Figure 4.8. When the resulting values were plotted, a linear equation could be easily calculated that correlated all calibration test datasets with the "4" iris setting. This linear equation became the standard equation for which to test all image values against in order to determine an image weight value output.

LBS	LB TEST	10/26/2012	10/27/2012a	10/27/2012b	11/7/2012	AVG AVG	y = 0.1177x - 31.842
0	-32.0462	-31.87303418	-31.89755294	-31.92058244	-31.87441695	-31.89139662	-0.419682455
5	-31.53055556	-31.32891799	-31.39700691	-31.29538806	-31.39828672	-31.35489992	4.138488356
10	-31.14886667	-30.54149348	-30.80156742	-30.73149508	-30.72101767	-30.69889341	9.712035581
15	-30.53274444	-29.95968142	-30.11408626	-30.03325273	-30.00837385	-30.02884857	15.404855
20	-29.84412222	-29.35657345	-29.30357966	-29.3573266	-29.39932498	-29.35420117	21.13677849
25	-29.52061429	-28.76130218	-29.43669018	-28.84327899	-28.77159568	-28.95321676	24.54361292
30	-29.00611429	-28.26018245	-28.23717697	-28.17808512	-28.16215276	-28.20939932	30.86321729
35	-28.4557	-27.84831189	-27.58346228	-27.58586617	-27.56119224	-27.64470815	35.66093333
40	-28.0641	-27.33488769	-26.99564248	-26.95630118	-27.03996977	-27.08170028	40.44434766
45	-27.68687143	-26.84455717	-26.49266609	-26.50052271	-26.52794529	-26.59142282	44.60983163
50	-27.03322857	-26.23013197	-26.07747324	-25.96035327	-25.76481871	-26.0081943	49.5650442
55		-25.64736826	-25.37236261		-25.14672664	-25.38881917	54.82736474
60		-25.07608147	-25.15071396		-24.26810739	-24.83163427	59.56130611

Figure 4.6 – Calibration test scan dataset averages comparison.

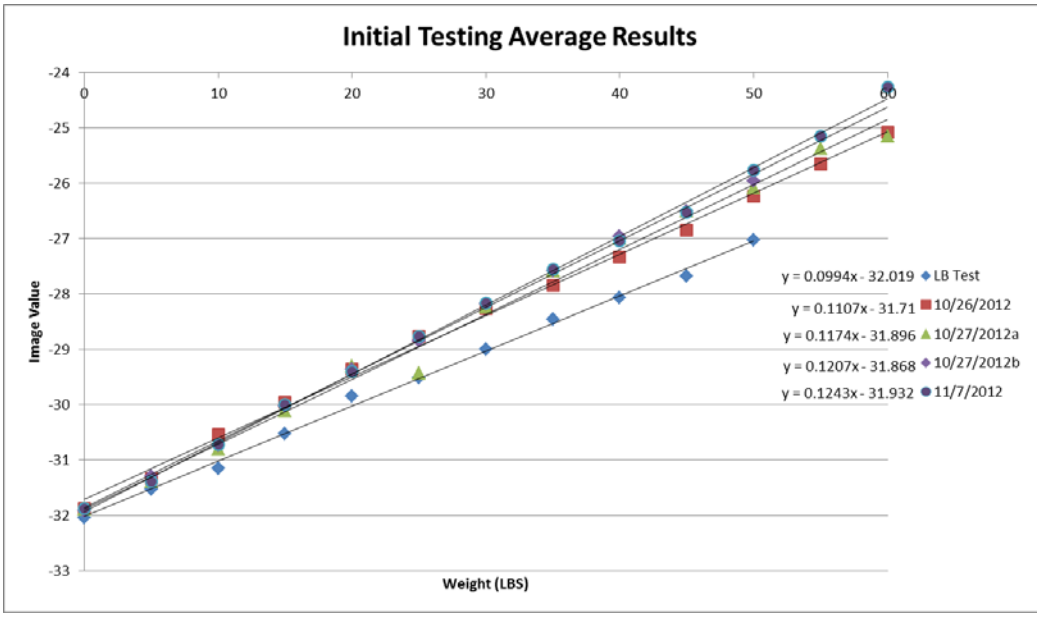

Figure 4.7 – Comparison plot of calibration test scans.

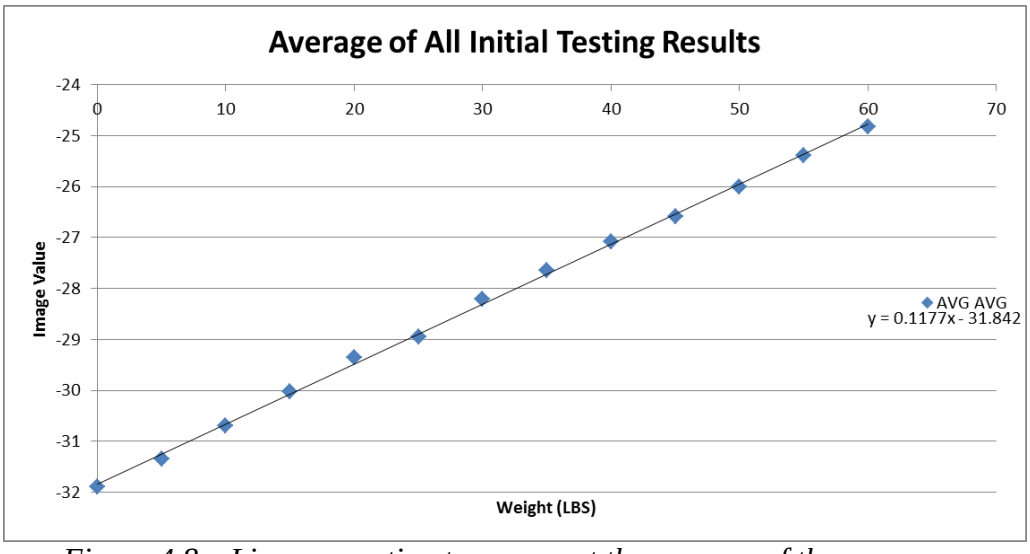

Figure 4.8 – Linear equation to represent the average of the averages.

This linear equation was then tested as shown in the last column of data in Figure 4.6 against the known weight sample averages of the calibration test scans data by changing the Y-value to the average value. As seen in Figure 4.6, nearly every image weight value is within one pound of the actual average value for each 5 pound increment. The linear equation was then tested against the image values determined by the software for each phase image. The result for the majority of scans was a value that was within one or two pounds of the physical scale measured weight. A sample of these output values can be seen in Figure 4.9.

Image Title	Image Value	Image Weight	Scale Weight	Difference
30lbscanblb\PhaseImage.tif	-27.86382246	33.80	30	3.80
30lbscanbrb\PhaseImage.tif	-28.09839196	31.81	30	1.81
30lbscancb\PhaseImage.tif	-27.5883515	36.14	30	6.14
30lbscanf\PhaseImage.tif	-28.48376053	28.53	30	-1.47
30lbscanf2\PhaseImage.tif	-28.48740013	28.50	30	-1.50
30lbscanflb\PhaseImage.tif	-28.18144889	31.10	30	1.10
30lbscanfrb\PhaseImage.tif	-28.34066949	29.75	30	-0.25
30lbscanh\PhaseImage.tif	-28.25337713	30.49	30	0.49
35lbscanblb\PhaseImage.tif	-27.29985071	38.59	35	3.59
35lbscanbrb\PhaseImage.tif	-27.46116538	37.22	35	2.22
35lbscancb\PhaseImage.tif	-26.9709789	41.39	35	6.39
35lbscanf\PhaseImage.tif	-27.86144033	33.82	35	-1.18
35lbscanf2\PhaseImage.tif	-27.86391075	33.80	35	-1.20
35lbscanflb\PhaseImage.tif	-27.53280576	36.61	35	1.61
35lbscanfrb\PhaseImage.tif	-27.74223737	34.83	35	-0.17
35lbscanh\PhaseImage.tif	-27.75714872	34.71	35	-0.29
40lbscanblb\PhaseImage.tif	-26.84784216	42.43	40	2.43
40lbscanbrb\PhaseImage.tif	-26.8902608	42.07	40	2.07
40lbscancb\PhaseImage.tif	-26.466576	45.67	40	5.67
40lbscanf\PhaseImage.tif	-27.28320027	38.73	40	-1.27
40lbscanf2\PhaseImage.tif	-27.28651453	38.70	40	-1.30
40lbscanflb\PhaseImage.tif	-26.99331792	41.20	40	1.20
40lbscanfrb\PhaseImage.tif	-27.2713019	38.83	40	-1.17
40lbscanh\PhaseImage.tif	-27.28074459	38.75	40	-1.25
45lbscanblb\PhaseImage.tif	-26.40577464	46.19	45	1.19
45lbscanbrb\PhaseImage.tif	-26.46189139	45.71	45	0.71
45lbscancb\PhaseImage.tif	-25.93341983	50.20	45	5.20
45lbscanf\PhaseImage.tif	-26.79866239	42.85	45	-2.15
45lbscanf2\PhaseImage.tif	-26.8060244	42.79	45	-2.21
45lbscanflb\PhaseImage.tif	-26.41955168	46.07	45	1.07
45lbscanfrb\PhaseImage.tif	-26.60508284	44.49	45	-0.51
45lbscanh\PhaseImage.tif	-26.79315518	42.90	45	-2.10
50lbscanblb\PhaseImage.tif	-25.62987803	52.78	50	2.78
50lbscanbrb\PhaseImage.tif	-25.76230366	51.65	50	1.65
50lbscancb\PhaseImage.tif	-25.29307289	55.64	50	5.64
50lbscanf\PhaseImage.tif	-25.95448737	50.02	50	0.02
50lbscanf2\PhaseImage.tif	-25.96559585	49.93	50	-0.07
50lbscanflb\PhaseImage.tif	-25.71993362	52.01	50	2.01
50lbscanfrb\PhaseImage.tif	-25.85599459	50.86	50	0.86
50lbscanh\PhaseImage.tif	-25.93728367	50.17	50	0.17

Figure 4.9 – Example of calibration test scan image pound weight values calculated.

Once the calibration test datasets were collected, the research was then able to proceed towards determining the correlation between image value and scale measured weight value of these calibration tests. The X and Y directions are not as significant as the Z direction values. It is on the Z-axis that the image value is calculated. The controlled bias shown in the feed bin is clearly represented in the triangulation data plots. The various data points shown are the triangulations computed by the software and therefore have a contour similar to that of the actual feed. Some points are higher (closer to the camera) on the Z-axis than others and most of the triangulation data contains its own individual contour information. When all of these data points are averaged together, the average image value for the entire phase image dataset can be determined.

Of particular notice is the fact that the flat scans do show a slight slope. This is because the camera is tilted at a slight angle from the plane of the surface of the bin. This slope is considered to be only marginal and has little effect on the outcomes of the imaging system. The factor that does play a major role is the light intensity of the projector concerning biasing. From the data collected, the images that contained feed physically closer to the projector or the central point of light projection from the projector (the areas with greater light intensity) appeared to have a slightly higher image value than other biased and unbiased control test scans. As well, images that contained feed physically further away from the projector or the central point of light projection (the areas with lower intensities of light) appeared to have a slightly lower image value than the other biased and unbiased calibration test scans. In general, the rank of image values from highest to lowest (least negative to most negative) for each 5 pound increment level

were center bias (CB), back left bias (BLB), back right bias (BRB), and then all other scans at near parity in value.

For this research, we are not generally concerned with the center bias (CB) values as much since the chances of the feed ever being severally biased towards the center of the feed bin are virtually zero. When cow eat feed, their feeding characteristics and habits tend to push the feed towards the exterior boundaries and not towards the center of any container. As for the variations among the other images and their respective image values, this research study concluded that the difference in image value (and therefore image weight value) is of a minor order as the image weight values of the calibration scans are generally within one or two pounds of the scale measured weight values. The only values that consistently did not fit this result are the central bias scans image weight values and scale measured weight values, which tended to be off by approximately 0 to 5 pounds.

The difference between the scale measured weight and scan weight value can very easily be discernible in the fact that analog weighing scales, such as those used in this study, are neither as exact as digital scales nor was the precision of weight measured in the bin on the scales taken in sub-pound exactitude. Meaning, the difference between the actual weight in the bin and the scale measured weight could be off by as much as 0 to 5 pounds, with most being well under 2 pounds in difference. Taking this factor into consideration for the calibration test data, the scan weight value was actually more precise than the scale measured weight value, which further proved the successful use of this system to accurately measure the amount of feed in a bin.

With all of the calibration data results collected, the evaluation method for determining the image weight was then revisited in order to determine the amount of error in the calibration data. In this manner, the goal was to determine if a linear analysis was the best representation of this data or if another method should be utilized. Figures 4.10 to 4.13 show the calibration test results once again, but this time the individual scans for each 5 pound weight increment are combined into a t-test statistical analysis for each 5 pound weight interval with a confidence interval of 95%. The error bars on each 5 pound data point indicate the amount of t-test statistical error form the mean value. For example, in Calibration Test 1, the mean image value for a weight of 30 pounds was -28 with an error interval that ranges from approximately -27.5 to -28.5. Figure 4.14 is the averaged values of the calibration tests that result in a final determination of image value versus weight. As can be seen, the image value for a weight of 30 pounds had been estimated as approximately -28.2 with an error interval that had been greatly reduced for a range of approximately -28.1 to -28.3. This reduction in error in Figure 4.14 is similar for all 5 pound intervals after averaging the calibration tests data together. Again, it can be seen that there was somewhat of a linear relationship between image value and weight.

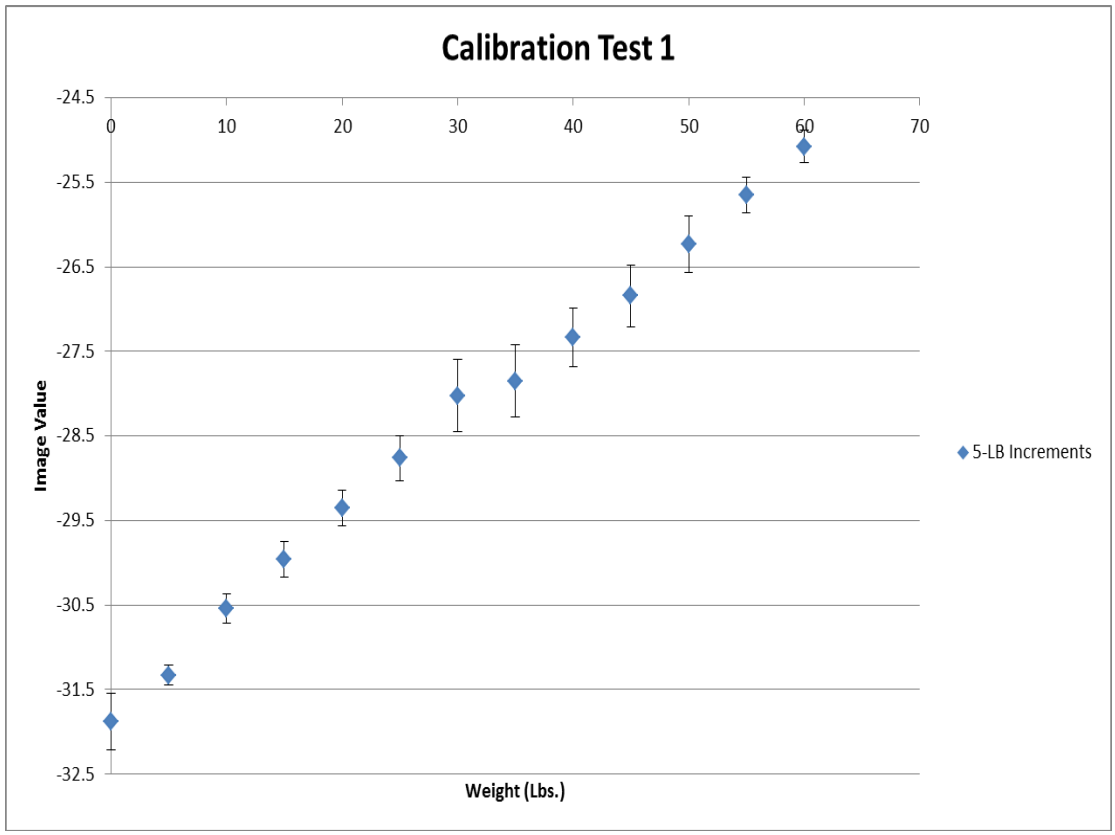

Figure 4.10 – t-test of first calibration dataset with error shown.

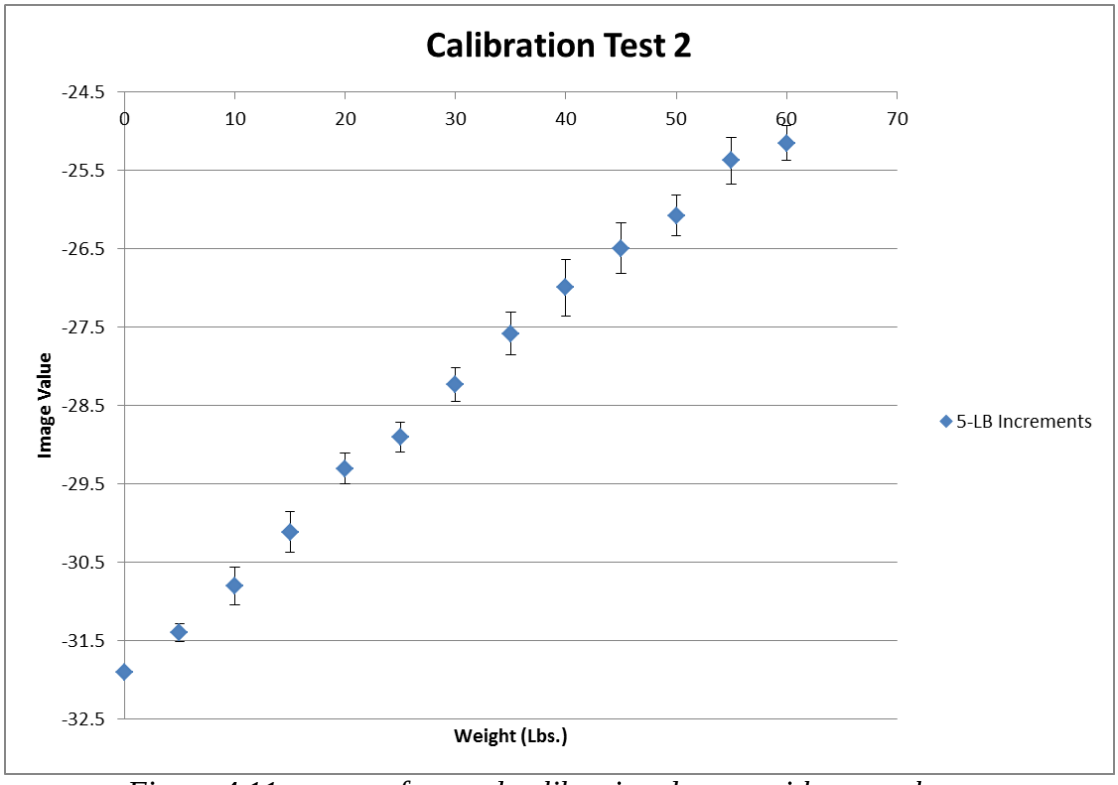

Figure 4.11 – t-test of second calibration dataset with error shown.

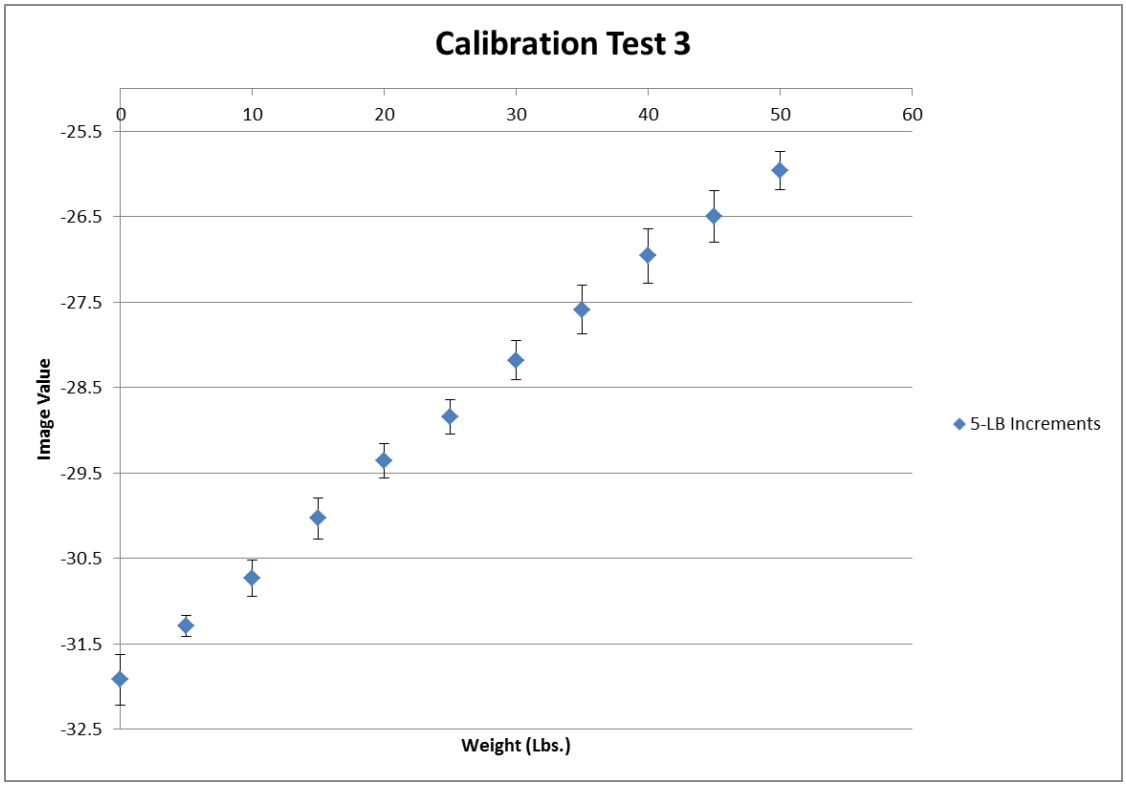

Figure 4.12 – t-test of third calibration dataset with error shown.

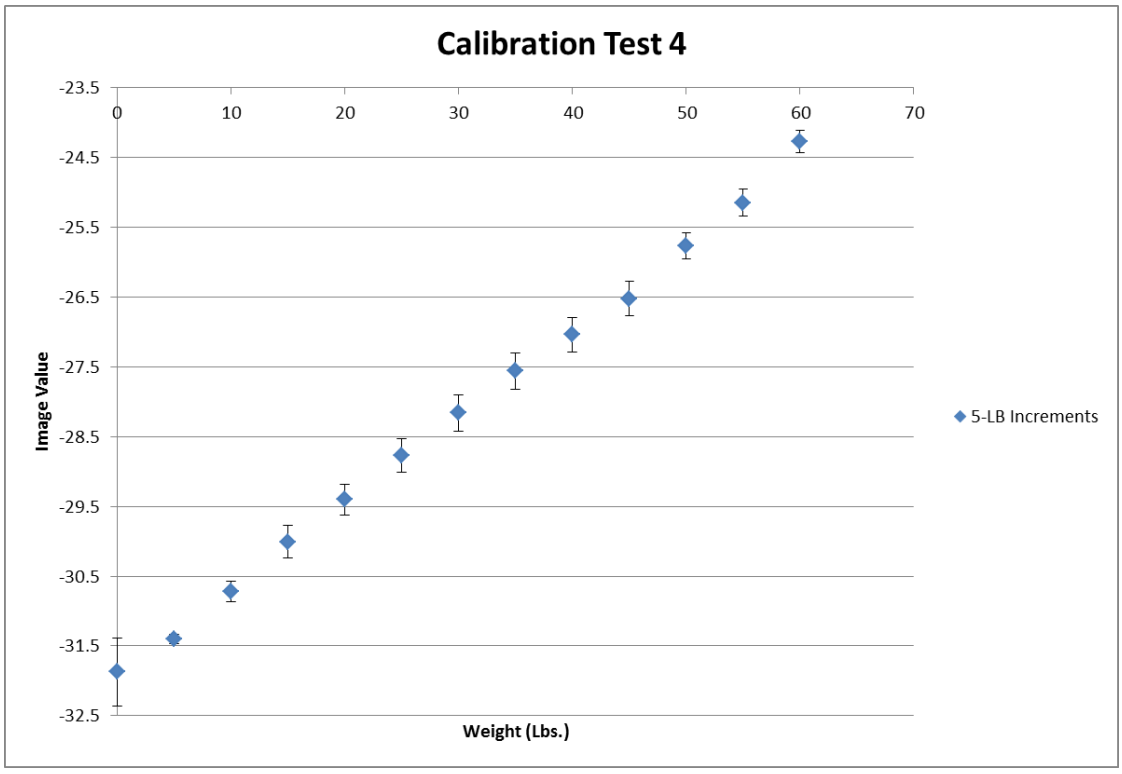

Figure 4.13 – t-test of fourth calibration dataset with error shown.

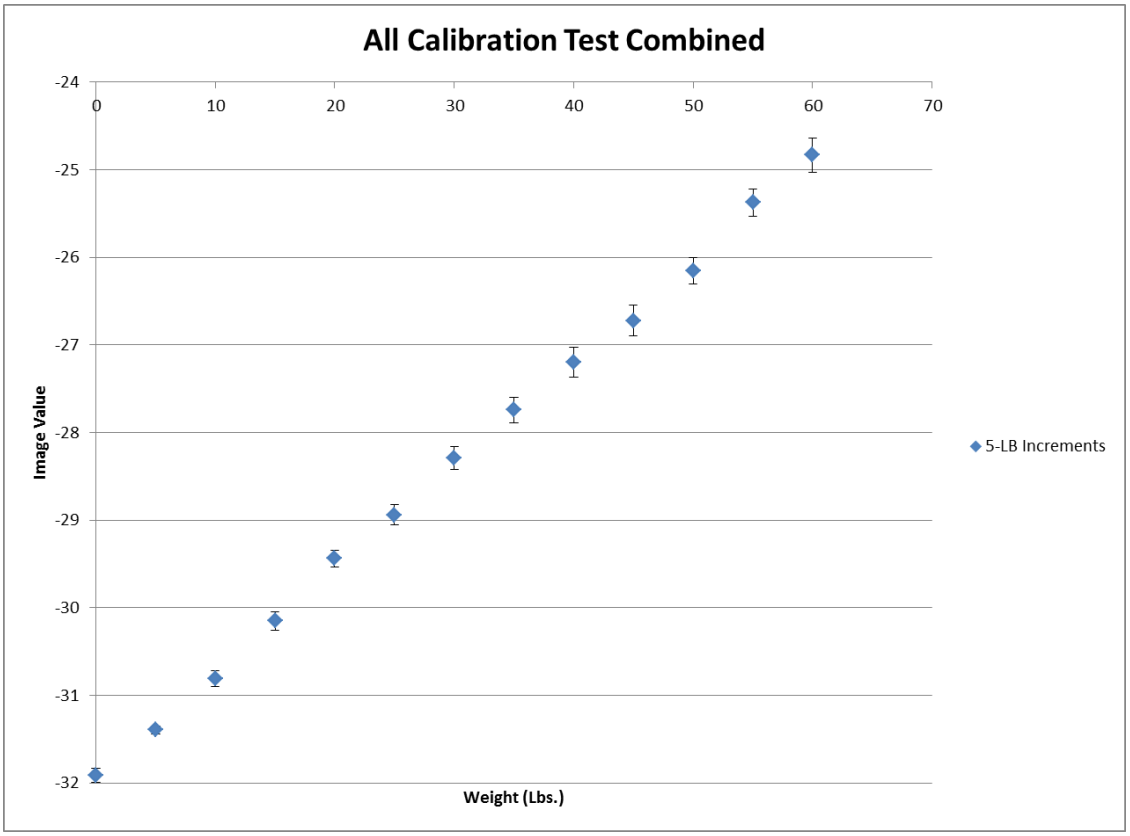

Figure 4.14 – t-test of all calibration datasets combined and averaged with error shown.

If we now look closer at the individual biasing averages plotted separately versus weight, as shown in Figure 4.15, we can see the differences in biasing averages. For example, the image values range from approximately -27.5 to -28.5 for the 30 pound weight interval, depending on which type of bias is present in the feed in the bin. This tells us that the bin biasing plays a major factor in determining the output weight value.

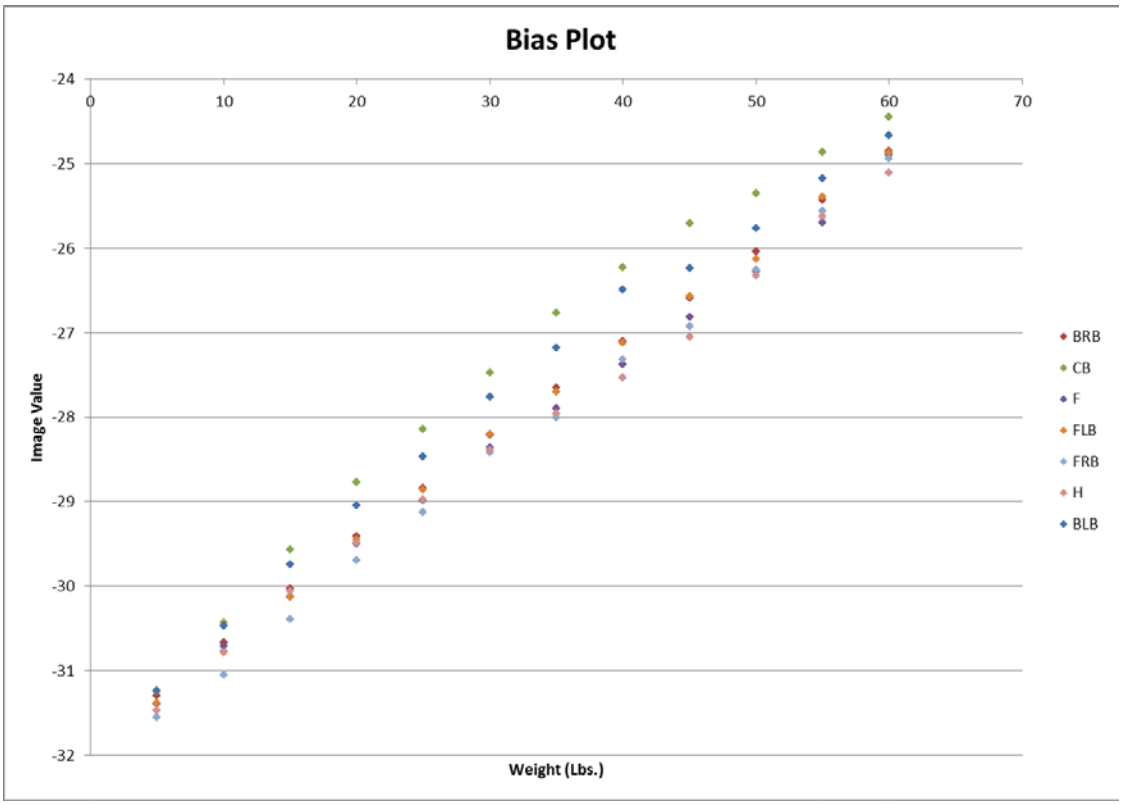

Figure 4.15 – Bin biasing versus resulting 5 pound incremental average image value.

If we again look closer at the data to see how the biasing affects the mean value, such as in Figure 4.16, we can see a clear difference in biasing from the mean value. What this tells us is that if the biasing did not affect the image value, and ultimately the output weight value, then the biasing would have a mean of 0. As we can see from Figure 4.16, though, the biasing caused the data to underestimate or overestimate the image and weight values. The increments of the *X*-axis were determined to have a relationship of 0.1 being equal to 1 pound. The back right biasing (BRB) does fall very close to the mean value, but with a 95% confidence interval t-test average of plus or minus approximately 1 pound of error. Likewise, the front left biasing (FLB), flat (F) scan, hole biasing (H), and front right biasing (FRB) tend to have an error of plus or minus 1 pound, even though their mean values underestimate the amount of feed in the bin by, respectively and approximately, 0.5, 1.8, 2.3, and 2.8 pounds. For the center bias

(CB), the weight values calculated tended to overestimate by nearly 6 pounds with plus or minus about 1 pound of error. As well, the back left biasing (BLB) overestimated the weight by approximately 3 pounds with plus or minus about 1 pound of error.

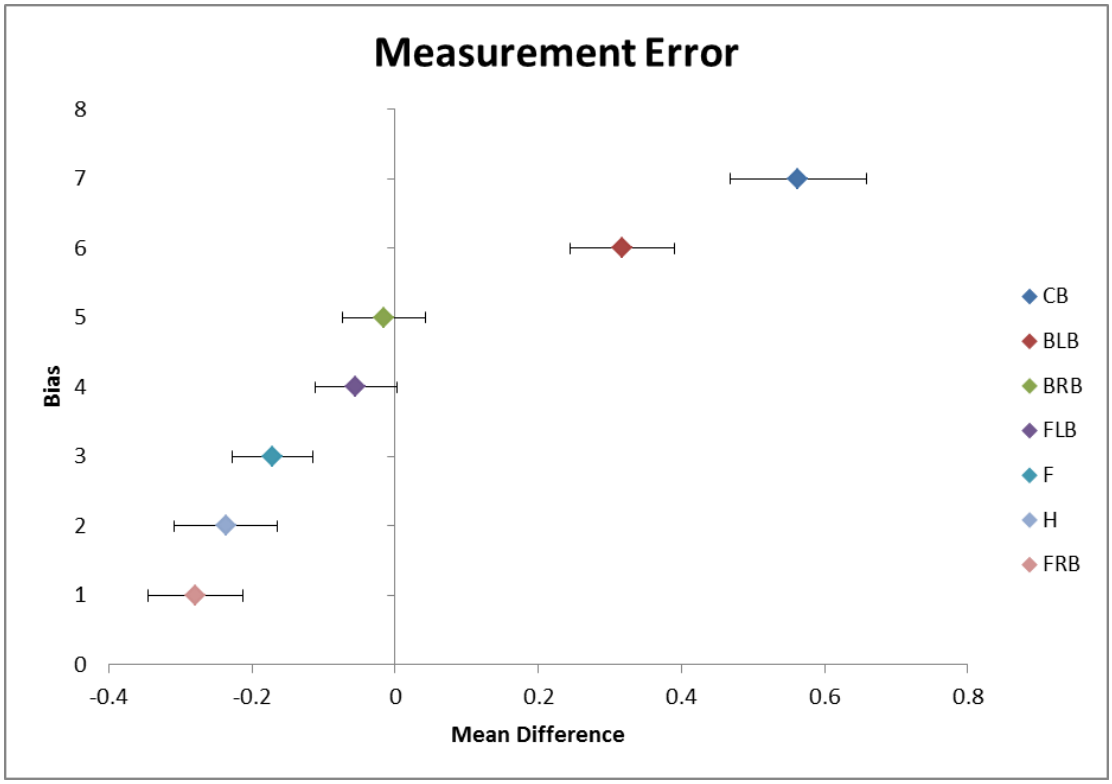

Figure 4.16 – Statistical deviation error of biasing from the mean value.

What this result tells us is that there is inherent error in the previous evaluation of the system by using a linear relationship between image value and weight, but it is a consistent interval of error, it just depends on which biasing we are looking at. What this suggests is that using a singular linear equation to represent the conversion from image value to image weight is the wrong approach. Instead, using look up tables (LUT) that depend on the bias, would provide a much more robust system evaluation of image values into weight values.

CHAPTER V: CONCLUSION, SUMMARY, AND RECOMMENDATIONS

The research study concluded with testing the linear correlation assumption in control testing to determine if this relationship continued outside of calibration testing and to test the assumptions made about the resulting scan image weight value analysis. The control testing was conducted over a period from 1/7/2013 through 1/26/2013, Monday through Saturday of each week and excluding Sundays, at the daily 1pm feeding time. A dry matter analysis was conducted on a sample of the feed from each day of feeding and can be seen in Figure 5.1. The Koster testing method [12,31] was utilized by the farm management in order to determine dry matter percentage. As can be seen, the dry matter content remained fairly constant over the duration of the testing period.

Date Sampled	Dry Matter (%)	% Moisture Content	Date Tested
1/7/2013	49	51	1/11/2013
1/8/2013	51.5	48.5	1/11/2013
1/9/2013	50	50	1/11/2013
1/10/2013	49.5	50.5	1/11/2013
1/11/2013	51	49	1/14/2013
1/12/2013	55	45	1/14/2013
1/13/2013	49	51	1/14/2013
1/14/2013	51	49	1/17/2013
1/15/2013	50	50	1/17/2013
1/16/2013	49.5	50.5	1/17/2013
1/17/2013	51	49	1/23/2013
1/18/2013	50	50	1/23/2013
1/19/2013	48	52	1/23/2013
1/20/2013	53	47	1/23/2013
1/21/2013	52	48	1/23/2013
1/22/2013	53	47	1/23/2013
1/23/2013	54	46	1/28/2013
1/24/2013	48	52	1/28/2013
1/25/2013	49	51	1/28/2013
1/26/2013	48.5	51.5	1/28/2013

Figure 5.1 – Moisture content of feed used during control testing.

The control testing cows utilized in this research were fresh cows, isolated in their feeding habits as discussed in Chapter 3 and shown in Figures 3.1 to 3.7. A summary plot of each cow's feedings can be seen in Figures 5.2 to 5.8. The individual cow's

number is the title of the plot. These plots show both the scale measured weight and the scan image weight values calculated for each cow's feed bin(s) for both output feed and weighback feed. In addition, shown in Figure 5.9 is only the data for bins of feed output and in Figure 5.10 is only the data for the bins of weighback feed. Figures 5.11 to 5.13 plot the scale measured weights against the scan image calculated weights and compares them to parity (one-to-one correspondence) for, respectively, output feed, weighback feed, and all the control scan data points collected.

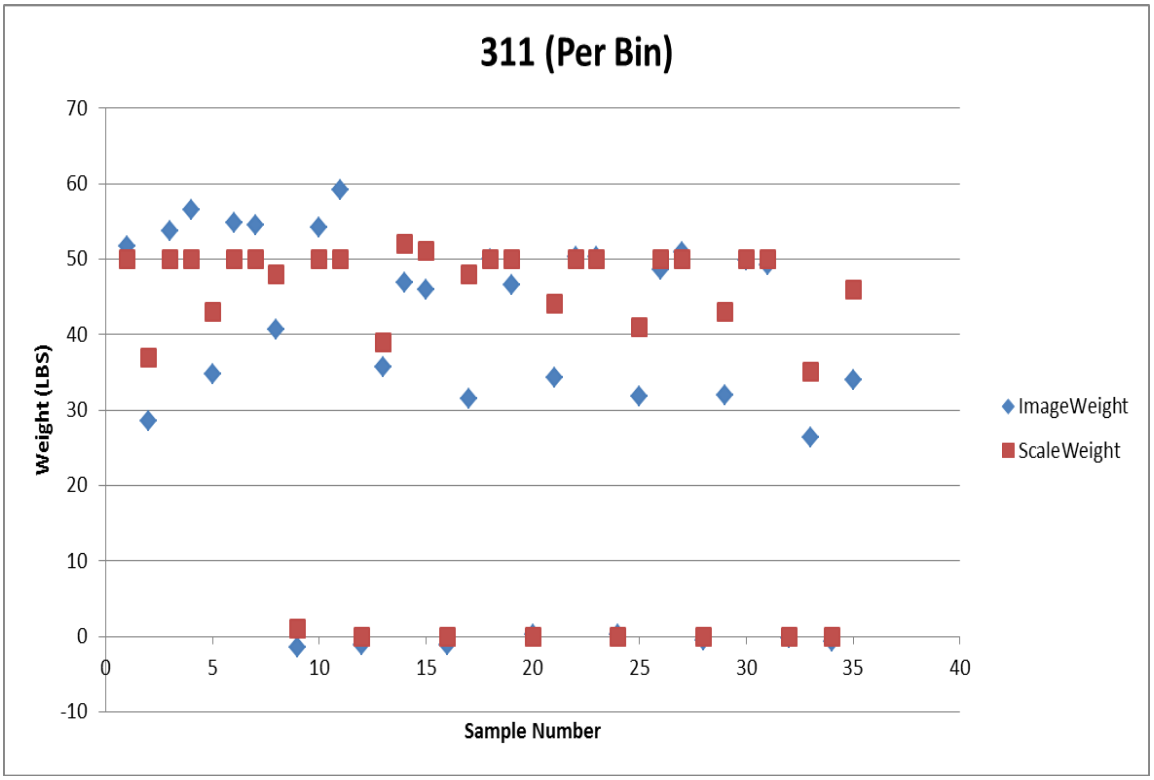

Figure 5.2 – Data for cow number 311.

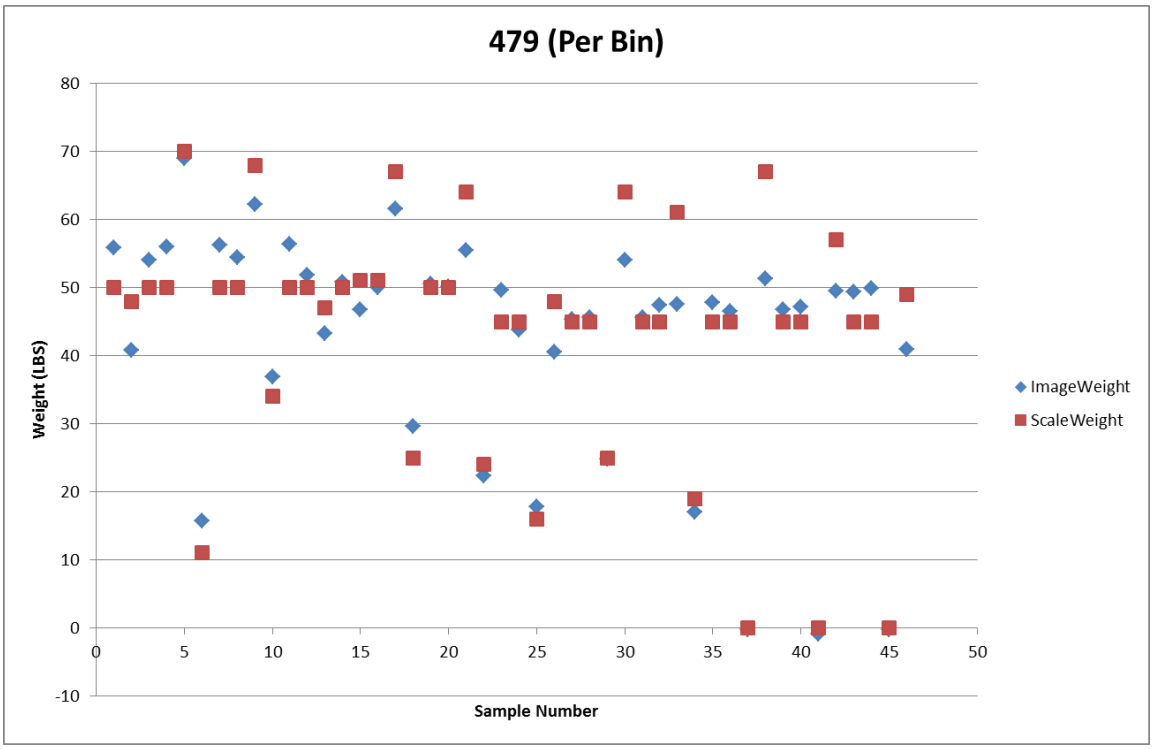

Figure 5.3 – Data for cow number 479.

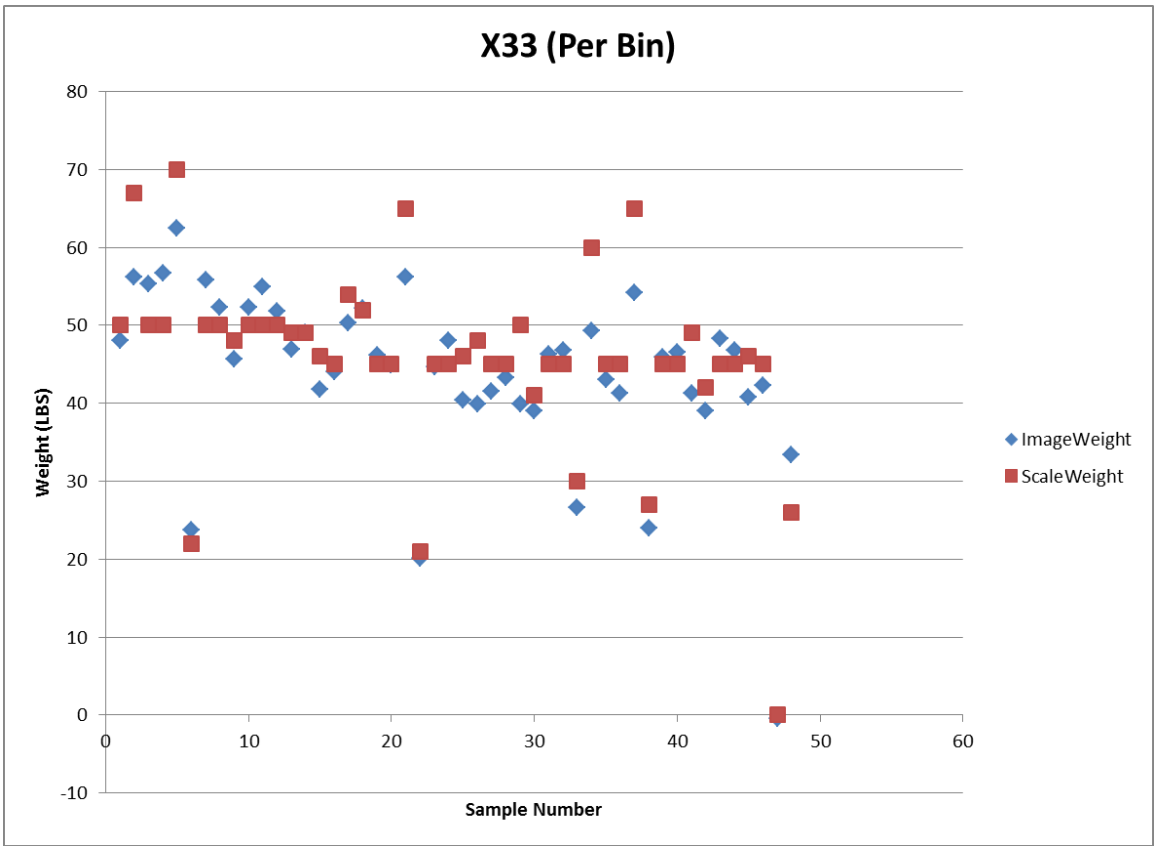

Figure 5.4 – Data for cow number X33.

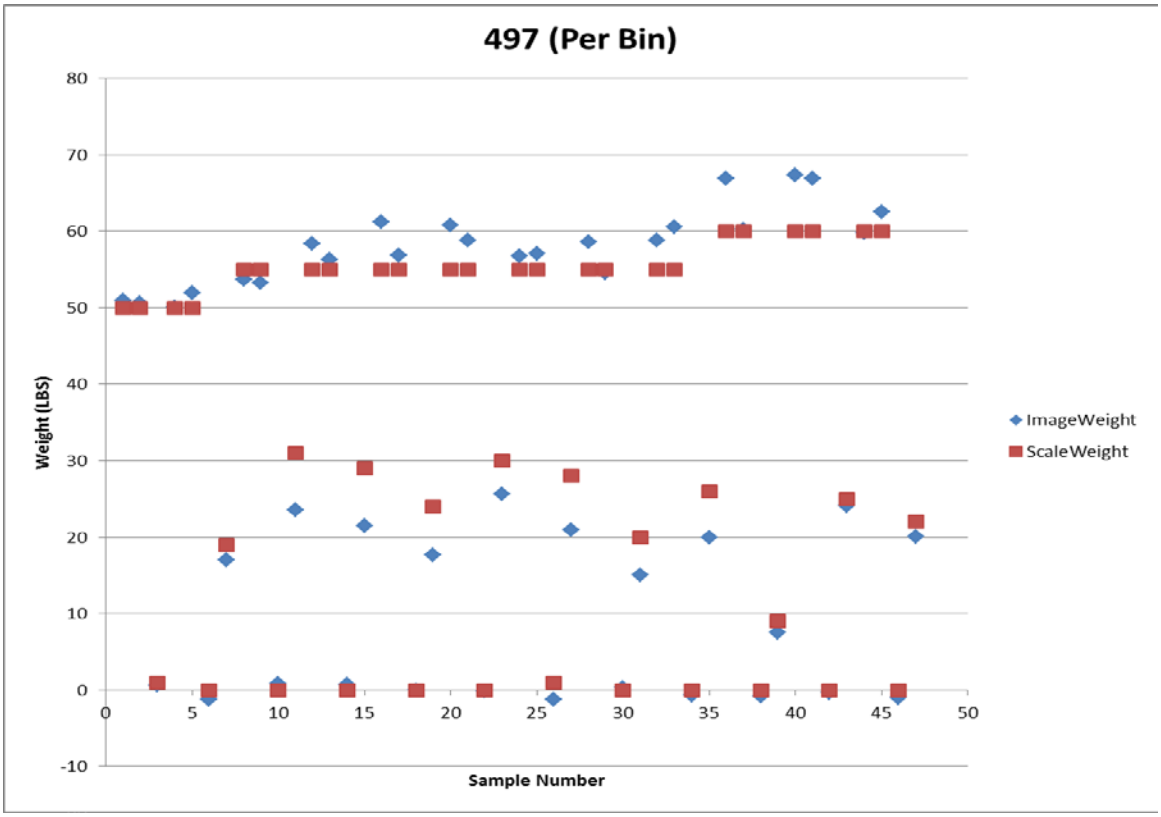

Figure 5.5 – Data for cow number 497.

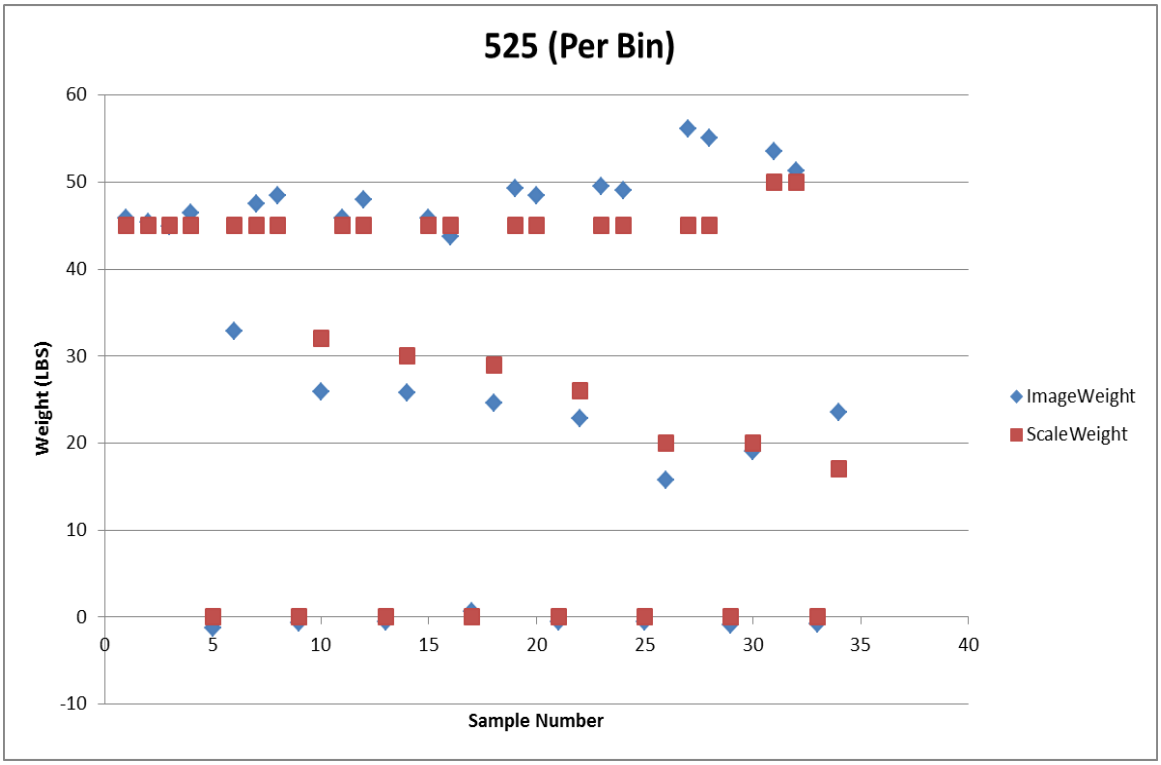

Figure 5.6 – Data for cow number 525.

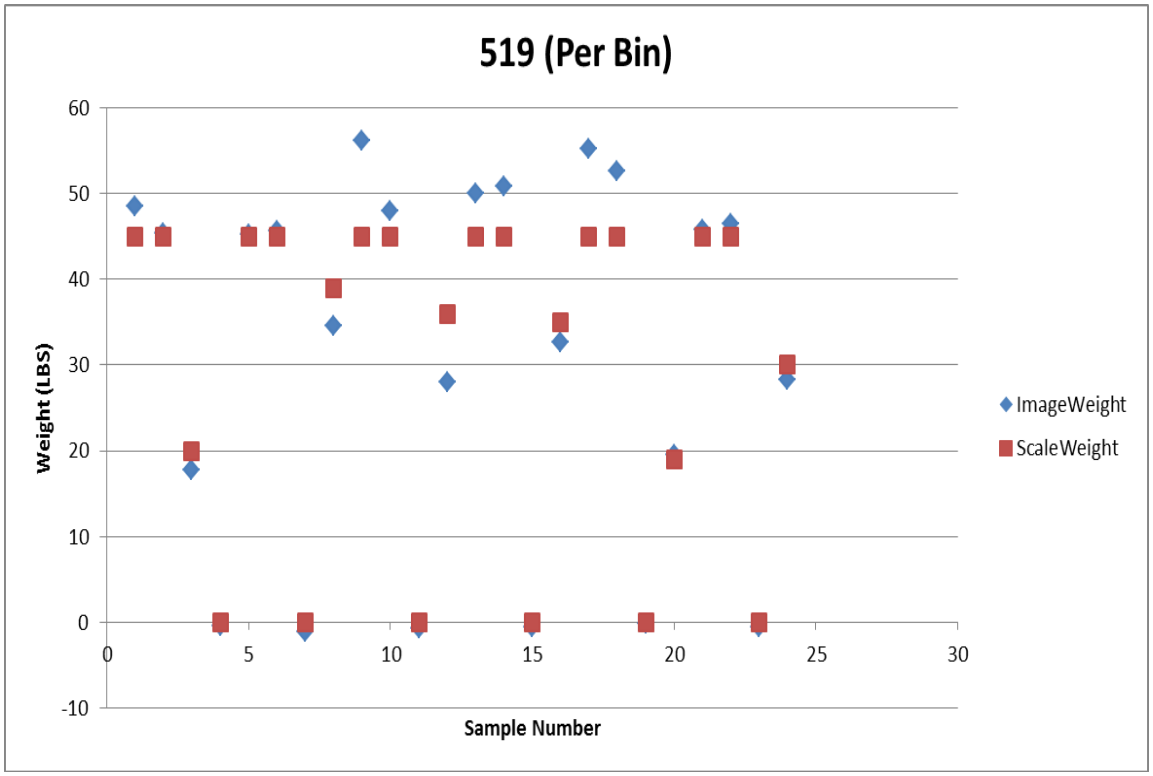

Figure 5.7 – Data for cow number 519.

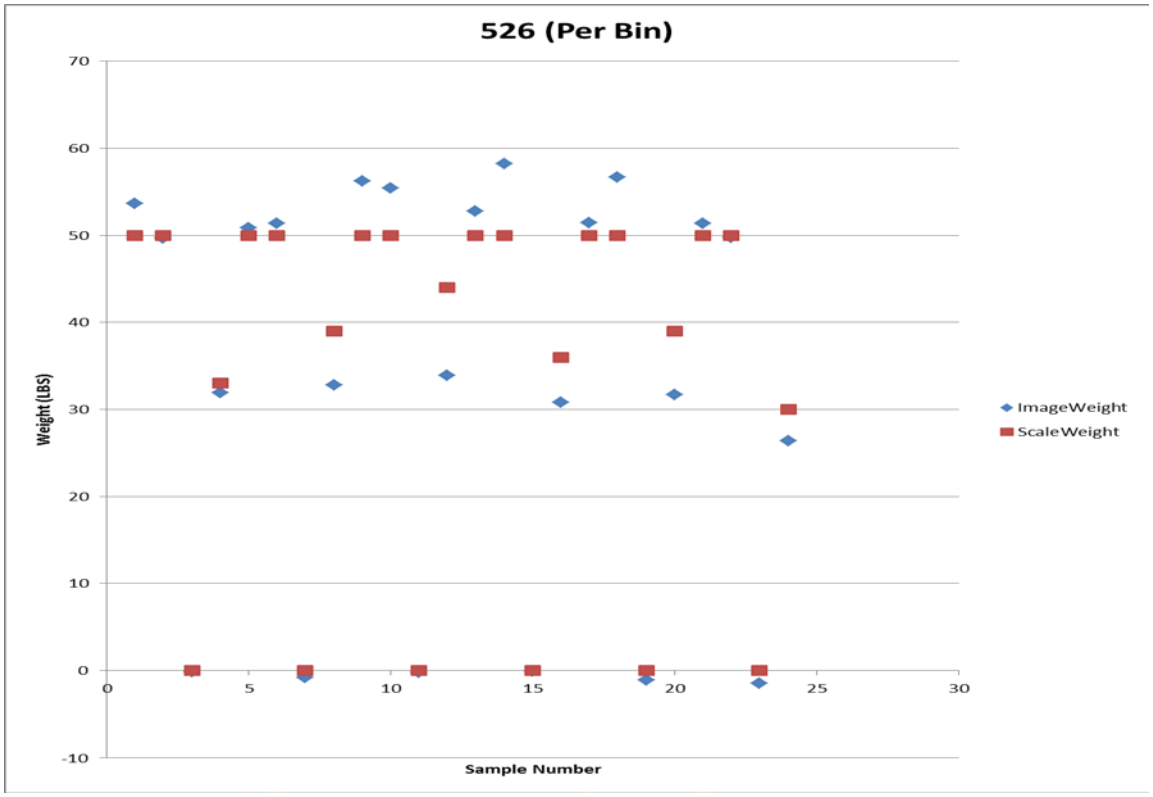

Figure 5.8 – Data for cow number 526.

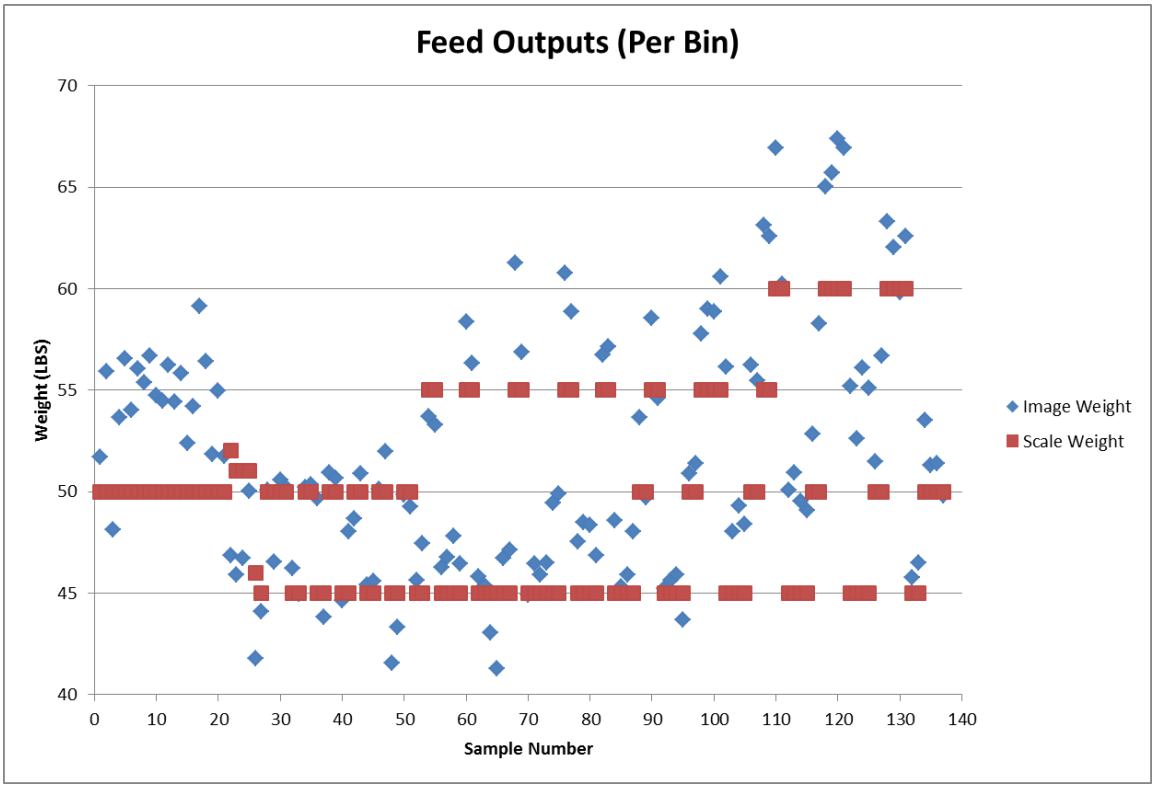

Figure 5.9 – Output feed data points.

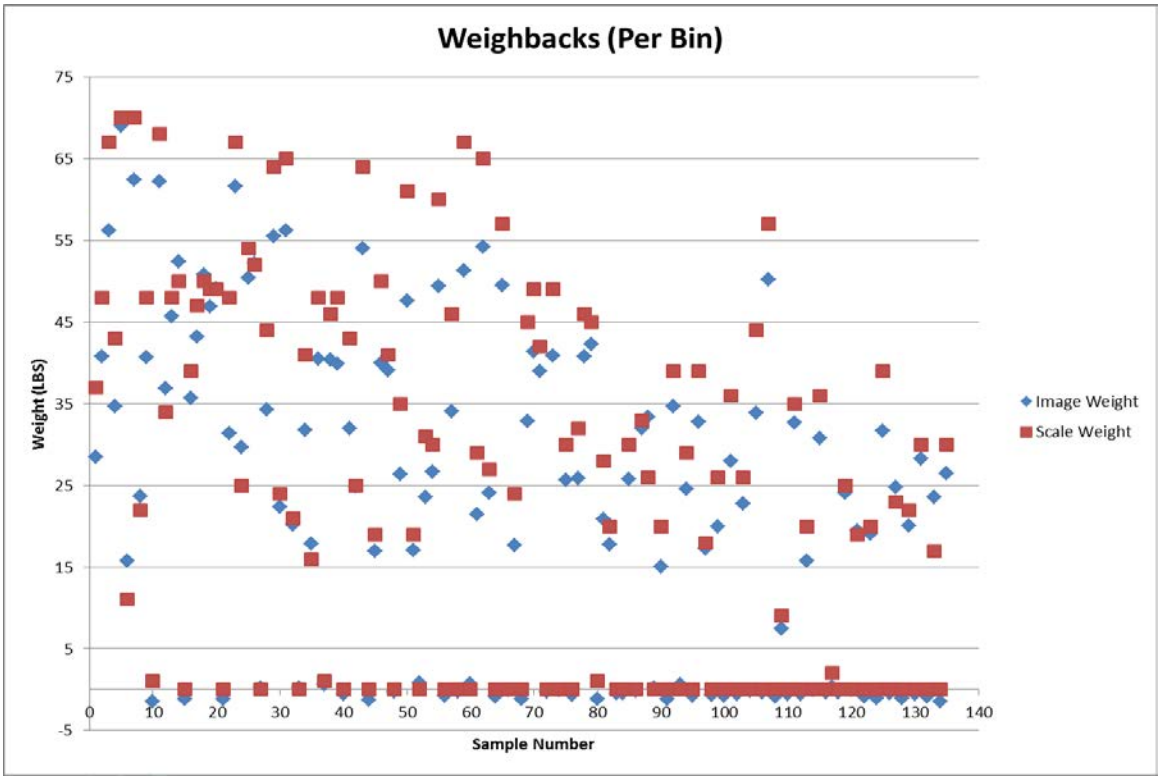

Figure 5.10 – Weighback feed data points.

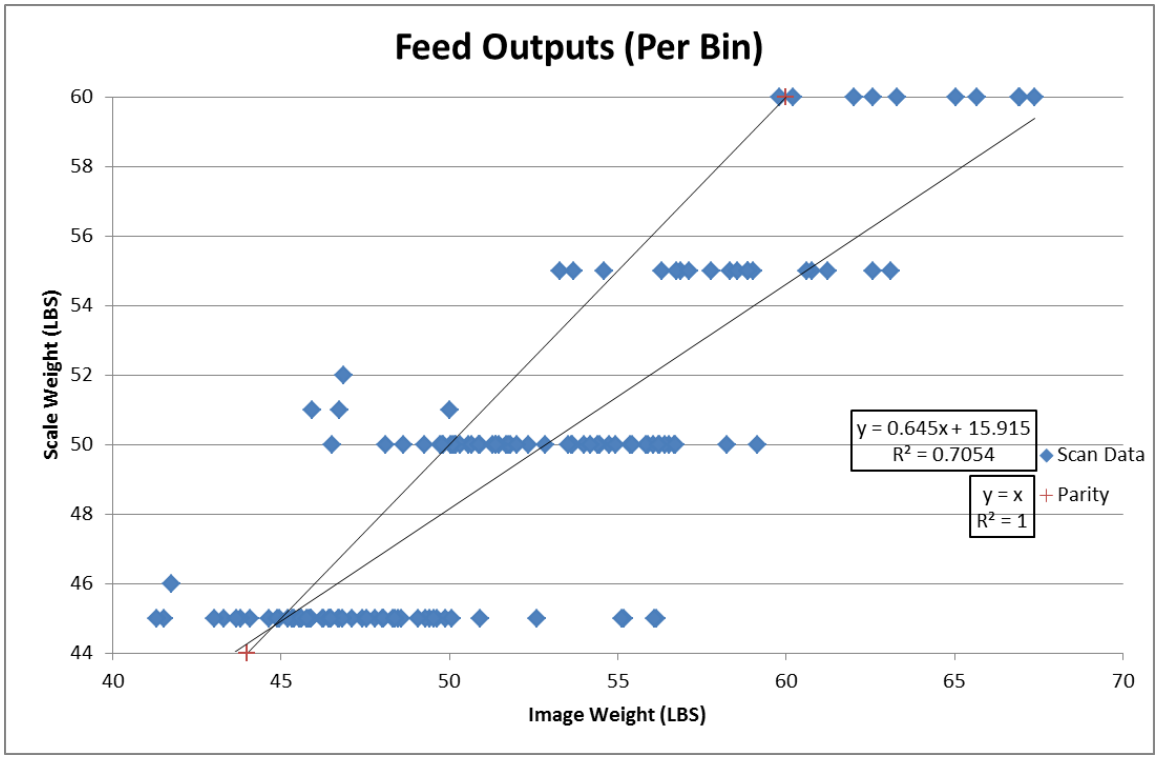

Figure 5.11 – Output feed values versus parity (1=1).

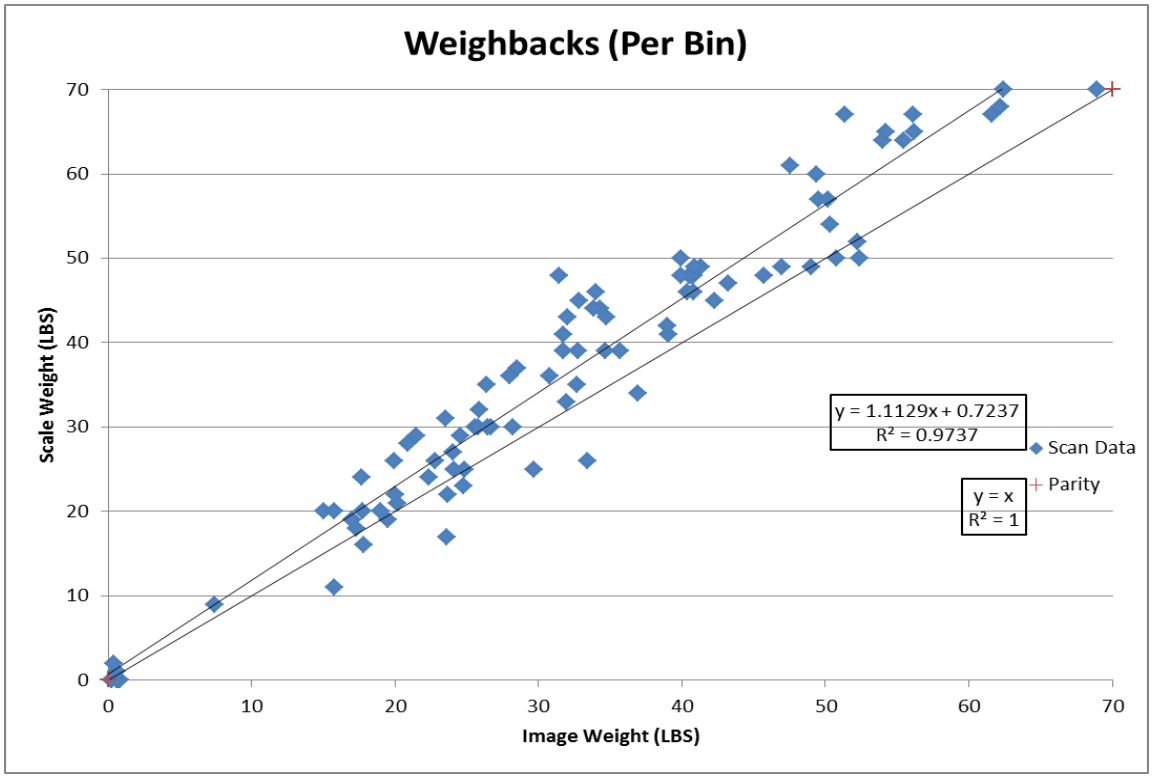

Figure 5.12 – Weighback feed values versus parity (1=1).

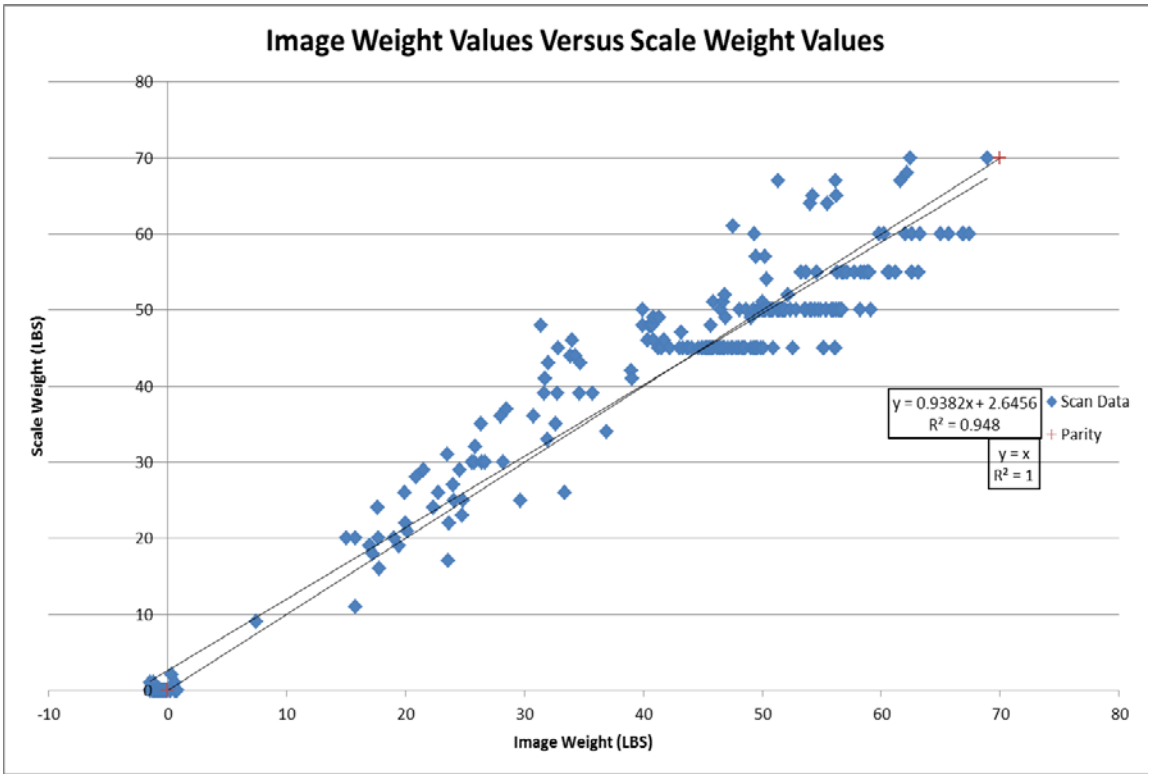

Figure 5.13 – All control data values versus parity (1=1).

In total, there were 272 control scan data values collected, processed, and analyzed. Statistical calculated image weight error information for the control test scans can be seen in Figure 5.14. The statistical data shows us that even though there were differences between scale measured weight and image value calculated weight, the correlation is very strong between both sets of values.

Pound Error	Data Points	Percentage	
16	1	0.367647	
15	1	0.367647	
14	0	0	
13	1	0.367647	
12	1	0.367647	
11	4	1.470588	2.941176
10	7	2.573529	
9	4	1.470588	
8	10	3.676471	
7	14	5.147059	
6	16	5.882353	
5	17	6.25	25
4	23	8.455882	
3	24	8.823529	
2	22	8.088235	
1	48	17.64706	
0	79	29.04412	72.05882
	272	100	100

Figure 5.14 – Calculated pound weight error for control test results.

The results shown in Figure 5.14 further proves the capability of this SLI system as 196 out of the 272 scans, or roughly 72% of the results, were within 4 pounds of the difference between the calculated image weight value and the scale measured weight value. As well, 149 out of 272, or almost 55%, of all the results are within 2 pounds of difference between calculated and scale measured weight. The nearly 3% of data that is 11 pounds or greater occurs at scale weights of 60 pounds or greater. The initial calibration testing was not calibrated for bin weights greater than 60 pounds as the feed in the bin at these values is either spilling out over the edges of the bin or is severely center biased (CB) as it must be piled in the center of the bin in order to accommodate this much feed. Therefore, the highly central biased nature of the feed placed more of the feed closer to the projector and camera than necessary and led to calculated values that did not accurately represent the actual amount of feed in the bin. Had the bins used been large

enough to properly accommodate such feed weight, then the system would have been further calibrated to higher weights of feed. This study did not take into consideration the scanning of bins of more than 60 pounds as most bins were typically filled at 45, 50, or 55 pounds with only a few at 60 pounds.

The 25% of data that was 5 to 10 pounds in difference between calculated and scale weight values can best be attributable to a combination of both types of errors discussed in Chapter 4; scale weight measure errors and linear analysis calculation errors. Another difference that was not directly investigated that may lead to resolving errors in this error range of 5 to 10 pounds is due to water content that had been added to the feed as many of the data points that calculate an underestimated weight are weighback feed data that may contain water added during the eating of the feed by the cow. As well, many of the calculated weights that overestimate weight occur during the period of 1/23/2012 and 1/26/2012 when the feed mixture had changed to incorporate a feed that encompassed a larger volume with the same amount of weight as the previous feed.

When all these uncontrollable externalities were considered, the ability of the system to nearly consistently calculate a weight value from the scan data that was within 4 pounds of the scale measured weight proves that this system is rather robust and quite accurate in monitoring dairy cow feed intake by means of machine vision utilizing the pilot SLI system and correlation assumptions of this research study.

The feed intake system developed in this study was a very closely correlated system to the actual amount of feed in the bin. The controlled testing data showed a tight correlation between separate testing datasets with feed of slightly differing dry matter content. This allowed interpretation of the results as having a linearly based relationship,

as expected since this was a linear system. The deviation from measured and actual weights was a direct result of the small number of test datasets used to produce the standard linear equation for the system and a few minor variables as mentioned in Chapters 3 and 4 and in this chapter. More calibrated and controlled testing datasets would have inevitably led to a more refined mathematical representation of the system as well as a minimization in variables influencing both the scale measured weights and image values, but the linear representation derived here was a quantifiably close approximation.

As can be seen from the resulting data, the ability of the system utilized in this study to measure the amount of feed distributed in the bin was closely correlated to the same value as read using weighing scales. The added benefit comes from the ability of the feed intake system used in this study to scan the amount of feed left over from the feeding period just as accurately. By calculating the difference from the amount fed to the amount left over, the producer is able to see exactly how much feed the cow actually consumed.

This greatly aids the producer in preparing future rations that best meet the needs of the individual cow. If any feed was left over, then the producer knows that the feed ration should be reduced or the dietary content revised in order to suit the needs of that cow. Alternatively, if there was no feed left over, then the producer may wish to steadily increase the amount of feed rationed to that individual cow to meet the desired amount by that cow. The producer can monitor small changes in eating habits to determine changes in the individual cow's health. This allows the producer to make timely decisions that

affect profitability and herd health, which is the basis of both precision dairy farming and this study.

The feed intake system used in this study was able to output values closely correlated to the same physical scale weights determined of the feed. This means that the system was able to determine the volume and thus the weight derivative of that value by means of machine vision, in particular, by means of SLI. Even when the feed was extremely biased in the feed bin, the system was capable of producing an output scan value that was within a few pounds of the actual physical scale weight of the same bin of feed. Therefore, this study proved that machine vision can be utilized to monitor dairy cow feed intake as accurately as any other current method, but with the added benefits of: (i) calculating the actual amount of feed consumed by the individual cow and not just the amount of feed distributed, (ii) maintaining an unobstructed workflow area, and (iii) that does not affect the feeding behavior of cow.

In future versions, the software should include the automated conversion of the scan value into an output weight value for the producer. Being able to see how much the cow consumes in pounds or kilograms will be much more beneficial to the individual producer than the scan values achieved in this study. The conversion already exists as outlined in this study, but should be integrated in the software. As well, the ability of the software to be able to automatically calculate the difference between the amount of output feed and amount of feed left over in order to produce a value of how much was actually consumed would be beneficial. The feeding scenario used in this research study was not best suited for this nor was it the main focus of the research, but these capabilities would be of use in future versions of the software used in this study.

The data collected here was all manually done so. In a consumer version, the scans should be automated to minimize the time used for individual scanning of feed output and weighbacks. It took approximately 5 hours to collect about 120 individual scans with a single system during the calibration testing. In an actual farm setting, the producer will not have 5 hours to spend taking scans daily. Therefore, the system should be able to scan the feed as soon as it is output and again just before the subsequent feeding automatically.

This technology would benefit from integration with other such precision dairy farming technologies. For instance, if this technology was used along with radio frequency identification (RFID) tags, then the computer could automatically save the scan data with that specific cow's RFID. In addition, the feed intake data collected could be used in conjunction with milk yield data in order to follow the ratio of feed intake to milk production as well as the effective nutritional use of feed by the cow. In this manner, the diet of the cow could be adjusted to increase milk yield and decrease the amount of feed that just goes to nutritional waste byproduct.

Another issue that will have to be addressed is the problem of inconsistent lighting in a real-world consumer version. If there is too much light, the image will be oversaturated and the resulting data will be useless as the contour of the feed will not be able to be collected for analysis. If there is too little light, the resultant image will not accurately resemble the contour of the feed, which will lead to deviances of accurate estimation. It will either overestimate or underestimate the actual weight. The greater the deviation will be from the actual contour and thus the actual weight with less light.

The camera and projector used in this study are not best suited for a dairy farm environment. An actual consumer system would need to include a camera and projector that would be able to be resilient against the changing weather and environmental conditions where it is used. Most importantly, the system would need to be able to remain cool as to avoid overheating. It would also need to be able to tolerate moisture and dust as both issues can quickly render an unfit camera or projector useless. The data collected in this study was conducted in a controlled environment, so such considerations were not necessary.

With all uncontrollable externalities considered that could have affected the precision of this system, it was determined that the resulting data collected in this study proves the capability of such a machine vision SLI 3D scanning system to accurately monitor dairy cow feed intake. When the statistical error data were studied and compared to the difference in calculated image weight value and scale measured weight value, it was easily discernible that this was a robust system that can be calibrated to differing feeds with different biasing and feeding situations by the end user. Once the system was calibrated, the user will have little need to change the system's weight calculation method if the feed used and the feeding habits remain fairly consistent. Such a system, therefore, has been proven that it can aid in precision dairy farming and can be used in conjunction with other technologies to increase yields and profits as well as monitor herd health.

The future system goal is to have a system such as the one depicted in Figure 5.15. In this system, the camera and projector are moved to the ceiling of the feeding area and out into the natural feeding environment. This is a more realistic workflow of

the dairy farm. Because we have utilized machine vision, such a system setup is possible in future research since the system remains out of the way of workflow and does not interrupt the natural feeding behavior of the dairy cows, which will give a more accurate representation of feed intake when compared to other technologies already in use.

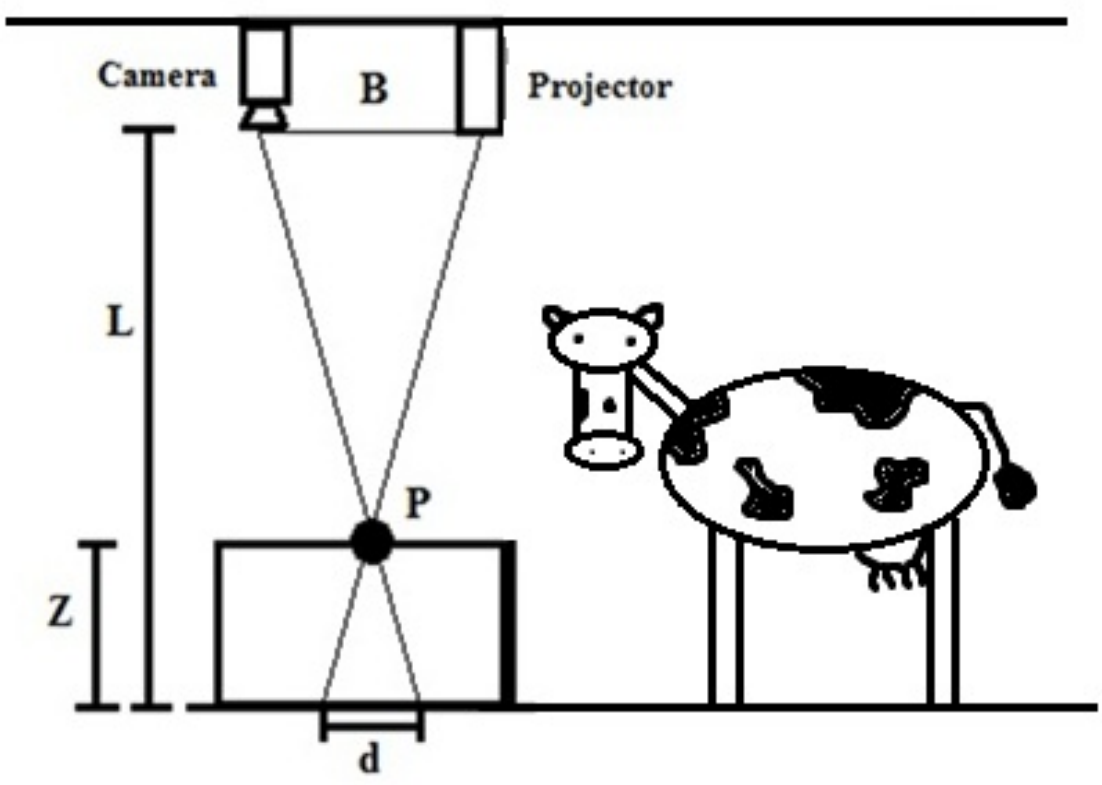

Figure 5.15 – Future SLI system shown as least intrusive as possible.

APPENDIX A

Calibration Tests Data Image Values

First Calibration Test Data Image Values		Second Calibration Test Data Image Values		Third Calibration Test Data Image Values		Fourth Calibration Test Data Image Values	
nothing6\PhaseImage.tif	-32.3393	0lbscan1\PhaseImage.tif	-31.8983	0lbscan1\PhaseImage.tif	-31.8970	0lbscan\PhaseImage.tif	-31.83646
0lbscan28\PhaseImage.tif	-31.6651	0lbscan2\PhaseImage.tif	-31.8968	0lbscan2\PhaseImage.tif	-31.9442	0lbscan2\PhaseImage.tif	-31.91238
0lbscan4\PhaseImage.tif	-31.7194	5lbscanblb\PhaseImage.tif	-31.2097	5lbscanbrb\PhaseImage.tif	-31.1419	5lbscanblb\PhaseImage.tif	-31.25987
0lbscan6_1\PhaseImage.tif	-32.0592	5lbscanbrb\PhaseImage.tif	-31.2875	5lbscancb\PhaseImage.tif	-31.1640	5lbscanbrb\PhaseImage.tif	-31.45773
0lbscan6_2\PhaseImage.tif	-32.0485	5lbscancb\PhaseImage.tif	-31.3008	5lbscanf\PhaseImage.tif	-31.3116	5lbscancb\PhaseImage.tif	-31.29342
5lbscanblb\PhaseImage.tif	-31.2442	5lbscanf\PhaseImage.tif	-31.4088	5lbscanf2\PhaseImage.tif	-31.3071	5lbscanf\PhaseImage.tif	-31.42941
5lbscanbrb\PhaseImage.tif	-31.2821	5lbscanf2\PhaseImage.tif	-31.4043	5lbscanflb\PhaseImage.tif	-31.4016	5lbscanf2\PhaseImage.tif	-31.42406
5lbscancb\PhaseImage.tif	-31.2134	5lbscanflb\PhaseImage.tif	-31.4238	5lbscanfr\PhaseImage.tif	-31.5113	5lbscanflb\PhaseImage.tif	-31.38334
5lbscanf1\PhaseImage.tif	-31.4052	5lbscanfrb\PhaseImage.tif	-31.6023	5lbscanfrb\PhaseImage.tif	-31.1070	5lbscanfrb\PhaseImage.tif	-31.49285
5lbscanf2\PhaseImage.tif	-31.2576	5lbscanh\PhaseImage.tif	-31.5389	5lbscanh\PhaseImage.tif	-31.4186	5lbscanh\PhaseImage.tif	-31.44562
5lbscanflb\PhaseImage.tif	-31.3264	10lbscanblb\PhaseImage.tif	-30.5541	10lbscanblb\PhaseImage.tif	-30.4759	10lbscanblb\PhaseImage.tif	-30.47428
5lbscanfrb\PhaseImage.tif	-31.5736	10lbscanbrb\PhaseImage.tif	-30.8450	10lbscanbrb\PhaseImage.tif	-30.6420	10lbscanbrb\PhaseImage.tif	-30.75735
10lbscanblb\PhaseImage.tif	-30.3654	10lbscancb\PhaseImage.tif	-30.4380	10lbscancb\PhaseImage.tif	-30.4689	10lbscancb\PhaseImage.tif	-30.48415
10lbscanbrb\PhaseImage.tif	-30.4198	10lbscanf\PhaseImage.tif	-30.7625	10lbscanf\PhaseImage.tif	-30.7359	10lbscanf\PhaseImage.tif	-30.80466
10lbscancb\PhaseImage.tif	-30.3365	10lbscanflb\PhaseImage.tif	-30.8888	10lbscanflb\PhaseImage.tif	-30.9177	10lbscanf2\PhaseImage.tif	-30.80888
10lbscanf\PhaseImage.tif	-30.5259	10lbscanfrb\PhaseImage.tif	-31.2290	10lbscanfrb\PhaseImage.tif	-31.1234	10lbscanflb\PhaseImage.tif	-30.67403
10lbscanflb\PhaseImage.tif	-30.5957	10lbscanh\PhaseImage.tif	-30.8935	10lbscanh\PhaseImage.tif	-30.7567	10lbscanfrb\PhaseImage.tif	-30.98881
10lbscanfrb\PhaseImage.tif	-30.8561	15lbscanblb\PhaseImage.tif	-29.8215	15lbscanblb\PhaseImage.tif	-29.7627	10lbscanh\PhaseImage.tif	-30.77599
10lbscanh\PhaseImage.tif	-30.6911	15lbscanbrb\PhaseImage.tif	-30.2089	15lbscanbrb\PhaseImage.tif	-30.1632	15lbscanblb\PhaseImage.tif	-29.74825
15lbscanblb\PhaseImage.tif	-29.6336	15lbscancb\PhaseImage.tif	-29.5734	15lbscancb\PhaseImage.tif	-29.6307	15lbscanbrb\PhaseImage.tif	-29.90702
15lbscanbrb\PhaseImage.tif	-29.8373	15lbscanf\PhaseImage.tif	-30.1784	15lbscanf\PhaseImage.tif	-30.0919	15lbscancb\PhaseImage.tif	-29.49429
15lbscanf\PhaseImage.tif	-29.9922	15lbscanf2\PhaseImage.tif	-30.1919	15lbscanflb\PhaseImage.tif	-30.1121	15lbscanf\PhaseImage.tif	-30.21887
15lbscanflb\PhaseImage.tif	-30.0117	15lbscanflb\PhaseImage.tif	-30.2511	15lbscanfrb\PhaseImage.tif	-30.4279	15lbscanf2\PhaseImage.tif	-30.22362
15lbscanfrb\PhaseImage.tif	-30.1885	15lbscanfrb\PhaseImage.tif	-30.6131	15lbscanh\PhaseImage.tif	-30.0443	15lbscanflb\PhaseImage.tif	-30.14531
15lbscanh\PhaseImage.tif	-30.0947	15lbscanh\PhaseImage.tif	-30.0744	20lbscanblb\PhaseImage.tif	-29.0395	15lbscanfrb\PhaseImage.tif	-30.32433
20lbscanblb\PhaseImage.tif	-29.0274	20lbscanblb\PhaseImage.tif	-28.9632	20lbscanblb2\PhaseImage.tif	-28.6913	15lbscanh\PhaseImage.tif	-30.00529
20lbscanbrb\PhaseImage.tif	-29.2640	20lbscanblb2\PhaseImage.tif	-28.7699	20lbscanbrb\PhaseImage.tif	-29.6263	20lbscanblb\PhaseImage.tif	-29.13877
20lbscanf\PhaseImage.tif	-29.4744	20lbscanbrb\PhaseImage.tif	-29.4610	20lbscanbrb2\PhaseImage.tif	-29.4097	20lbscanbrb\PhaseImage.tif	-29.29835
20lbscanflb\PhaseImage.tif	-29.3093	20lbscanbrb2\PhaseImage.tif	-29.3415	20lbscancb\PhaseImage.tif	-28.6818	20lbscancb\PhaseImage.tif	-28.9337
20lbscanfrb\PhaseImage.tif	-29.5912	20lbscancb\PhaseImage.tif	-28.6846	20lbscanf\PhaseImage.tif	-29.5011	20lbscanf\PhaseImage.tif	-29.55486
20lbscanh\PhaseImage.tif	-29.4732	20lbscanf\PhaseImage.tif	-29.4705	20lbscanf2\PhaseImage.tif	-29.5113	20lbscanf2\PhaseImage.tif	-29.57931
25lbscanblb\PhaseImage.tif	-28.3026	20lbscanf2\PhaseImage.tif	-29.4731	20lbscanflb\PhaseImage.tif	-29.5169	20lbscanflb\PhaseImage.tif	-29.45018
25lbscanbrb\PhaseImage.tif	-28.7177	20lbscanflb\PhaseImage.tif	-29.5284	20lbscanflb2\PhaseImage.tif	-29.3370	20lbscanfrb\PhaseImage.tif	-29.74791
25lbscanf\PhaseImage.tif	-28.9585	20lbscanflb2\PhaseImage.tif	-29.0417	20lbscanfrb\PhaseImage.tif	-29.7268	20lbscanh\PhaseImage.tif	-29.49153
25lbscanflb\PhaseImage.tif	-28.6925	20lbscanfrb\PhaseImage.tif	-29.6970	20lbscanfrb2\PhaseImage.tif	-29.6516	25lbscanblb\PhaseImage.tif	-28.569
25lbscanfrb\PhaseImage.tif	-28.9723	20lbscanfrb2\PhaseImage.tif	-29.5481	20lbscanh\PhaseImage.tif	-29.4938	25lbscanbrb\PhaseImage.tif	-28.74869
25lbscanh\PhaseImage.tif	-28.9241	20lbscanh\PhaseImage.tif	-29.4869	20lbscanh2\PhaseImage.tif	-29.4581	25lbscancb\PhaseImage.tif	-28.1861
30lbscanblb\PhaseImage.tif	-27.2582	20lbscanh2\PhaseImage.tif	-29.4807	25lbscanblb\PhaseImage.tif	-28.5024	25lbscanf\PhaseImage.tif	-29.03823
30lbscanbrb\PhaseImage.tif	-27.9444	25lbscanblb\PhaseImage.tif	-35.8368	25lbscanblb2\PhaseImage.tif	-28.3129	25lbscanf2\PhaseImage.tif	-29.04477
30lbscanf\PhaseImage.tif	-28.3560	25lbscanblb2\PhaseImage.tif	-28.4866	25lbscanbrb\PhaseImage.tif	-28.9505	25lbscanflb\PhaseImage.tif	-28.75997
30lbscanflb\PhaseImage.tif	-28.0508	25lbscanbrb\PhaseImage.tif	-28.9539	25lbscanbrb2\PhaseImage.tif	-28.8383	25lbscanfrb\PhaseImage.tif	-29.02164
30lbscanfrb\PhaseImage.tif	-28.1895	25lbscanbrb2\PhaseImage.tif	-28.7999	25lbscancb\PhaseImage.tif	-28.0756	25lbscanh\PhaseImage.tif	-28.80438
30lbscanh\PhaseImage.tif	-28.3454	25lbscancb\PhaseImage.tif	-28.1560	25lbscanf\PhaseImage.tif	-28.9624	30lbscanblb\PhaseImage.tif	-27.86382
30lbscanblb\PhaseImage.tif	-27.5120	25lbscanf\PhaseImage.tif	-28.9716	25lbscanf2\PhaseImage.tif	-28.9646	30lbscanbrb\PhaseImage.tif	-28.09839
30lbscanbrb\PhaseImage.tif	-28.0978	25lbscanf2\PhaseImage.tif	-28.9731	25lbscanflb\PhaseImage.tif	-28.9597	30lbscancb\PhaseImage.tif	-27.58835
30lbscanf\PhaseImage.tif	-28.7299	25lbscanflb\PhaseImage.tif	-29.0127	25lbscanflb2\PhaseImage.tif	-28.8572	30lbscanf\PhaseImage.tif	-28.48376
30lbscanflb\PhaseImage.tif	-28.1561	25lbscanflb2\PhaseImage.tif	-28.9201	25lbscanfrb\PhaseImage.tif	-29.2413	30lbscanf2\PhaseImage.tif	-28.4874
30lbscanfrb\PhaseImage.tif	-28.4581	25lbscanfrb\PhaseImage.tif	-29.2750	25lbscanfrb2\PhaseImage.tif	-29.0670	30lbscanflb\PhaseImage.tif	-28.18145
30lbscanh\PhaseImage.tif	-28.6071	25lbscanfrb2\PhaseImage.tif	-29.1944	25lbscanh\PhaseImage.tif	-29.1326	30lbscanfrb\PhaseImage.tif	-28.34067
35lbscanblb\PhaseImage.tif	-27.0736	25lbscanh\PhaseImage.tif	-29.0435	25lbscanh2\PhaseImage.tif	-29.0980	30lbscanh\PhaseImage.tif	-28.25338
35lbscanbrb\PhaseImage.tif	-27.8108	25lbscanh2\PhaseImage.tif	-29.0536	30lbscanblb\PhaseImage.tif	-27.9236	35lbscanblb\PhaseImage.tif	-27.29985
35lbscanf\PhaseImage.tif	-28.1063	30lbscanblb\PhaseImage.tif	-27.9828	30lbscanblb2\PhaseImage.tif	-27.4246	35lbscanbrb\PhaseImage.tif	-27.46117
35lbscanflb\PhaseImage.tif	-27.8604	30lbscanblb2\PhaseImage.tif	-27.6828	30lbscanbrb\PhaseImage.tif	-28.4542	35lbscancb\PhaseImage.tif	-26.97098
35lbscanfrb\PhaseImage.tif	-28.2236	30lbscanbrb\PhaseImage.tif	-28.3583	30lbscanbrb2\PhaseImage.tif	-28.3015	35lbscanf\PhaseImage.tif	-27.86144
35lbscanh\PhaseImage.tif	-28.0152	30lbscanbrb2\PhaseImage.tif	-28.2344	30lbscancb\PhaseImage.tif	-27.4319	35lbscanf2\PhaseImage.tif	-27.86391
40lbscanblb\PhaseImage.tif	-26.8029	30lbscancb\PhaseImage.tif	-27.3981	30lbscanf\PhaseImage.tif	-28.2502	35lbscanflb\PhaseImage.tif	-27.53281
40lbscanbrb\PhaseImage.tif	-27.1748	30lbscanf\PhaseImage.tif	-28.3504	30lbscanf2\PhaseImage.tif	-28.2588	35lbscanfrb\PhaseImage.tif	-27.74224
40lbscanf\PhaseImage.tif	-27.6668	30lbscanf2\PhaseImage.tif	-28.3548	30lbscanflb\PhaseImage.tif	-28.2460	35lbscanh\PhaseImage.tif	-27.75715
40lbscanflb\PhaseImage.tif	-27.2687	30lbscanflb\PhaseImage.tif	-28.3245	30lbscanflb2\PhaseImage.tif	-28.1302	40lbscanblb\PhaseImage.tif	-26.84784
40lbscanfrb\PhaseImage.tif	-27.4396	30lbscanflb2\PhaseImage.tif	-28.2237	30lbscanfrb\PhaseImage.tif	-28.5107	40lbscanbrb\PhaseImage.tif	-26.89026
40lbscanh\PhaseImage.tif	-27.6566	30lbscanfrb\PhaseImage.tif	-28.6310	30lbscanfrb2\PhaseImage.tif	-28.4213	40lbscancb\PhaseImage.tif	-26.46658
45lbscanblb\PhaseImage.tif	-26.2426	30lbscanfrb2\PhaseImage.tif	-28.5631	30lbscanh\PhaseImage.tif	-28.4722	40lbscanf\PhaseImage.tif	-27.2832
45lbscanbrb\PhaseImage.tif	-26.7238	30lbscanh\PhaseImage.tif	-28.4834	30lbscanh2\PhaseImage.tif	-28.4899	40lbscanf2\PhaseImage.tif	-27.28652
45lbscanf\PhaseImage.tif	-27.0926	30lbscanh2\PhaseImage.tif	-28.4960	35lbscanblb\PhaseImage.tif	-27.1689	40lbscanflb\PhaseImage.tif	-26.99332
45lbscanflb\PhaseImage.tif	-26.7462	35lbscanblb\PhaseImage.tif	-27.1704	35lbscanblb2\PhaseImage.tif	-26.7761	40lbscanfrb\PhaseImage.tif	-27.2713
45lbscanfrb\PhaseImage.tif	-27.1468	35lbscanblb2\PhaseImage.tif	-26.6929	35lbscanbrb\PhaseImage.tif	-27.5647	40lbscanh\PhaseImage.tif	-27.28075
45lbscanh\PhaseImage.tif	-27.1154	35lbscanbrb\PhaseImage.tif	-27.7700	35lbscanbrb2\PhaseImage.tif	-27.4440	45lbscanblb\PhaseImage.tif	-26.40578
47lbscanblb\PhaseImage.tif	-26.0053	35lbscanbrb2\PhaseImage.tif	-27.6012	35lbscancb\PhaseImage.tif	-26.6382	45lbscanbrb\PhaseImage.tif	-26.46189
47lbscanbrb\PhaseImage.tif	-26.3275	35lbscancb\PhaseImage.tif	-26.7023	35lbscanf\PhaseImage.tif	-27.7919	45lbscancb\PhaseImage.tif	-25.93342
47lbscanf\PhaseImage.tif	-26.8381	35lbscanf\PhaseImage.tif	-27.8303	35lbscanf2\PhaseImage.tif	-27.7975	45lbscanf\PhaseImage.tif	-26.79866
47lbscanflb\PhaseImage.tif	-26.3037	35lbscanf2\PhaseImage.tif	-27.8361	35lbscanflb\PhaseImage.tif	-27.6886	45lbscanf2\PhaseImage.tif	-26.80602
47lbscanfrb\PhaseImage.tif	-26.5903	35lbscanflb\PhaseImage.tif	-27.7362	35lbscanflb2\PhaseImage.tif	-27.5471	45lbscanflb\PhaseImage.tif	-26.41955
47lbscanh1\PhaseImage.tif	-27.2239	35lbscanflb2\PhaseImage.tif	-27.5226	35lbscanfrb\PhaseImage.tif	-28.1148	45lbscanfrb\PhaseImage.tif	-26.60508
47lbscanh2\PhaseImage.tif	-27.2160	35lbscanfrb\PhaseImage.tif	-27.9356	35lbscanfrb2\PhaseImage.tif	-27.9709	45lbscanh\PhaseImage.tif	-26.79316

Calibration Tests Data Image Values (Continued)

First Calibration Test Data Image Values	
48lbscanblb\PhaseImage.tif	-25.4204
48lbscanbrb\PhaseImage.tif	-26.0940
48lbscanf\PhaseImage.tif	-26.6400
48lbscanflb\PhaseImage.tif	-26.2734
48lbscanfrb\PhaseImage.tif	-26.4490
48lbscanh\PhaseImage.tif	-27.0592
49lbscanblb\PhaseImage.tif	-25.7000
49lbscanbrb\PhaseImage.tif	-25.8043
49lbscanf\PhaseImage.tif	-26.5595
49lbscanflb\PhaseImage.tif	-25.8795
49lbscanfrb\PhaseImage.tif	-26.2081
49lbscanh\PhaseImage.tif	-26.5949
50lbscanblb\PhaseImage.tif	-25.7285
50lbscanbrb\PhaseImage.tif	-26.0261
50lbscanf\PhaseImage.tif	-26.1043
50lbscanflb\PhaseImage.tif	-25.9495
50lbscanfrb\PhaseImage.tif	-26.2436
50lbscanh\PhaseImage.tif	-26.3657
50lbscanblb\PhaseImage.tif	-25.7645
50lbscanbrb\PhaseImage.tif	-26.2216
50lbscancb\PhaseImage.tif	-25.7019
50lbscanf\PhaseImage.tif	-26.5759
50lbscanflb\PhaseImage.tif	-26.2825
50lbscanfrb\PhaseImage.tif	-26.5017
50lbscanh\PhaseImage.tif	-26.5627
51lbscanblb\PhaseImage.tif	-25.5581
51lbscanbrb\PhaseImage.tif	-26.0284
51lbscanf\PhaseImage.tif	-26.2311
51lbscanflb\PhaseImage.tif	-26.0121
51lbscanfrb\PhaseImage.tif	-26.2250
51lbscanh\PhaseImage.tif	-26.5888
52lbscanblb\PhaseImage.tif	-25.4515
52lbscanbrb\PhaseImage.tif	-26.0688
52lbscanf\PhaseImage.tif	-26.2547
52lbscanflb\PhaseImage.tif	-25.9763
52lbscanfrb\PhaseImage.tif	-26.0672
52lbscanh\PhaseImage.tif	-26.4986
53lbscanblb\PhaseImage.tif	-25.2862
53lbscanbrb\PhaseImage.tif	-25.3779
53lbscanf\PhaseImage.tif	-26.1927
53lbscanflb\PhaseImage.tif	-25.5402
53lbscanfrb\PhaseImage.tif	-25.9359
53lbscanh\PhaseImage.tif	-26.2465
55lbscanblb\PhaseImage.tif	-25.4260
55lbscanbrb\PhaseImage.tif	-25.7055
55lbscancb\PhaseImage.tif	-25.2574
55lbscanf1\PhaseImage.tif	-25.8613
55lbscanf2\PhaseImage.tif	-25.6616
55lbscanflb\PhaseImage.tif	-25.8158
55lbscanfrb\PhaseImage.tif	-25.8039
60lbscanblb\PhaseImage.tif	-24.8678
60lbscanbrb\PhaseImage.tif	-25.2171
60lbscancb\PhaseImage.tif	-24.6641
60lbscanf28\PhaseImage.tif	-25.0535
60lbscanf4\PhaseImage.tif	-25.0594
60lbscanf6\PhaseImage.tif	-25.0524
60lbscanflb\PhaseImage.tif	-25.3375
60lbscanfrb\PhaseImage.tif	-25.3570

Second Calibration Test Data Image Values	
35lbscanfrb2\PhaseImage.tif	-27.8810
35lbscanh\PhaseImage.tif	-27.9546
35lbscanh2\PhaseImage.tif	-27.9518
40lbscanblb\PhaseImage.tif	-25.7964
40lbscanblb22\PhaseImage.tif	-26.4002
40lbscanbrb\PhaseImage.tif	-27.1860
40lbscanbrb2\PhaseImage.tif	-27.1368
40lbscancb\PhaseImage.tif	-25.9993
40lbscanf\PhaseImage.tif	-27.2907
40lbscanf2\PhaseImage.tif	-27.3008
40lbscanflb\PhaseImage.tif	-27.0433
40lbscanflb2\PhaseImage.tif	-26.8434
40lbscanfrb\PhaseImage.tif	-27.2615
40lbscanfrb2\PhaseImage.tif	-27.1365
40lbscanh\PhaseImage.tif	-27.7613
40lbscanh2\PhaseImage.tif	-27.7871
45lbscanblb\PhaseImage.tif	-26.0694
45lbscanblb2\PhaseImage.tif	-25.4334
45lbscanbrb\PhaseImage.tif	-26.6864
45lbscanbrb2\PhaseImage.tif	-26.4446
45lbscancb\PhaseImage.tif	-25.5348
45lbscanf\PhaseImage.tif	-26.7372
45lbscanf2\PhaseImage.tif	-26.7404
45lbscanflb\PhaseImage.tif	-26.4795
45lbscanflb2\PhaseImage.tif	-26.3130
45lbscanfrb\PhaseImage.tif	-26.9383
45lbscanfrb2\PhaseImage.tif	-26.7300
45lbscanh\PhaseImage.tif	-27.1491
45lbscanh2\PhaseImage.tif	-27.1485
50lbscanblb\PhaseImage.tif	-25.8695
50lbscanblb2\PhaseImage.tif	-25.5995
50lbscanbrb\PhaseImage.tif	-26.0394
50lbscanbrb2\PhaseImage.tif	-25.8042
50lbscancb\PhaseImage.tif	-25.0787
50lbscanf\PhaseImage.tif	-26.3012
50lbscanf2\PhaseImage.tif	-26.3085
50lbscanflb\PhaseImage.tif	-26.3689
50lbscanflb2\PhaseImage.tif	-26.0099
50lbscanfrb\PhaseImage.tif	-26.3654
50lbscanfrb2\PhaseImage.tif	-26.0126
50lbscanh\PhaseImage.tif	-26.6340
50lbscanh2\PhaseImage.tif	-26.6152
55lbscanblb\PhaseImage.tif	-25.2744
55lbscanblb2\PhaseImage.tif	-24.5791
55lbscanbrb\PhaseImage.tif	-25.4430
55lbscanbrb2\PhaseImage.tif	-25.3287
55lbscancb\PhaseImage.tif	-24.4895
55lbscanf\PhaseImage.tif	-25.7857
55lbscanf2\PhaseImage.tif	-25.7942
55lbscanflb\PhaseImage.tif	-25.2748
55lbscanflb2\PhaseImage.tif	-24.8597
55lbscanfrb\PhaseImage.tif	-25.7899
55lbscanfrb2\PhaseImage.tif	-25.3180
55lbscanh\PhaseImage.tif	-25.9694
55lbscanh2\PhaseImage.tif	-25.9343
60lbscanblb\PhaseImage.tif	-25.0869
60lbscanbrb\PhaseImage.tif	-25.1388
60lbscancb\PhaseImage.tif	-24.6598
60lbscanf\PhaseImage.tif	-25.2706
60lbscanf2\PhaseImage.tif	-25.2753
60lbscanflb\PhaseImage.tif	-25.0339
60lbscanfrb\PhaseImage.tif	-25.1616
60lbscanh\PhaseImage.tif	-25.5787

Third Calibration Test Data Image Values	
35lbscanh\PhaseImage.tif	-28.0991
35lbscanh2\PhaseImage.tif	-28.0144
40lbscanblb\PhaseImage.tif	-26.5328
40lbscanblb2\PhaseImage.tif	-25.8466
40lbscanbrb\PhaseImage.tif	-27.1655
40lbscanbrb2\PhaseImage.tif	-26.9142
40lbscancb\PhaseImage.tif	-26.2059
40lbscanf\PhaseImage.tif	-27.2462
40lbscanf2\PhaseImage.tif	-27.2268
40lbscanflb\PhaseImage.tif	-27.1701
40lbscanflb2\PhaseImage.tif	-27.0223
40lbscanfrb\PhaseImage.tif	-27.3010
40lbscanh\PhaseImage.tif	-27.4346
40lbscanh2\PhaseImage.tif	-27.4095
45lbscanblb\PhaseImage.tif	-26.2476
45lbscanblb2\PhaseImage.tif	-25.5193
45lbscanbrb\PhaseImage.tif	-26.5061
45lbscanbrb2\PhaseImage.tif	-26.2532
45lbscancb\PhaseImage.tif	-25.6607
45lbscanf\PhaseImage.tif	-26.6402
45lbscanf2\PhaseImage.tif	-26.6479
45lbscanflb\PhaseImage.tif	-26.6335
45lbscanflb2\PhaseImage.tif	-26.3901
45lbscanfrb\PhaseImage.tif	-27.0045
45lbscanfrb2\PhaseImage.tif	-26.7189
45lbscanh\PhaseImage.tif	-27.1516
45lbscanh2\PhaseImage.tif	-27.1333
50lbscanblb\PhaseImage.tif	-25.7935
50lbscanblb2\PhaseImage.tif	-25.1455
50lbscanbrb\PhaseImage.tif	-26.1377
50lbscanbrb2\PhaseImage.tif	-25.8660
50lbscancb\PhaseImage.tif	-25.3339
50lbscanf\PhaseImage.tif	-26.2651
50lbscanf2\PhaseImage.tif	-26.2671
50lbscanflb\PhaseImage.tif	-26.1607
50lbscanflb2\PhaseImage.tif	-25.8220
50lbscanfrb\PhaseImage.tif	-26.2888
50lbscanfrb2\PhaseImage.tif	-26.0631
50lbscanh\PhaseImage.tif	-26.1775
50lbscanh2\PhaseImage.tif	-26.1635

Fourth Calibration Test Data Image Values	
50lbscanblb\PhaseImage.tif	-25.62988
50lbscanbrb\PhaseImage.tif	-25.7623
50lbscancb\PhaseImage.tif	-25.29307
50lbscanf\PhaseImage.tif	-25.95449
50lbscanf2\PhaseImage.tif	-25.9656
50lbscanflb\PhaseImage.tif	-25.71993
50lbscanfrb\PhaseImage.tif	-25.856
50lbscanh\PhaseImage.tif	-25.93728
55lbscanblb\PhaseImage.tif	-24.8308
55lbscanbrb\PhaseImage.tif	-25.14877
55lbscancb\PhaseImage.tif	-24.85447
55lbscanf\PhaseImage.tif	-25.43379
55lbscanf2\PhaseImage.tif	-25.43965
55lbscanflb\PhaseImage.tif	-25.09143
55lbscanfrb\PhaseImage.tif	-25.08434
55lbscanh\PhaseImage.tif	-25.29058
60lbscanblb\PhaseImage.tif	-24.05432
60lbscanbrb\PhaseImage.tif	-24.215
60lbscancb\PhaseImage.tif	-24.01289
60lbscanf\PhaseImage.tif	-24.33737
60lbscanf2\PhaseImage.tif	-24.34255
60lbscanflb\PhaseImage.tif	-24.2462
60lbscanfrb\PhaseImage.tif	-24.30558
60lbscanh\PhaseImage.tif	-24.63097

APPENDIX B

Control Test Data Results

FileName	ImageValue	ImageWeight	ScaleWeight	Difference	Abs. Diff.
1_7_311_f(50)\PhaseImage.tif	-25.75762743	51.69390455	50	1.693904549	1.693904549
1_7_311_w(37)\PhaseImage.tif	-28.48841997	28.49260859	37	-8.507391409	8.507391409
1_7_479_f(50)\PhaseImage.tif	-25.25988774	55.92278899	50	5.922788992	5.922788992
1_7_479_w(48)\PhaseImage.tif	-27.04222506	40.77973607	48	-7.220263933	7.220263933
1_7_x33_f(50)\PhaseImage.tif	-26.17910682	48.11294119	50	-1.887058809	1.887058809
1_7_x33_w(67)\PhaseImage.tif	-25.23320117	56.14952275	67	-10.85047725	10.85047725
1_8_311_f1(50)\PhaseImage.tif	-25.52940787	53.63289834	50	3.632898341	3.632898341
1_8_311_f2(50)\PhaseImage.tif	-25.18651258	56.54619726	50	6.546197259	6.546197259
1_8_311_w(43)\PhaseImage.tif	-27.75522629	34.72195165	43	-8.278048348	8.278048348
1_8_479_f1(50)\PhaseImage.tif	-25.48394333	54.01917305	50	4.019173052	4.019173052
1_8_479_f2(50)\PhaseImage.tif	-25.24513011	56.04817242	50	6.048172417	6.048172417
1_8_479_w1(70)\PhaseImage.tif	-23.72531436	68.96079558	70	-1.039204422	1.039204422
1_8_479_w2(11)\PhaseImage.tif	-29.98559506	15.77234443	11	4.772344432	4.772344432
1_8_x33_f1(50)\PhaseImage.tif	-25.32466651	55.37241712	50	5.372417119	5.372417119
1_8_x33_f2(50)\PhaseImage.tif	-25.16935732	56.69195141	50	6.691951411	6.691951411
1_8_x33_w1(70)\PhaseImage.tif	-24.49195658	62.44726778	70	-7.552732219	7.552732219
1_8_x33_w2(22)\PhaseImage.tif	-29.05210057	23.7034786	22	1.703478597	1.703478597
1_9_311_f1(50)\PhaseImage.tif	-25.39899291	54.74092684	50	4.740926845	4.740926845
1_9_311_f2(50)\PhaseImage.tif	-25.43190693	54.46128355	50	4.461283548	4.461283548
1_9_311_w1(48)\PhaseImage.tif	-27.05845154	40.64187303	48	-7.35812697	7.35812697
1_9_311_w2(1)\PhaseImage.tif	-32.01219953	-1.446045256	1	-2.446045256	2.446045256
1_9_479_f1(50)\PhaseImage.tif	-25.22133667	56.25032563	50	6.250325626	6.250325626
1_9_479_f2(50)\PhaseImage.tif	-25.43706308	54.41747594	50	4.417475943	4.417475943
1_9_479_w1(68)\PhaseImage.tif	-24.52337513	62.18033029	68	-5.819669712	5.819669712
1_9_479_w2(34)\PhaseImage.tif	-27.49779976	36.90909294	34	2.909092939	2.909092939
1_9_x33_f1(50)\PhaseImage.tif	-25.27029123	55.83439909	50	5.834399093	5.834399093
1_9_x33_f2(50)\PhaseImage.tif	-25.67945801	52.3580458	50	2.358045803	2.358045803
1_9_x33_w1(48)\PhaseImage.tif	-26.46237664	45.70623079	48	-2.293769211	2.293769211
1_9_x33_w2(50)\PhaseImage.tif	-25.67748519	52.37480726	50	2.374807262	2.374807262
1_10_311_f1(50)\PhaseImage.tif	-25.46209617	54.20479038	50	4.204790378	4.204790378
1_10_311_f2(50)\PhaseImage.tif	-24.88064972	59.14486216	50	9.144862164	9.144862164
1_10_311_w1(0)\PhaseImage.tif	-31.98372555	-1.204125309	0	-1.204125309	1.204125309
1_10_311_w2(39)\PhaseImage.tif	-27.63762891	35.72107979	39	-3.278920209	3.278920209
1_10_479_f1(50)\PhaseImage.tif	-25.20122262	56.42121816	50	6.42121816	6.42121816
1_10_479_f2(50)\PhaseImage.tif	-25.74286441	51.81933381	50	1.819333815	1.819333815
1_10_479_w1(47)\PhaseImage.tif	-26.75498054	43.22021627	47	-3.779783729	3.779783729
1_10_479_w2(50)\PhaseImage.tif	-25.86665945	50.76754927	50	0.767549271	0.767549271
1_10_x33_f1(50)\PhaseImage.tif	-25.37454065	54.94867761	50	4.94867761	4.94867761
1_10_x33_f2(50)\PhaseImage.tif	-25.75026837	51.75642846	50	1.756428458	1.756428458
1_10_x33_w1(49)\PhaseImage.tif	-26.3183208	46.93015459	49	-2.069845406	2.069845406
1_10_x33_w2(49)\PhaseImage.tif	-26.06847834	49.05286033	49	0.052860334	0.052860334
1_11_311_f1(52)\PhaseImage.tif	-26.32655425	46.86020179	52	-5.139798208	5.139798208
1_11_311_f2(51)\PhaseImage.tif	-26.43749356	45.91764177	51	-5.082358225	5.082358225
1_11_311_w1(0)\PhaseImage.tif	-31.97467844	-1.127259482	0	-1.127259482	1.127259482
1_11_311_w2(48)\PhaseImage.tif	-28.14442313	31.41526652	48	-16.58473348	16.58473348

Control Test Data Results (Continued)

FileName	ImageValue	ImageWeight	ScaleWeight	Difference	Abs. Diff.
1_11_479_f1(51)\PhaseImage.tif	-26.34149938	46.73322532	51	-4.266774681	4.266774681
1_11_479_f2(51)\PhaseImage.tif	-25.95522489	50.01508169	51	-0.984918314	0.984918314
1_11_479_w1(67)\PhaseImage.tif	-24.58713627	61.63860436	67	-5.361395639	5.361395639
1_11_479_w2(25)\PhaseImage.tif	-28.34829603	29.68312636	25	4.683126361	4.683126361
1_11_x33_f1(46)\PhaseImage.tif	-26.92606457	41.76665612	46	-4.233343877	4.233343877
1_11_x33_f2(45)\PhaseImage.tif	-26.6534102	44.08317583	45	-0.916824168	0.916824168
1_11_x33_w1(54)\PhaseImage.tif	-25.91503033	50.3565817	54	-3.643418298	3.643418298
1_11_x33_w2(52)\PhaseImage.tif	-25.69741486	52.20548123	52	0.205481233	0.205481233
1_12_311_f1(50)\PhaseImage.tif	-25.95143795	50.04725619	50	0.047256189	0.047256189
1_12_311_f2(50)\PhaseImage.tif	-26.36495714	46.53392406	50	-3.466075938	3.466075938
1_12_311_w1(0)\PhaseImage.tif	-31.81274495	0.248556045	0	0.248556045	0.248556045
1_12_311_w2(44)\PhaseImage.tif	-27.80310171	34.31519366	44	-9.68480634	9.68480634
1_12_479_f1(50)\PhaseImage.tif	-25.88931699	50.57504679	50	0.575046792	0.575046792
1_12_479_f2(50)\PhaseImage.tif	-25.93514221	50.18570765	50	0.185707649	0.185707649
1_12_479_w1(64)\PhaseImage.tif	-25.31258331	55.47507807	64	-8.524921932	8.524921932
1_12_479_w2(24)\PhaseImage.tif	-29.20989815	22.36280248	24	-1.63719752	1.63719752
1_12_x33_f1(45)\PhaseImage.tif	-26.40031948	46.23347935	45	1.233479349	1.233479349
1_12_x33_f2(45)\PhaseImage.tif	-26.54890173	44.9710983	45	-0.028901696	0.028901696
1_12_x33_w1(65)\PhaseImage.tif	-25.22408744	56.22695467	65	-8.773045334	8.773045334
1_12_x33_w2(21)\PhaseImage.tif	-29.47227859	20.13357189	21	-0.866428106	0.866428106
1_14_311_f1(50)\PhaseImage.tif	-25.93188659	50.21336795	50	0.213367953	0.213367953
1_14_311_f2(50)\PhaseImage.tif	-25.91729616	50.33733082	50	0.337330824	0.337330824
1_14_311_w1(0)\PhaseImage.tif	-31.81571609	0.223312751	0	0.223312751	0.223312751
1_14_311_w2(41)\PhaseImage.tif	-28.10587299	31.74279533	41	-9.257204666	9.257204666
1_14_479_f1(45)\PhaseImage.tif	-25.99924546	49.64107513	45	4.641075131	4.641075131
1_14_479_f2(45)\PhaseImage.tif	-26.68517524	43.8132945	45	-1.186705499	1.186705499
1_14_479_w1(16)\PhaseImage.tif	-29.74384754	17.82627406	16	1.826274059	1.826274059
1_14_479_w2(48)\PhaseImage.tif	-27.07568837	40.49542592	48	-7.504574085	7.504574085
1_14_497_f1(50)\PhaseImage.tif	-25.84808496	50.92536144	50	0.925361441	0.925361441
1_14_497_f2(50)\PhaseImage.tif	-25.87725713	50.67750951	50	0.677509506	0.677509506
1_14_497_w1(1)\PhaseImage.tif	-31.76904972	0.619798505	1	-0.380201495	0.380201495
1_14_x33_f1(45)\PhaseImage.tif	-26.58663899	44.6504759	45	-0.349524104	0.349524104
1_14_x33_f2(45)\PhaseImage.tif	-26.18630138	48.05181493	45	3.051814934	3.051814934
1_14_x33_w1(46)\PhaseImage.tif	-27.09270591	40.35084186	46	-5.649158143	5.649158143
1_14_x33_w2(48)\PhaseImage.tif	-27.14252794	39.92754509	48	-8.072454915	8.072454915
1_15_311_f1(50)\PhaseImage.tif	-26.11608891	48.64835248	50	-1.351647522	1.351647522
1_15_311_f2(50)\PhaseImage.tif	-25.8520469	50.8917001	50	0.8917001	0.8917001
1_15_311_w1(0)\PhaseImage.tif	-31.9082656	-0.563004264	0	-0.563004264	0.563004264
1_15_311_w2(43)\PhaseImage.tif	-28.07661549	31.99137224	43	-11.00862776	11.00862776
1_15_479_f1(45)\PhaseImage.tif	-26.49884986	45.39634787	45	0.396347872	0.396347872
1_15_479_f2(45)\PhaseImage.tif	-26.47842146	45.56991112	45	0.569911115	0.569911115
1_15_479_w1(25)\PhaseImage.tif	-28.91751397	24.84695009	25	-0.153049906	0.153049906
1_15_479_w2(64)\PhaseImage.tif	-25.48535907	54.00714468	64	-9.992855324	9.992855324
1_15_497_f1(50)\PhaseImage.tif	-25.94356396	50.11415494	50	0.114154941	0.114154941
1_15_497_f2(50)\PhaseImage.tif	-25.72217682	51.99509924	50	1.995099237	1.995099237

Control Test Data Results (Continued)

FileName	ImageValue	ImageWeight	ScaleWeight	Difference	Abs. Diff.
1_15_497_w1(0)\PhaseImage.tif	-31.98916307	-1.250323446	0	-1.250323446	1.250323446
1_15_497_w2(19)\PhaseImage.tif	-29.84305255	16.98341077	19	-2.016589233	2.016589233
1_15_x33_f1(45)\PhaseImage.tif	-26.95258206	41.54135891	45	-3.458641085	3.458641085
1_15_x33_f2(45)\PhaseImage.tif	-26.74386273	43.31467523	45	-1.685324768	1.685324768
1_15_x33_w1(50)\PhaseImage.tif	-27.14064638	39.9435312	50	-10.0564688	10.0564688
1_15_x33_w2(41)\PhaseImage.tif	-27.24585532	39.04965743	41	-1.95034257	1.95034257
1_16_311_f1(50)\PhaseImage.tif	-25.97637572	49.83538047	50	-0.164619532	0.164619532
1_16_311_f2(50)\PhaseImage.tif	-26.04451216	49.25648125	50	-0.743518754	0.743518754
1_16_311_w1(0)\PhaseImage.tif	-31.87332184	-0.266115903	0	-0.266115903	0.266115903
1_16_311_w2(35)\PhaseImage.tif	-28.73867598	26.36638928	35	-8.633610724	8.633610724
1_16_479_f1(45)\PhaseImage.tif	-26.47270686	45.61846338	45	0.618463378	0.618463378
1_16_479_f2(45)\PhaseImage.tif	-26.25920049	47.43245121	45	2.432451214	2.432451214
1_16_479_w1(61)\PhaseImage.tif	-26.24241909	47.57502896	61	-13.42497104	13.42497104
1_16_479_w2(19)\PhaseImage.tif	-29.83622788	17.04139443	19	-1.958605568	1.958605568
1_16_497_f1(55)\PhaseImage.tif	-25.52176319	53.69784884	55	-1.302151156	1.302151156
1_16_497_f2(55)\PhaseImage.tif	-25.56975091	53.29013667	55	-1.709863326	1.709863326
1_16_497_w1(0)\PhaseImage.tif	-31.74823788	0.796619576	0	0.796619576	0.796619576
1_16_497_w2(31)\PhaseImage.tif	-29.06937284	23.5567303	31	-7.443269704	7.443269704
1_16_x33_f1(45)\PhaseImage.tif	-26.39573585	46.27242269	45	1.272422688	1.272422688
1_16_x33_f2(45)\PhaseImage.tif	-26.34025337	46.74381161	45	1.743811613	1.743811613
1_16_x33_w1(30)\PhaseImage.tif	-28.70209865	26.67715678	30	-3.322843224	3.322843224
1_16_x33_w2(60)\PhaseImage.tif	-26.03356247	49.3495117	60	-10.6504883	10.6504883
1_17_311_w1(0)\PhaseImage.tif	-31.93009591	-0.748478448	0	-0.748478448	0.748478448
1_17_311_w2(46)\PhaseImage.tif	-27.83597584	34.03588918	46	-11.96411082	11.96411082
1_17_479_f1(45)\PhaseImage.tif	-26.21534568	47.80504948	45	2.805049478	2.805049478
1_17_479_f2(45)\PhaseImage.tif	-26.37336439	46.4624946	45	1.462494604	1.462494604
1_17_479_w1(0)\PhaseImage.tif	-31.87381361	-0.27029404	0	-0.27029404	0.27029404
1_17_479_w2(67)\PhaseImage.tif	-25.80079907	51.32711069	67	-15.67288931	15.67288931
1_17_497_f1(55)\PhaseImage.tif	-24.97435319	58.34874093	55	3.348740934	3.348740934
1_17_497_f2(55)\PhaseImage.tif	-25.21341271	56.31764898	55	1.317648983	1.317648983
1_17_497_w1(0)\PhaseImage.tif	-31.7493251	0.787382344	0	0.787382344	0.787382344
1_17_497_w2(29)\PhaseImage.tif	-29.31099901	21.50383172	29	-7.496168278	7.496168278
1_17_525_f1(45)\PhaseImage.tif	-26.4476911	45.83100168	45	0.831001676	0.831001676
1_17_525_f2(45)\PhaseImage.tif	-26.50284115	45.3624371	45	0.362437099	0.362437099
1_17_x33_f1(45)\PhaseImage.tif	-26.77584604	43.04293934	45	-1.95706066	1.95706066
1_17_x33_f2(45)\PhaseImage.tif	-26.98101373	41.29979838	45	-3.70020162	3.70020162
1_17_x33_w1(65)\PhaseImage.tif	-25.46053843	54.21802526	65	-10.78197474	10.78197474
1_17_x33_w2(27)\PhaseImage.tif	-29.01523596	24.01668686	27	-2.983313136	2.983313136
1_18_479_f1(45)\PhaseImage.tif	-26.34374378	46.71415652	45	1.714156522	1.714156522
1_18_479_f2(45)\PhaseImage.tif	-26.29606885	47.11921111	45	2.119211109	2.119211109
1_18_479_w1(0)\PhaseImage.tif	-31.940522	-0.837060295	0	-0.837060295	0.837060295
1_18_479_w2(57)\PhaseImage.tif	-26.01510398	49.50633834	57	-7.49366166	7.49366166
1_18_497_f1(55)\PhaseImage.tif	-24.63399638	61.24047259	55	6.240472593	6.240472593
1_18_497_f2(55)\PhaseImage.tif	-25.14790152	56.8742437	55	1.874243703	1.874243703
1_18_497_w1(0)\PhaseImage.tif	-31.84550567	-0.029784769	0	-0.029784769	0.029784769

Control Test Data Results (Continued)

FileName	ImageValue	ImageWeight	ScaleWeight	Difference	Abs. Diff.
1_18_497_w2(24)\PhaseImage.tif	-29.75960144	17.69242615	24	-6.307573848	6.307573848
1_18_525_f1(45)\PhaseImage.tif	-26.55576276	44.91280579	45	-0.087194214	0.087194214
1_18_525_f2(45)\PhaseImage.tif	-26.37591837	46.44079546	45	1.440795463	1.440795463
1_18_525_w1(0)\PhaseImage.tif	-31.98422532	-1.208371473	0	-1.208371473	1.208371473
1_18_525_w2(45)\PhaseImage.tif	-27.9766884	32.84037048	45	-12.15962952	12.15962952
1_18_x33_f1(45)\PhaseImage.tif	-26.43898776	45.90494683	45	0.904946835	0.904946835
1_18_x33_f2(45)\PhaseImage.tif	-26.36897943	46.49974995	45	1.499749947	1.499749947
1_18_x33_w1(49)\PhaseImage.tif	-26.97589208	41.34331283	49	-7.656687167	7.656687167
1_18_x33_w2(42)\PhaseImage.tif	-27.2500791	39.01377142	42	-2.986228581	2.986228581
1_19_479_f1(45)\PhaseImage.tif	-26.02529418	49.41976055	45	4.419760547	4.419760547
1_19_479_f2(45)\PhaseImage.tif	-25.97045482	49.88568545	45	4.885685447	4.885685447
1_19_479_w1(0)\PhaseImage.tif	-31.87456494	-0.276677487	0	-0.276677487	0.276677487
1_19_479_w2(49)\PhaseImage.tif	-27.03086597	40.87624495	49	-8.123755053	8.123755053
1_19_497_f1(55)\PhaseImage.tif	-24.69070109	60.75869932	55	5.758699318	5.758699318
1_19_497_f2(55)\PhaseImage.tif	-24.91255921	58.87375353	55	3.873753529	3.873753529
1_19_497_w1(0)\PhaseImage.tif	-31.85407202	-0.102566044	0	-0.102566044	0.102566044
1_19_497_w2(30)\PhaseImage.tif	-28.82666207	25.6188439	30	-4.381156102	4.381156102
1_19_525_f1(45)\PhaseImage.tif	-26.24676875	47.53807351	45	2.538073505	2.538073505
1_19_525_f2(45)\PhaseImage.tif	-26.13572766	48.48149825	45	3.48149825	3.48149825
1_19_525_w1(0)\PhaseImage.tif	-31.92340688	-0.691647205	0	-0.691647205	0.691647205
1_19_525_w2(32)\PhaseImage.tif	-28.79948388	25.84975464	32	-6.150245356	6.150245356
1_19_x33_f1(45)\PhaseImage.tif	-26.15199973	48.34324785	45	3.343247853	3.343247853
1_19_x33_f2(45)\PhaseImage.tif	-26.32860842	46.84274922	45	1.842749217	1.842749217
1_19_x33_w1(46)\PhaseImage.tif	-27.03735408	40.82112084	46	-5.178879156	5.178879156
1_19_x33_w2(45)\PhaseImage.tif	-26.86883445	42.25289337	45	-2.747106628	2.747106628
1_21_497_f1(55)\PhaseImage.tif	-25.16373092	56.73975426	55	1.739754259	1.739754259
1_21_497_f2(55)\PhaseImage.tif	-25.11836785	57.12516692	55	2.125166924	2.125166924
1_21_497_w1(1)\PhaseImage.tif	-31.98379234	-1.204692762	1	-2.204692762	2.204692762
1_21_497_w2(28)\PhaseImage.tif	-29.38394346	20.88408277	28	-7.115917232	7.115917232
1_21_519_f1(45)\PhaseImage.tif	-26.1231523	48.58834069	45	3.588340687	3.588340687
1_21_519_f2(45)\PhaseImage.tif	-26.50655562	45.33087832	45	0.330878319	0.330878319
1_21_519_w1(20)\PhaseImage.tif	-29.75504353	17.73115095	20	-2.26884905	2.26884905
1_21_519_x33_w1(0)\PhaseImage.tif	-31.89704037	-0.467632738	0	-0.467632738	0.467632738
1_21_525_f1(45)\PhaseImage.tif	-26.43909635	45.90402423	45	0.904024232	0.904024232
1_21_525_f2(45)\PhaseImage.tif	-26.19031909	48.01767981	45	3.017679812	3.017679812
1_21_525_w1(0)\PhaseImage.tif	-31.9021233	-0.510818222	0	-0.510818222	0.510818222
1_21_525_w2(30)\PhaseImage.tif	-28.80721155	25.78409897	30	-4.21590103	4.21590103
1_21_526_f1(50)\PhaseImage.tif	-25.52516581	53.66893963	50	3.668939628	3.668939628
1_21_526_f2(50)\PhaseImage.tif	-25.98970953	49.72209409	50	-0.277905908	0.277905908
1_21_526_w1(0)\PhaseImage.tif	-31.8595716	-0.149291398	0	-0.149291398	0.149291398
1_21_526_w2(33)\PhaseImage.tif	-28.08113765	31.95295117	33	-1.047048826	1.047048826
1_21_x33_w2(36)\PhaseImage.tif	-27.91061322	33.40175684	26	7.401756841	7.401756841
1_22_497_f1(55)\PhaseImage.tif	-24.94908588	58.56341648	55	3.563416481	3.563416481
1_22_497_f2(55)\PhaseImage.tif	-25.41728084	54.58554933	55	-0.41445067	0.41445067
1_22_497_w1(0)\PhaseImage.tif	-31.81149506	0.259175372	0	0.259175372	0.259175372

Control Test Data Results (Continued)

FileName	ImageValue	ImageWeight	ScaleWeight	Difference	Abs. Diff.
1_22_497_w2(20)\PhaseImage.tif	-30.06981009	15.05683866	20	-4.943161335	4.943161335
1_22_519_f1(45)\PhaseImage.tif	-26.52200981	45.19957684	45	0.19957684	0.19957684
1_22_519_f2(45)\PhaseImage.tif	-26.47396663	45.60776015	45	0.607760147	0.607760147
1_22_519_w1(0)\PhaseImage.tif	-31.97807924	-1.156153313	0	-1.156153313	1.156153313
1_22_519_w2(39)\PhaseImage.tif	-27.76587867	34.63144716	39	-4.368552841	4.368552841
1_22_525_f1(45)\PhaseImage.tif	-26.44148707	45.88371227	45	0.883712266	0.883712266
1_22_525_f2(45)\PhaseImage.tif	-26.70016594	43.68593082	45	-1.314069176	1.314069176
1_22_525_w1(0)\PhaseImage.tif	-31.77044227	0.607967104	0	0.607967104	0.607967104
1_22_525_w2(29)\PhaseImage.tif	-28.94924688	24.57734173	29	-4.422658271	4.422658271
1_22_526_f1(50)\PhaseImage.tif	-25.85395333	50.87550271	50	0.875502713	0.875502713
1_22_526_f2(50)\PhaseImage.tif	-25.79350121	51.38911462	50	1.389114619	1.389114619
1_22_526_w1(0)\PhaseImage.tif	-31.9329094	-0.772382286	0	-0.772382286	0.772382286
1_22_526_w2(39)\PhaseImage.tif	-27.98389786	32.77911759	39	-6.220882408	6.220882408
1_23_429_f1(55)\PhaseImage.tif	-25.04033129	57.78817936	55	2.788179361	2.788179361
1_23_429_f2(55)\PhaseImage.tif	-24.89640828	59.01097467	55	4.010974666	4.010974666
1_23_429_w1(18)\PhaseImage.tif	-29.80845051	17.2773958	18	-0.722604205	0.722604205
1_23_497_f1(55)\PhaseImage.tif	-24.91333398	58.86717092	55	3.867170919	3.867170919
1_23_497_f2(55)\PhaseImage.tif	-24.70922926	60.60128075	55	5.601280755	5.601280755
1_23_497_w1(0)\PhaseImage.tif	-31.9222427	-0.681756146	0	-0.681756146	0.681756146
1_23_497_w2(26)\PhaseImage.tif	-29.49731383	19.9208681	26	-6.079131903	6.079131903
1_23_519_f1(45)\PhaseImage.tif	-25.23188926	56.16066898	45	11.16066898	11.16066898
1_23_519_f2(45)\PhaseImage.tif	-26.18778984	48.0391687	45	3.039168697	3.039168697
1_23_519_w1(0)\PhaseImage.tif	-31.9323773	-0.767861529	0	-0.767861529	0.767861529
1_23_519_w2(36)\PhaseImage.tif	-28.54763847	27.98947778	36	-8.010522222	8.010522222
1_23_525_f1(45)\PhaseImage.tif	-26.04091151	49.28707302	45	4.28707302	4.28707302
1_23_525_f2(45)\PhaseImage.tif	-26.14453683	48.40665397	45	3.406653973	3.406653973
1_23_525_w1(0)\PhaseImage.tif	-31.91307628	-0.603876667	0	-0.603876667	0.603876667
1_23_525_w2(26)\PhaseImage.tif	-29.16022028	22.7848744	26	-3.215125599	3.215125599
1_23_526_f1(50)\PhaseImage.tif	-25.22384166	56.22904283	50	6.229042833	6.229042833
1_23_526_f2(50)\PhaseImage.tif	-25.31622341	55.44415112	50	5.444151123	5.444151123
1_23_526_w1(0)\PhaseImage.tif	-31.86311697	-0.179413507	0	-0.179413507	0.179413507
1_23_526_w2(44)\PhaseImage.tif	-27.85312051	33.89022504	44	-10.10977496	10.10977496
1_24_429_f1(55)\PhaseImage.tif	-24.41238334	63.12333613	55	8.123336126	8.123336126
1_24_429_f2(55)\PhaseImage.tif	-24.47622632	62.58091487	55	7.580914868	7.580914868
1_24_429_w1(0)\PhaseImage.tif	-31.88739192	-0.385657792	0	-0.385657792	0.385657792
1_24_429_w2(57)\PhaseImage.tif	-25.93158754	50.21590874	57	-6.78409126	6.78409126
1_24_497_f1(60)\PhaseImage.tif	-23.96380203	66.93456216	60	6.934562158	6.934562158
1_24_497_f2(60)\PhaseImage.tif	-24.75397389	60.22112245	60	0.221122449	0.221122449
1_24_497_w1(0)\PhaseImage.tif	-31.94072285	-0.838766811	0	-0.838766811	0.838766811
1_24_497_w2(9)\PhaseImage.tif	-30.96463131	7.454279472	9	-1.545720528	1.545720528
1_24_519_f1(45)\PhaseImage.tif	-25.94869168	50.07058892	45	5.070588925	5.070588925
1_24_519_f2(45)\PhaseImage.tif	-25.85009232	50.90830652	45	5.908306524	5.908306524
1_24_519_w1(0)\PhaseImage.tif	-31.90587987	-0.542734684	0	-0.542734684	0.542734684
1_24_519_w2(35)\PhaseImage.tif	-27.99909937	32.64996285	35	-2.350037152	2.350037152
1_24_525_f1(45)\PhaseImage.tif	-26.01025978	49.54749549	45	4.547495494	4.547495494

Control Test Data Results (Continued)

FileName	ImageValue	ImageWeight	ScaleWeight	Difference	Abs. Diff.
1_24_525_f2(45)\PhaseImage.tif	-26.06503422	49.08212217	45	4.082122168	4.082122168
1_24_525_w1(0)\PhaseImage.tif	-31.90464895	-0.532276535	0	-0.532276535	0.532276535
1_24_525_w2(20)\PhaseImage.tif	-29.98544834	15.773591	20	-4.226408999	4.226408999
1_24_526_f1(50)\PhaseImage.tif	-25.62255354	52.84151626	50	2.841516263	2.841516263
1_24_526_f2(50)\PhaseImage.tif	-24.9847834	58.26012403	50	8.260124032	8.260124032
1_24_526_w1(0)\PhaseImage.tif	-31.84999516	-0.067928319	0	-0.067928319	0.067928319
1_24_526_w2(36)\PhaseImage.tif	-28.21778099	30.79200515	36	-5.20799485	5.20799485
1_25_429_f1(60)\PhaseImage.tif	-24.1874972	65.03400854	60	5.034008537	5.034008537
1_25_429_f2(60)\PhaseImage.tif	-24.11142156	65.68036059	60	5.680360587	5.680360587
1_25_429_w1(0)\PhaseImage.tif	-31.88825924	-0.39302665	0	-0.39302665	0.39302665
1_25_429_w2(2)\PhaseImage.tif	-31.79769856	0.37639284	2	-1.62360716	1.62360716
1_25_497_f1(60)\PhaseImage.tif	-23.90948448	67.3960537	60	7.396053705	7.396053705
1_25_497_f2(60)\PhaseImage.tif	-23.96731748	66.90469429	60	6.90469429	6.90469429
1_25_497_w1(0)\PhaseImage.tif	-31.88319449	-0.349995678	0	-0.349995678	0.349995678
1_25_497_w2(25)\PhaseImage.tif	-29.00407553	24.11150778	25	-0.888492215	0.888492215
1_25_519_f1(45)\PhaseImage.tif	-25.3462114	55.18936791	45	10.18936791	10.18936791
1_25_519_f2(45)\PhaseImage.tif	-25.65213723	52.59016797	45	7.590167967	7.590167967
1_25_519_w1(0)\PhaseImage.tif	-31.85463818	-0.107376177	0	-0.107376177	0.107376177
1_25_519_w2(19)\PhaseImage.tif	-29.54918379	19.48017167	19	0.480171675	0.480171675
1_25_525_f1(45)\PhaseImage.tif	-25.24103779	56.08294148	45	11.08294148	11.08294148
1_25_525_f2(45)\PhaseImage.tif	-25.35456086	55.11842939	45	10.11842939	10.11842939
1_25_525_w1(0)\PhaseImage.tif	-31.94736414	-0.895192345	0	-0.895192345	0.895192345
1_25_525_w2(20)\PhaseImage.tif	-29.60254075	19.02684158	20	-0.973158418	0.973158418
1_25_526_f1(50)\PhaseImage.tif	-25.78244591	51.48304241	50	1.483042408	1.483042408
1_25_526_f2(50)\PhaseImage.tif	-25.16767244	56.70626644	50	6.706266436	6.706266436
1_25_526_w1(0)\PhaseImage.tif	-31.96742314	-1.065617149	0	-1.065617149	1.065617149
1_25_526_w2(39)\PhaseImage.tif	-28.11039976	31.70433511	39	-7.295664894	7.295664894
1_26_429_f1(60)\PhaseImage.tif	-24.39081574	63.30657828	60	3.306578277	3.306578277
1_26_429_f2(60)\PhaseImage.tif	-24.54145922	62.02668463	60	2.026684626	2.026684626
1_26_429_w1(0)\PhaseImage.tif	-31.89659526	-0.463850978	0	-0.463850978	0.463850978
1_26_429_w2(23)\PhaseImage.tif	-28.92605908	24.7743494	23	1.774349403	1.774349403
1_26_497_f1(60)\PhaseImage.tif	-24.80233083	59.81027333	60	-0.189726673	0.189726673
1_26_497_f2(60)\PhaseImage.tif	-24.47638029	62.57960669	60	2.579606693	2.579606693
1_26_497_w1(0)\PhaseImage.tif	-31.96162315	-1.01633942	0	-1.01633942	1.01633942
1_26_497_w2(22)\PhaseImage.tif	-29.48574324	20.01917382	22	-1.980826176	1.980826176
1_26_519_f1(45)\PhaseImage.tif	-26.45461061	45.77221231	45	0.772212312	0.772212312
1_26_519_f2(45)\PhaseImage.tif	-26.37120573	46.4808349	45	1.480834899	1.480834899
1_26_519_w1(0)\PhaseImage.tif	-31.91063604	-0.583143925	0	-0.583143925	0.583143925
1_26_519_w2(30)\PhaseImage.tif	-28.51767769	28.24402979	30	-1.755970209	1.755970209
1_26_525_f1(50)\PhaseImage.tif	-25.54197918	53.52609023	50	3.526090234	3.526090234
1_26_525_f2(50)\PhaseImage.tif	-25.80577646	51.28482191	50	1.284821908	1.284821908
1_26_525_w1(0)\PhaseImage.tif	-31.94036162	-0.835697708	0	-0.835697708	0.835697708
1_26_525_w2(17)\PhaseImage.tif	-29.0662539	23.58322941	17	6.583229415	6.583229415
1_26_526_f1(50)\PhaseImage.tif	-25.79270154	51.39590874	50	1.395908742	1.395908742
1_26_526_f2(50)\PhaseImage.tif	-25.98037389	49.80141127	50	-0.198588725	0.198588725
1_26_526_w1(0)\PhaseImage.tif	-32.01092755	-1.435238321	0	-1.435238321	1.435238321
1_26_526_w2(30)\PhaseImage.tif	-28.73099647	26.43163575	30	-3.568364253	3.568364253

REFERENCES

[1] Friggens, N. C., Nielsen, B. L., Kyriazakis, I., Tolkamp, B. J., & Emmans, G. C. (1998). Effects of feed composition and stage of lactation on the short-term feeding behavior of dairy cows. *Journal of dairy science, 81*(12), 3268-3277.

[2] Huisma, C. (2002). *U.S. Patent No. 6,427,627*. Washington, DC: U.S. Patent and Trademark Office.

[3] "Calan Broadbent Feeding System." *American Calan*. American Calan, 1997. Retrieved April 25, 2013, from http://americancalan.com

[4] Mendes, E. D. M., Carstens, G. E., Tedeschi, L. O., Pinchak, W. E., & Friend, T. H. (2011). Validation of a system for monitoring feeding behavior in beef cattle. *Journal of animal science, 89*(9), 2904-2910.

[5] Krawczel, P. D., Klaiber, L. M., Thibeau, S. S., & Dann, H. M. (2012). Technical note: Data loggers are a valid method for assessing the feeding behavior of dairy cows using the Calan Broadbent Feeding System. *Journal of dairy science, 95*(8), 4452-4456.

[6] DeVries, T. J., von Keyserlingk, M. A. G., Weary, D. M., & Beauchemin, K. A. (2003). Technical note: Validation of a system for monitoring feeding behavior of dairy cows. *Journal of dairy science, 86*(11), 3571-3574.

[7] Chapinal, N., Veira, D. M., Weary, D. M., & Von Keyserlingk, M. A. G. (2007). Technical Note: Validation of a System for Monitoring Individual Feeding and Drinking Behavior and Intake in Group-Housed Cattle. *Journal of dairy science, 90*(12), 5732-5736.

[8] Nielsen, B. L. (1999). On the interpretation of feeding behaviour measures and the use of feeding rate as an indicator of social constraint. Applied Animal Behaviour Science, 63(1), 79-91.

[9] Chiba, L. (2009). Animal Nutrition Handbook. *College of Agriculture - Auburn University*. Retrieved January 3, 2013, from http://www.ag.auburn.edu/~chibale/an15dairycattlefeeding.pdf

[10] Looper, M., & University of Arkansas (1998). Individually Feeding Dairy Cows in the Milking Parlor. *U of A Division of Agriculture Cooperative Extension Service*. Retrieved January 3, 2013, from http://www.uaex.edu/Other_Areas/publications/PDF/FSA-4011.pdf

[11] Amaral-Phillips, D., Hemken, R., Crist, W., & University of Kentucky Cooperative Extension Service (1997). More Feed = More Milk. *Learning, Discovery, Service | in the College of Agriculture*. Retrieved January 3, 2013, from http://www.ca.uky.edu/agc/pubs/asc/asc135/asc135.pdf

[12] The University of Tennessee Agricultural Extension Service (1997, October). PB1598-Managing Intake of Lactating Dairy Cows. Retrieved January 3, 2013, from https://utextension.tennessee.edu/publications/Documents/pb1598.pdf

[13] Grant, R., & University of Nebraska (1990). G90-1003 Maximizing Feed Intake for Maximum Milk Production. *Historical Materials from University of Nebraska-Lincoln Extension. Paper 439*. Retrieved January 3, 2013, from http://digitalcommons.unl.edu/cgi/viewcontent.cgi?article=1435&context=extensionhist

[14] Albright, J. L. (1993). Nutrition, Feeding, and Calves. *Journal of Dairy Science*, *76*, 485-498.

[15] DeVries, T. J., Von Keyserlingk, M. A. G., & Beauchemin, K. A. (2003). Short Communication: Diurnal Feeding Pattern of Lactating Dairy Cows. *Journal of dairy science*, *86*(12), 4079-4082.

[16] Hutjens, M. F. (2005, March). Dairy Efficiency and Dry Matter Intake. *Western Dairy Management Conference*. Retrieved January 3, 2013, from http://www.wdmc.org/2005/8Hutjens.pdf

[17] Grant, R. J., & Albright, J. L. (2001). Effect of animal grouping on feeding behavior and intake of dairy cattle. *Journal of dairy science*, *84*, E156-E163.

[18] Rim, J., Lee, S., Cho, Y., Kim, E., Kim, J., & Ha, J. (2008). Prediction of Dry Matter Intake in Lactating Holstein Dairy Cows Offered High Levels of Concentrate. *Asian-Australasian Journal of Animal Science*, *21*(5), 677-684. Retrieved from http://www.ajas.info/Editor/manuscript/upload/21-95.pdf

[19] Schwartzkopf-Genswein, K. S., Huisma, C., & McAllister, T. A. (1999). Validation of a radio frequency identification system for monitoring the feeding patterns of feedlot cattle. *Livestock production science*, *60*(1), 27-31.

[20] Bach, A., Iglesias, C., & Busto, I. (2004). Technical Note: A Computerized System for Monitoring Feeding Behavior and Individual Feed Intake of Dairy Cattle. *Journal of dairy science*, *87*(12), 4207-4209.

[21] Shultz, T. (1989). Computerized corral feed stations for dairy cows. *California Agriculture*, *43*(5), 26-27. doi:10.3733/ca.v043n05p26

[22] Ferris, C. P., Keady, T. W. J., Gordon, F. J., & Kilpatrick, D. J. (2006). Comparison of a Calan gate and a conventional feed barrier system for dairy cows: feed intake and cow behaviour. *Irish Journal of Agricultural and Food Research*, 149-156.

[23] Halachmi, I., Edan, Y., Maltz, E., Peiper, U. M., Moallem, U., & Brukental, I. (1998). A real-time control system for individual dairy cow food intake. *Computers and Electronics in Agriculture*, *20*(2), 131-144.

[24] University of Kentucky (n.d.). Dairy Research | Dairy. *Learning, Discovery, Service | in the College of Agriculture*. Retrieved January 13, 2013, from http://www2.ca.uky.edu/afsdairy/research

[25] Liu, K., Wang, Y., Lau, D., Hao, Q., & Hassebrook, L. (2010). Dual-frequency pattern scheme for high-speed 3-D shape measurement. *Optics Express*, *18*(5), 5229-5244. doi:10.1364/OE.18.005229

[26] Wang, Y. (2010). *Novel Approaches in Structured Light Illumination*. PhD Dissertation, University of Kentucky, 2010. Retrieved January 13, 2013, from http://uknowledge.uky.edu/cgi/viewcontent.cgi?article=1124&context=gradschool_diss

[27] Du, Q., Faber, V., & Gunzburger, M. (1999). Centroidal Voronoi tessellations: Applications and algorithms. *SIAM review*, *41*(4), 637-676.

[28] Lee, D. T., & Schachter, B. J. (1980). Two algorithms for constructing a Delaunay triangulation. *International Journal of Computer & Information Sciences*, *9*(3), 219-242.

[29] Fang, T. P., & Piegl, L. A. (1995). Delaunay triangulation in three dimensions. *Computer Graphics and Applications, IEEE*, *15*(5), 62-69.

[30] Tanemura, M., Ogawa, T., & Ogita, N. (1983). A new algorithm for three-dimensional Voronoi tessellation. *Journal of Computational Physics, 51*(2), 191-207.

[31] Koster, E. C. (1976). *U.S. Patent No. 3,994,156*. Washington, DC: U.S. Patent and Trademark Office.

VITA

ANTHONY NEAL SHELLEY
Morehead, Kentucky

Education

M.S., Engineering Technology (3.818 GPA)
Morehead State University, Morehead, KY (August 2009 - December 2010)
Thesis: "A 24FT/7.3M PARABOLIC REFLECTOR ANTENNA PERFORMANCE & FEED DESIGN ANALYSIS"
Thesis Committee: Ahmad Zargari (Advisor), Ph.D., Hans Chapman, Ph.D., & Capp Yess, Ph.D.

B.S., Space Science (3.077 GPA)
Minor, International Studies
Morehead State University, Morehead, KY (August 2004 - May 2009)
Senior Research: "Implementation of A Secondary Space Tracking Antenna at Morehead State University"
Undergraduate Advisor: Benjamin Malphrus, Ph.D.

Research & Teaching Experience

- Graduate Research Assistant: August 2012 – Present
  Department of Electrical Engineering
  University of Kentucky, Lexington, KY

- Graduate Assistant: January 2010 – December 2010
  Department of Applied Engineering & Technology
  Morehead State University, Morehead, KY

- Undergraduate Fellowship: August 2008 – May 2009
  Space Science Center
  Morehead State University, Morehead, KY

- Work-Study: August 2004 – May 2008
  Space Science Center
  Morehead State University, Morehead, KY

Publications, Presentations, & Awards

- Shelley, A. N., "A 24ft/7.3m Parabolic Reflector Antenna Performance & Feed Design Analysis," 2010 Kentucky Academy of Science (KAS) Annual Meeting, Bowling Green, KY, 13-14 November 2010. (Won 1st place for Engineering).

- Shelley, A.N., Midden, D.P., and Arabmakki, E., "Digital Signal Processing and Medical Imaging," International Association of Journals and Conferences – American Society for Engineering Education (IAJC – ASEE) 2011 Joint International Conference, University of Hartford, CT, 15-16 April 2011.

- Outstanding Senior in Space Science, May 2009.